Decoding the Trafficking Motifs in the Mammalian VNUT N- and C-Termini

by
Stephanie Rayner

B.Sc. (Hons., Psychology and Neuroscience), University of Sussex, 2017

Thesis Submitted in Partial Fulfilment of the
Requirements for the Degree of
Master of Science

in the
Department of Biomedical Physiology and Kinesiology
Faculty of Science

SIMON FRASER UNIVERSITY
Summer 2024

Declaration of Committee

Name:	Stephanie Rayner
Degree:	Master of Science
Title:	Decoding the Trafficking Motifs in the Mammalian VNUT N- and C-Termini
Committee:	Chair: **Andrew Blaber** Professor, Biomedical Physiology and Kinesiology
	Damon Poburko Supervisor Associate Professor, Biomedical Physiology and Kinesiology
	Peter Ruben Committee Member Professor, Biomedical Physiology and Kinesiology
	Michael Silverman Committee Member Professor, Biological Sciences
	Nadine Wicks Committee Member Senior Lecturer, Biomedical Physiology and Kinesiology
	Thomas Claydon Examiner Associate Professor, Biomedical Physiology and Kinesiology

Abstract

Rationale: The vesicular nucleotide transporter (VNUT) is crucial for loading adenosine triphosphate (ATP) into vesicles. ATP acts as a neurotransmitter in the central and peripheral nervous systems and is implicated in diverse physiological functions. We have shown that mammalian VNUT localises to the Golgi apparatus and endoplasmic reticulum (ER), diverging from the vesicular localisation of other neurotransmitter transporters.

Objective: To identify trafficking motifs in VNUT's termini that explain its unexpected subcellular localisation.

Methods: Bioinformatics analyses mapped phylogenetic changes in VNUT's C-terminus and uncovered a putative N-terminal retrograde transport motif. We used chimeric and mutagenic analyses to dissect functional motifs in regions of the N- and C-termini of VNUT.

Results: Epifluorescence microscopy revealed that mammalian C-terminal motifs promote ER-Golgi retention compared to avian (tyrosine, dileucine) motifs. Truncation of the putative N-terminal COPI-interacting motif disrupted retrograde Golgi-ER transport.

Conclusions: Terminal motifs mediate mammalian VNUT trafficking, advancing our understanding of purinergic signalling.

Keywords: purinergic signalling; VNUT; ATP; truncation; trafficking motifs.

For George and Fig

Acknowledgements

I thank my partner, George, for his consistent support throughout the Master's program. It has been incredible sharing this journey with you. Your patience and companionship have been truly invaluable, and I wouldn't be in this position without you.

Thank you to my supervisor, Dr Damon Poburko for pushing me when I needed it, having patience with teaching me, and showing kindness. Your breadth of knowledge will never cease to amaze me.

Thank you to the other Poburko Lab members, Josh Ham, Samantha Rothwell, Lara Gastaldello, Chloe Lindsay and Ziyanna Vallani, for your help with data collection, analysis, lab maintenance and camaraderie, along with all other members of the lab.

Thank you also to the wonderful friends I have made at SFU during this program. You have made Vancouver a wonderful place to live, and I will miss the people even more than the city.

Table of Contents

Declaration of Committee ii
Abstract iii
Dedication iv
Acknowledgements v
Table of Contents vi
List of Tables ix
List of Figures x
List of Acronyms xii

Chapter 1. Introduction 1
1.1. Synaptic Transmission 1
1.2. Purinergic Signalling 1
1.2.1. Physiological and Pathological Roles of ATP 5
1.2.2. Mechanisms of Purinergic Signalling 7
1.3. VNUT 9
1.3.1. VNUT Expression 11
1.3.2. The Roles of VNUT and Vesicular ATP Release 12
1.3.3. VNUT Subcellular Localisation 14
1.4. Vesicle Trafficking Dynamics 18
1.4.1. Retention Mechanisms 19
1.4.2. Secretory Pathways from the Golgi Apparatus 21
1.4.3. Chimera Proteins Used for Researching Transporter Trafficking 22
1.5. VNUT Phylogeny 24
1.6. Methods Featured in This Thesis 24
1.6.1. Image Acquisition Techniques 25
1.6.2. Image Analysis Methods 26
1.6.3. Research Hypotheses 27

Chapter 2. General Methods 30
2.1. Molecular Biology 30
2.2. Cell Culture 30
2.2.1. Maintenance and Differentiation 30
2.2.2. Transfection 31
2.3. Fixed Cell Imaging 32
2.3.1. Sample Preparation 32
2.3.2. Image Acquisition 32
2.4. Live Cell Imaging 33
2.5. Image Analysis 34
2.5.1. ImageJ and FIJI 34

2.5.2. Deconvolution 34
2.5.3. Maximal Intensity Projections 36
2.5.4. RIPA 36
2.5.5. MINER 37
2.5.6. JACOP 39
2.6. Data Analyses 39
2.6.1. Correlational analyses 39
2.6.2. Puncta analyses 39
2.6.3. Statistical Analyses 41

Chapter 3. Deciphering the C-terminal Sorting Motifs in Mammalian VNUT 42

3.1. Rationale 42
3.2. Methods 43
3.2.1. Bioinformatics 43
Motif search 43
Evolutionary Tree 43
3.2.2. Molecular Biology 43
Insert Design 43
Primer Design 44
PCR Protocol 45
Gel Electrophoresis 45
PCR Clean-up 45
Construct Assembly 45
Transformation 46
Colony PCR 46
Colony PCR 46
Plasmid Creation 46
3.2.3. Live Imaging 47
Sample Preparation 47
Image Acquisition 48
pH Excursions and Calibrations 49
3.2.4. Fixed Imaging 50
3.2.5. Image Analysis 51
pHluorin Analysis 51
EGFP-Analysis 51
3.2.6. Statistical Analysis 52
3.3. Results 52
3.3.1. Evolutionary Conservation of VNUT C-terminus Motifs Across Species 52
3.3.2. Subcellular Localisation of Fixed EGFP-VNUT Chimera Constructs 57
3.3.3. Using pH Excursions to Determine Localisation of VNUT PHluorin Chimera Constructs 67

3.4. Summary 73

Chapter 4. Identification of a Putative N-terminal ER-retention Sequence in the VNUT N-terminus 76
4.1. Rationale 76
4.2. Methods 77
4.2.1. Bioinformatics 77
Predicting Protein Interactions 77
4.2.2. Molecular Biology 77
Primer Design 77
Site Directed Mutagenesis 78
Transformation 78
Colony PCR 79
Plasmid Creation 79
4.2.3. Cell culture 79
4.2.4. Fixed Imaging 80
Sample Preparation 80
4.2.5. Image analysis 80
Golgi:ER Ratio 80
4.2.6. Data Analyses 81
4.2.7. Statistical Analyses 81
4.3. Results 81
4.3.1. Bioinformatics 82
4.3.2. Fixed Cell Microscopy 90
4.4. Summary 100

Chapter 5. Discussion and Future Directions 102
5.1. Identification of Amino Acid Motifs in VNUT's Termini 103
5.2. Correlation as a Measure of VNUT Localisation 106
5.3. The Effect of C-terminal Motifs in VNUT Localisation 108
5.4. Using pH to Locate VNUT-Containing Compartments 109
5.5. The Effect of N-terminal Truncations on VNUT Transport 111
5.6. Caveats and Limitations 113
5.7. Implications and Future Directions 114

References 117

Appendix. Supplemental Table 152

List of Tables

Table 1.1: Purinergic receptor expression and transduction mechanisms 4
Table 2.1: Transfection constructs used 31
Table 2.2: Point Spread Function parameters 35
Table 3.1: EGFP-VNUT and VNUT-pHluorin backbone amplification primers 44
Table 3.2: Colony PCR sequences 46
Table 3.3: Live imaging buffer recipes 47
Table 4.1: EGFP-VNUT N-terminus truncation primers 78
Table 4.2: EGFP-VNUT N-terminus truncation PCR protocol 78
Table 4.3: N-terminus truncations colony PCR primers 79

List of Figures

Figure 1.1: Co-release and co-transmission of neurotransmitters 2
Figure 1.2: Sequence and Predicted Topology of VNUT 10
Figure 1.3: Moriyama et al 2016 VNUT co-localisation 15
Figure 1.4: Colocalisation of VNUT and Golgi markers 18
Figure 1.5: Vesicular trafficking dynamics in the secretory pathway 19
Figure 1.6: PHluorins quenching and dequenching 26
Figure 2.1: Cell seeding to microscopy workflow 33
Figure 2.2: Born & Wolf PSF model of diffraction. 35
Figure 2.3: RIPA and MINER analysis Within the cell soma 38
Figure 2.4: Diagrammatic representation of puncta analyses 40
Figure 3.1: pH excursions protocol 50
Figure 3.2: Protocol for calibrating pH values to pHluorin fluorescence 50
Figure 3.3: Phylogenetic tree displaying VNUT C-terminal motif change in kingdom Animalia 54
Figure 3.4: Sequence alignment of C-terminal amino acid sequences in selected species 55
Figure 3.5: Evolutionary motif variations in monotreme and marsupial C-termini 56
Figure 3.6: Sequence alignment of human and rat VNUT C-termini 57
Figure 3.7: Comparative co-localisation of VNUT variants with the ER and Golgi 58
Figure 3.8: Correlation between VNUT C-terminus variants with ER and Golgi markers 59
Figure 3.9: 'Onion-peel' analysis: spatial distribution of VNUT construct puncta in 250 nm slices 61
Figure 3.10: Perimeter-proximal puncta counts across VNUT C-terminus variants 62
Figure 3.11: Normalised perimeter-proximal puncta distribution across VNUT C-terminus variants 64
Figure 3.12: Fluorescence intensity of perimeter VNUT puncta 66
Figure 3.13: Comparison of cell and puncta area across VNU C-terminus variants. 67
Figure 3.14: Representative normalised fluorescence trace by VNUT C-terminus variant 69
Figure 3.15: pH-calibrated fluorescence trace for VNUT pHluorin constructs 71
Figure 3.16: Average resting pH values for VNUT variants 72
Figure 4.1: N2a ER and Golgi ROIs 81

Figure 4.2: Evolutionary conservation of the Mammalian VNUT N-terminus 84
Figure 4.3: Comparative alignment of VNUT N-Terminus between human and rat 85
Figure 4.4: Protein folding predictions between αCOPI and human VNUT with N-terminal modifications 86
Figure 4.5: Changes in αCOPI-VNUT binding affinity due to N-Terminal alanine substitutions 87
Figure 4.6: Protein folding predictions between αCOPI and rat VNUT with N-terminal truncations 88
Figure 4.7: Changes in predicted αCOPI-VNUT binding affinity following N-terminal truncations 89
Figure 4.8: Sequence alignment of VNUT N-terminal truncations in EGFP-VNUT 90
Figure 4.9: Comparative co-localisation of VNUT N-terminus variants with ER and Golgi markers 91
Figure 4.10: Correlational analysis of VNUT N-Terminus variants with subcellular organelle markers 92
Figure 4.11: VNUT Localizationsin ER versus Golgi Across N-Terminal Variants 94
Figure 4.12: ‘Onion-peel’ Analysis: Distribution of VNUT N-Terminus Variants Near Cell Perimeter 95
Figure 4.13: Quantifying VNUT N-Terminus Variant Localisation Near the Cell Membrane 97
Figure 4.14: Perimeter-Localised VNUT Puncta Density by N-Terminus Variant. 98
Figure 4.15: Intensity of VNUT-Containing Puncta Close to Cell Membrane Across N-Terminus Variants 99
Figure 4.16: Comparative Analysis of Cell and Puncta Size Among VNUT N-Terminus Variants 100

List of Acronyms

ADP	Adenosine 5'-diphophate
AMP	Adenosine 5'-monophosphate
AP	Adaptor protein
ATP	Adenosine 5'-triphosphate
BFP	Blue fluorescent protein
CACNA1c	Calcium voltage-gated channel subunit alpha1 c
CalHMn	Calcium homeostasis modulator, isoform n
CaMK	Calcium or calmodulin protein kinase
cAMP	Cyclic AMP
CCTOP	Constrained Consensus Topology Predictor
CD39	Cluster of differentiation 39
CD73	Cluster of differentiation 73
COPI	Coatomer protein I
COPII	Coatomer protein II
DAG	Diacylglycerol
DIDS	4,4'-Diisothiocyanatostilbene-2,2'-disulfonic acid
DM	Differentiation media
DMEM	Dulbecco's Modified Eagle Medium
DNA	Deoxyribonucleic acid
dPBS	Distilled phosphate buffered saline
EDTA	Ethylenediaminetetraacetic Acid
ER	Endoplasmic reticulum
FBS	Fetal bovine serum
FWHM	Full width at half maximal fluorescent intensity
GABA	Gamma aminobutyric acid
GFAP	Glial fibrillary acidic protein
GFP	Green fluorescent protein

GM	Growth media
GOLPH3	Golgi phosphoprotein 3
HBSS	HEPES-buffered solution
HCN4	Hyperpolarization-activated cyclic nucleotide-gated channel 4
HEPES	4-(2-hydroxyethyl)-1-piperazineethanesulfonic acid
IP3	Inositol 1,4,5-trisphosphate
iTOL	interactive tree of life
ITP	Inosine 5'-triphosphate
JACOP	Just another colocalization plugin
LDCV	Large dense core vesicle
LRRC8	Leucine rich repeat containing 8
MANT-ATP	(2'-(or-3')-O-(N-methylanthraniloyl) adenosine 5'-triphosphate
MBSS	MES-buffered solution
MES	2-(N-morpholino)ethanesulfonic acid
MINER	Multi-Image Neighbourhood Exploring
N2a	Neuro-2A
NA	Numerical aperture
NCBI	National Center for Biotechnology Information
NMDA	N-Methyl-D-aspartate
P2X*n*	ATP-gated ion channel, subunit *n*
P2Y*n*	G-protein coupled ATP receptor, subunit *n*
PCR	Polymerase chain reaction
PKC	Protein kinase C
POROK8	Porokeratosis 8, disseminated superficial actinic type
PSF	Point spread function
Regex	Regular expression
RFP	Red fluorescent protein
RIPA	Recursive Image Particle Analyser
ROI	Region of interest

RSP	Regulated secretory pathway
shRNA	Short hairpin RNA
SLC	Solute carrier
SLC17	Solute carrier family 17
SLC17A*n*	Solute carrier 17 family 17, member *n*
SLC18	Solute carrier family 18
SLC18A*n*	Solute carrier family 18, member *n*
SOC	Super optimal broth with catabolite repression
TAE	TRIS-acetate-EDTA
TBSS	Tris-buffered saline solution
TGN	Trans-Golgi network
TRIS	Tris(hydroxymethyl)aminomethane
TRPV4	Transient receptor potential vanilloid 4
UDP	Uridine 5'-diphosphate
UTP	Uridine 5'-triphosphate
V-ATPase	Vacuolar H+-ATPase
VAChT	Vesicular acetylcholine transporter
VGAT	Vesicular GABA transporter
VGLUT	Vesicular glutamate transporter
VGLUT*n*	Vesicular glutamate transporter, isoform *n*
VMAT	Vesicular monoamine transporter
VMAT*n*	Vesicular monoamine transporter, isoform *n*
VNUT	Vesicular nucleotide transporter
VNUT*n*	Vesicular nucleotide transporter, isoform *n*
VRAC	Volume regulated anion channel

Chapter 1. Introduction

1.1. Synaptic Transmission

Neurons communicate through synapses, where they are in proximity with other neurons or effector tissues. Synapses can be classed into two main categories: electrical and chemical. Electrical synapses allow direct communication between two cells. The pre-synaptic and post-synaptic cells are connected by the docking of two hemichannels, allowing the direct flow of ions and metabolites between the two (Martin et al., 2020). Electrical transmission is superior for fast communication, whereas the benefit of chemical transmission is greater flexibility of communication. In chemical synapses, neurotransmitters are synthesised and packaged into vesicles within the presynaptic neuron. When a depolarisation current arrives at the axon terminal, voltage-gated calcium channels open, allowing the synaptic vesicles to fuse with the cell membrane. Neurotransmitters are then released into the synaptic cleft towards the post-synaptic target (Purves, 2012). At the post-synaptic target, neurotransmitters can interact with specific receptors to enact a wide range of effects, including the opening of ion channels and G-protein coupled signalling cascades. Such effects can alter the conductance of either neuron, mediate a variety of acute second messenger-mediated responses, and alter gene expression (Hao & Tatonetti, 2016).

1.2. Purinergic Signalling

Purinergic signalling involves the release and subsequent binding of purine nucleotides, such as adenosine triphosphate (ATP) and adenosine, to specific cell surface receptors, known as purinergic receptors. This signalling system was first introduced by Geoffrey Burnstock in 1972 to describe vesicular ATP neurotransmission (Burnstock, 1972). He later proposed the co-transmission of ATP with other neurotransmitters in the sympathetic and

parasympathetic nervous systems (Burnstock, 1976), the first suggestion of a co-transmission mechanism from a single neuron. Before this point was the ‘one neuron, one neurotransmitter’ doctrine known as Dale’s Principle. Co-release describes the concurrent release of multiple neurotransmitters from the same vesicles at the synapse. In contrast, co-transmission is the release of multiple neurotransmitters from distinct vesicle populations, either within the same axon terminal or distinct axons. Co-transmission from separate vesicle pool populations indicates separate neurotransmitter storage and vesicle release mechanisms, which can be differentially regulated (Trudeau & El Mestikawy, 2018). Co-transmitters can act as pre- or post-synaptic modulators of neurotransmitter release and the resulting response.

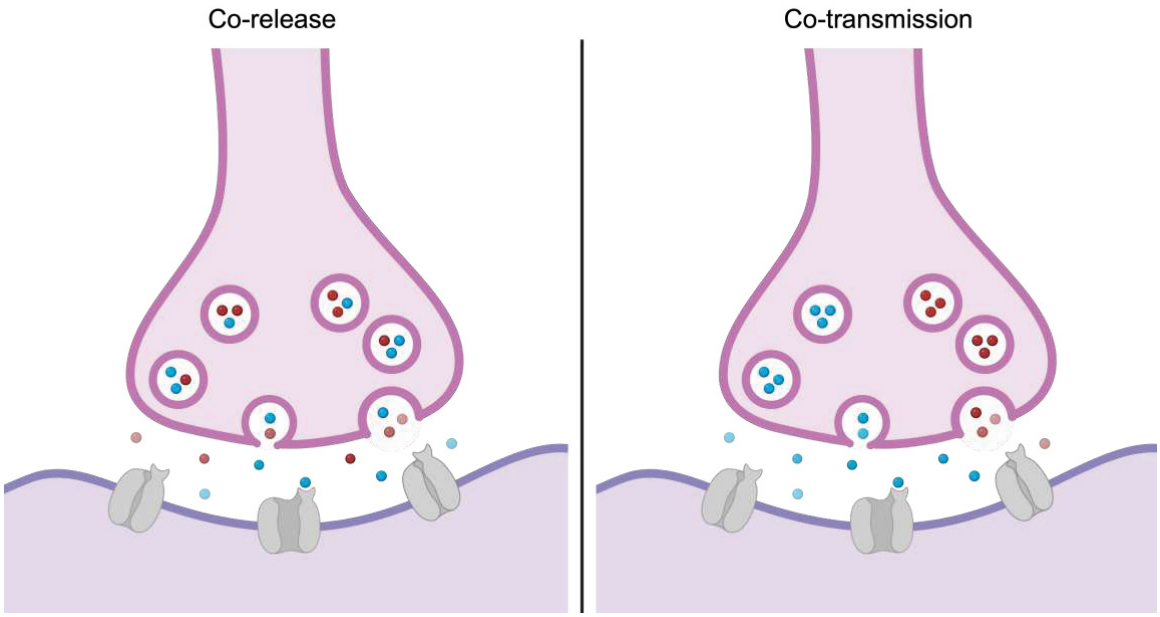

Figure 1.1: Co-release and co-transmission of neurotransmitters
This figure illustrates the difference between co-release and co-transmission of multiple neurotransmitters from the same neuron. Neurotransmitters that are co-released are packaged into, and released from, the same vesicles, whereas those that are co-transmitted are released from distinct vesicle pools. Created using Biorender.com.

In sympathetic nerves, ATP is co-transmitted with norepinephrine where it acts post-junctionally to evoke depolarisation, calcium influx and smooth muscle contraction (Kennedy, 2015). In the cardiovascular system, sympathetic neurons

innervate the heart, enhancing contractility and elevating heart rate. Additionally, these neurons act on the smooth muscle and endothelium of blood vessels, modulating vascular tone (McCorry, 2007). In the respiratory system, sympathetic fibres innervate the bronchioles, causing bronchodilation (McCorry, 2007). Elsewhere, sympathetic innervations controls blood flow to the gastrointestinal tract to inhibit secretion, contraction of the bladder to promote retention, and sweat glands to promote sweating (Herat et al., 2019; McCorry, 2007). Today, it is widely accepted that ATP acts as an independent neurotransmitter or co-transmitter in most nerves of the central and peripheral nervous systems (Burnstock, 2007). However, the mechanisms by which a neuron can independently store and release multiple neurotransmitters are poorly understood.

Purinergic receptors are divided into two families: the P1, adenosine receptors, and P2 receptors, which bind purines ATP and adenosine diphosphate (ADP), and pyrimidines uridine triphosphate (UTP) and uridine diphosphate (UDP) (Woo & Trinh, 2020). The P2 receptors are further divided into two subtypes: P2X and P2Y. A breakdown of the tissues that P2 receptors are expressed in can be found in Table 1.1: Purinergic receptor expression and transduction mechanisms. P2X receptors are trimeric ligand-gated ion channels, permeable to sodium, potassium and calcium ions upon ATP-binding (Burnstock, 2018). ATP binding to P2X receptors results in rapid depolarisation and increased cytosolic calcium (Kopp et al., 2019). Calcium ions entering the cell through P2X receptors can activate a variety of calcium-dependent intracellular signalling cascades, including those involving calmodulin, calcium/calmodulin protein kinases (CaMKs), phosphatases and phospholipases (Burnstock & Verkhratsky, 2010; Khakh & North, 2012). These pathways can modulate gene expression, synaptic strength, and neuronal excitability, resulting in acute and trophic effects.

P2Y receptors are G protein-coupled receptors (Dubyak, 2013). They can be functionally divided into two subfamilies: $P2Y_1$, $P2Y_2$, $P2Y_4$ and $P2Y_6$ receptors are G_q coupled, while $P2Y_{12}$, $P2Y_{13}$ and $P2Y_{14}$ receptors are G_i

coupled. Gq-coupled receptors activate phospholipase C, leading to the generation of second messengers inositol 1,4,5-trisphosphate (IP3) and diacylglycerol (DAG), releasing in intracellular calcium stores and activating protein kinase C (PKC), and a variety of downstream cellular responses (Van Kolen & Slegers, 2006). Gi-coupled receptors can inhibit adenylyl cyclase, reducing cyclic AMP (cAMP) levels and leading to an inhibition of protein kinase A, which is linked to a reduction in cellular activity and neurotransmitter release (Van Kolen & Slegers, 2006). Essentially, the two P2Y families often lead to opposing effects.

Table 1.1: Purinergic receptor expression and transduction mechanisms

Receptor		**Main Distribution**	**Transduction Mechanisms**
P2X	P2X1	Smooth muscle, platelets, cerebellum, dorsal horn spinal neurons	ATP-gated ion channel (Ca^{2+} and Na^{+})
	P2X2	Smooth muscle, central nervous system, retina, chromaffin cells, autonomic and sensory ganglia, pancreas	ATP-gated ion channel (mostly Ca^{2+})
	P2X3	Sensory neurons, nucleus tractus solitarius, some sympathetic neurons	ATP-gated channel (Ca^{2+}, K^{+}, Na^{+})
	P2X4	Central nervous system, testis, colon, endothelial cells, microglia	ATP-gated ion channel (mostly Ca^{2+})
	P2X5	Proliferating cells in the skin, gut, bladder, thymus, spinal cord, heart, adrenal medulla	ATP-gated ion channel (Ca^{2+} and Cl^{-}) (Mahmood et al., 2021; Schiller et al., 2022)
	P2X6	Central nervous system, spinal cord motor neurons	ATP-gated channel (Ca^{2+}, K^{+}, Na^{+})
	P2X7	**Neuro-2a cells** (Gutiérrez-Martín et al., 2011), immune cells, pancreas, skin, microglia	ATP-gated channel (Ca^{2+}, K^{+}, Na^{+}) with prolonged activation
P2Y	$P2Y_1$	Epithelium, endothelium platelets, immune cells, osteoclasts, the brain	G_q activation

$P2Y_2$	**Neuro-2a cells** (Miras-Portugal et al., 2015)**,** endothelium, epithelium, immune cells, kidney tubules, osteoblasts	G_q activation
$P2Y_4$	Endothelium, placenta, spleen, thymus	G_q activation
$P2Y_6$	Airway and intestinal epithelium, placenta, T-cells, thymus, microglia	G_q activation
$P2Y_{11}$	Spleen, intestine, granulocytes	G_q activation
$P2Y_{12}$	Platelets, glial cells	G_i activation
$P2Y_{13}$	Spleen, brain, lymph nodes, bone marrow, erythrocytes	G_i activation
$P2Y_{14}$	Placenta, adipose tissue, stomach, intestine, mast cells, oligodendrocytes	G_i activation

Information acquired from Burnstock (2018) unless otherwise stated.

ATP and other nucleotides are integral signalling molecules in diverse physiological and pathological processes. A wide variety of cell types can release ATP and nucleotides into the extracellular space under conditions of demand or stress, where they can act as both autocrine and paracrine signals, with a wide variety of effects depending on the environment.

1.2.1. Physiological and Pathological Roles of ATP

In the healthy nervous system, purinergic signalling modulates neurotransmission and neuromodulation, influencing processes such as synaptic plasticity (Lalo et al., 2016), pain sensation (Tsuda et al., 2003; Burnstock, 2007) and sleep-wake cycle regulation (Haydon, 2017; Hines & Haydon, 2014; Nadjar et al., 2013). Additionally, purinergic signalling is involved in neurodevelopment, regulating processes such as neural tube formation (Oliveira et al., 2016),

progenitor cell differentiation (Tang & Illes, 2017), and the development of the autonomic nervous system (Cheung & Burnstock, 2002).

Purinergic pathologies in the nervous system are associated with a wide gamut of neurological conditions. Disruptions to this signalling mechanism are known to contribute to neuroinflammation, excitotoxicity, and reduced regeneration of neurons. This contributes to pathologies in a range of neurodegenerative diseases, such as Alzheimer's disease (Erb et al., 2019), Parkinson's disease (Tóth et al., 2019) and multiple sclerosis (Nobili et al., 2022), as well as certain psychiatric disorders such as schizophrenia (Burnstock, 2017b) and depression (Zhao et al., 2022). Moreover, the underlying mechanisms of epilepsy have also been associated with purinergic signalling (Wong & Engel, 2023). This emphasises the pivotal role that purinergic signalling plays in the onset and progression of numerous neurological disorders, underscoring its potential value as a focus for therapeutic intervention.

In the cardiovascular system, purinergic signalling is key in maintaining cardiac health, particularly by regulating vascular tone, which influences blood pressure and flow. ATP release from perivascular sympathetic nerves leads to vasoconstriction (Burnstock, 2017a). Conversely, endothelial cells can release ATP in response to changes in blood flow or hypoxic conditions, causing vasodilation (Burnstock, 2017a). At low concentrations, ATP can enhance contractility, while high concentrations can lead to decreased contractility (Procopio et al., 2021). Additionally, heart rate is sensitive to ATP concentration. Small concentrations of ATP lead to tachycardia, whereas high concentration promotes bradycardia (Procopio et al., 2021). This dual mechanism ensures a balanced regulation of vascular responses for cardiac function. In addition, adenine can act directly upon purinoreceptors on myocytes, atrioventricular and sinoatrial nodes, and cardiac fibroblasts to modulate heart rate and cardiac contraction (Burnstock, 2017a).

Dysfunctional purinergic signalling has been linked to adverse immune responses, inflammation, and injuries in the cardiovascular system, contributing

to various circulatory conditions. Examples include atherosclerosis (Virgilio & Solini, 2002), ischemic heart disease (Burnstock & Pelleg, 2015), heart failure (Birkenfeld et al., 2019), hypertension (Brock & Van Helden, 1995), and thrombosis (Burnstock, 1990).

Additionally, purinergic signalling is the driving force behind the immune response. Necrotic cells release ATP, which serves as a warning signal that activates P2 receptors on immune cells, stimulating an immune response. The cells then produce ectoenzymes, which drive the breakdown of ATP to adenosine, thereby activating P1 receptors to dampen the immune response (Linden et al., 2019). High levels of inflammation are a hallmark of cancer (Hanahan & Weinberg, 2011). In addition, an abundance of ATP, adenosine and purinergic receptors are associated with a wide range of tumour types (Burnstock & Di Virgilio, 2013; Gilbert et al., 2019).

The appearance of purinergic signalling early in evolution, plus its wide distribution across cell types, proves its crucial role in healthy cellular communication and the damaging effects of its dysfunction (Verkhratsky & Burnstock, 2014). The potential as a target for therapeutic treatment is broad, but understanding each portion of the purinergic mechanism is crucial for mitigating wide-reaching side effects.

1.2.2. Mechanisms of Purinergic Signalling

Purines (ATP, ADP, and adenosine) and pyrimidines (UTP and UDP) are primarily released from the cell as ATP or UTP nucleotides. Within the scope of this thesis, the emphasis will be placed on purines in the context of purinergic signalling. ATP is released from cells using several distinct mechanisms – some more well-understood than others.

As mentioned above, the immune system utilises ATP and adenosine to mediate the inflammatory response. Lysing cells produce increased extracellular ATP, activating $P2X_7$ receptors on immune cells, which stimulates the release of caspase-1 and cytokines (Lopez-Castejon & Brough, 2011). This system

incorporates a feedback loop; immune cells express ectoenzymes CD39 and CD73 on their surface, which degrade ATP into adenosine monophosphate (AMP) and then adenosine. P1 receptors are then activated by the extracellular adenosine and suppress the release of caspase-1 and cytokines, thereby attenuating the inflammatory response (Huang et al., 2021).

In healthy cells, a significant mechanism of ATP release is mediated through transmembrane ion channels. ATP is known to permeate through five types of channels: connexins (Huckstepp et al., 2010; Nualart-Marti et al., 2013), pannexins (Bao et al., 2004; Narahari et al., 2021), a volume-regulated anion channel (VRAC) known as SWELL1 or LRRC8 (Gaitán-Peñas et al., 2016), calcium Homeostasis Modulator 1-3 (CalHM1-3) (Z. Ma et al., 2018; Taruno et al., 2013), and Maxi-anion chloride channels (Sabirov et al., 2001, 2017). Channel-mediated ATP release is triggered by various mechanisms, predominantly linked to cellular stress, although not exclusively. Connexins (Contreras et al., 2003), pannexins (Bruzzone et al., 2003) and CalHM channels (Z. Ma et al., 2012) open in response to voltage changes, particularly during strong depolarisation in excitable cells. Both pannexins (Locovei et al., 2007) and connexins (De Vuyst et al., 2006) can also respond to elevated intracellular calcium levels. In addition, pannexin1 can form a complex with $P2X_7Rs$ to enable the influx of ATP through the pannexin channel upon activation of the P2X receptor (Iglesias et al., 2008).

Osmotic or mechanical stress from cell swelling often triggers channel-mediated ATP release. Pannexins and SWELL1, a pannexin gene family member, are directly mechanosensitive and open to allow the efflux of ATP in response to shear stress (Bao et al., 2004; Jentsch et al., 2016). In contrast, most other ATP release channels are not inherently mechanosensitive and can instead be coupled to Piezo or transient receptor potential vanilloid (TRPV4) channels to allow the efflux of ATP in response to shear force (Coste et al., 2012; Turovsky et al., 2020). Beta connexins, a connexin subgroup, are also sensitive to CO2 levels (Huckstepp et al., 2010). An increased partial pressure of CO_2 can lead to the opposing effects of opening hemichannels or closing gap junctions

depending on minor differences in the connexin amino acid sequence (Nijjar et al., 2021). Finally, ATP release channels may be activated indirectly through G-protein coupled receptor-mediated phosphorylation (Pogoda et al., 2016), acetylation (Chiu et al., 2021) or nitrosylation (Retamal et al., 2006). These diverse mechanisms demonstrate the complexity and versatility of channel-mediated release mechanisms.

The final mechanism for ATP release, and the subject of this research, is vesicular exocytosis. ATP-filled vesicles can fuse with the plasma membrane, releasing ATP into the extracellular space. The vesicular nucleotide transporter (VNUT) was uncovered in 2008 by Sawada and colleagues as the key protein that transports ATP across the vesicle membrane in a membrane potential-dependent fashion (Sawada et al., 2008). Yet, the specifics regarding ATP-containing vesicles – their types, packaging location, and exocytotic processes – remain obscure. Our current understanding of these aspects will be explored in the upcoming sections.

1.3. VNUT

The vesicular nucleotide transporter (VNUT) is part of the Solute Carrier (SLC) family of membrane-spanning transporters responsible for carrying various substrates across membranes. VNUT is encoded by the SLC17A9 gene, making it a member of the SLC17 subgroup alongside the vesicular glutamate transporters (VGLUT1-3), Sialin and type I phosphate transporters (Reimer, 2013).

The human VNUT protein is found in two isoforms, ranging from 430 to 436 amino acids in length. VNUT2 differs from VNUT1 in that it has a shortened N-terminus, but little is known about the prevalence or functional qualities of VNUT2. VNUT1 assembles to form twelve putative transmembrane domains with cytosolic N- and C-termini.

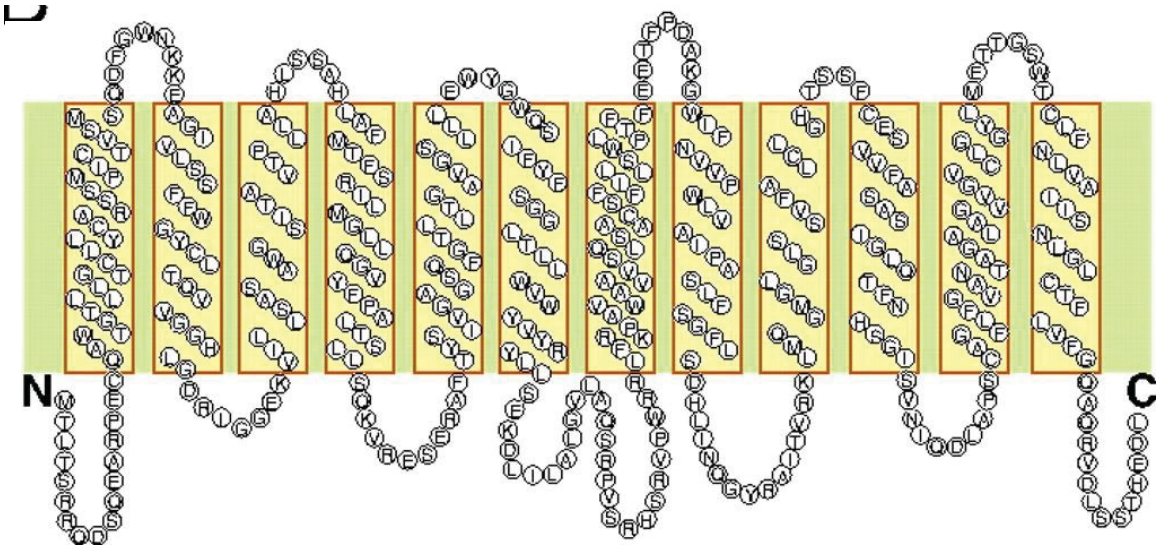

Figure 1.2: Sequence and Predicted Topology of VNUT
The figure obtained from (Sawada et al., 2008) shows the characterisation of human VNUT and predicted topology of twelve transmembrane domains. Reproduced with permission. Copyright (2008) National Academy of Sciences, U.S.A.

VNUT can transport various nucleotides across membranes. In order from most to least efficient, there are ATP > UTP > GTP > ITP > ADP >> AMP (Y. Moriyama et al., 2017a). In addition, VNUT is capable of transporting diadenosine polyphosphates. The substrate specificity of VNUT resembles the nucleotide composition of ATP storage vesicles (Sawada et al., 2008). VNUT is unique in its substrate specificity when compared to similar transporters. Where VNUT's substrates are varied, those of the vesicular transporters for glutamate (VGLUT), monoamines (VMAT) and acetylcholine (VAChT) are more selective.

VNUT mediates the vesicular storage of ATP. Vacuolar H+-ATPase (V-ATPase) pumps protons into the vesicle, creating an electrochemical gradient across the membrane comprised of an H+ ion gradient and the membrane potential. VNUT uses the voltage gradient to actively transport ATP into vesicles at the expense of further ATP hydrolysis (Y. Moriyama et al., 2017b).

There is one documented disease directly linked to a variant of the SLC17A9 gene: Porokeratosis 8, disseminated superficial actinic type (POROK8). A mutation of an N-terminal Arginine to a Cysteine at the ninth

residue (R9C) causes POROK8 (Cui et al., 2014). The disease is characterised by the development of multiple small keratotic lesions on areas of skin exposed to the sun. The disease is estimated to affect around 1 in 200,000 individuals (Pietkiewicz et al., 2023).

1.3.1. VNUT Expression

All animals possess the SLC17A9 gene, including vertebrates, insects, ascidians, hydras and nematodes (Jacobsson et al., 2010). Moreover, VNUT is expressed widely throughout the body, with notably high levels in the brain and adrenal gland. In the brain, VNUT is highly expressed in the cerebral cortex, hippocampal neurons, olfactory bulb and cerebellum (Larsson et al., 2012). VNUT is also found in dopaminergic neurons in the ventral tegmental area, substantia nigra (Ho et al., 2015) and dorsal root ganglion neurons (Nishida et al., 2014). Within the nerve terminals of enteric Musculo-motor neurons, VNUT co-localises with VAChT (Chaudhury et al., 2012). VNUT is also found extensively within sensory systems, including several retinal cells: photoreceptors, bipolar cells, amacrine cells, as well as in astrocytes (S. Moriyama & Hiasa, 2016; Pérez de Lara et al., 2015; Vessey & Fletcher, 2012). Type II taste cells in taste buds are known to express VNUT (Iwatsuki et al., 2009). Elsewhere, notable tissues with VNUT expression are alpha and beta cells in the pancreas (Geisler et al., 2013; Sakamoto et al., 2014), intestinal cells (Harada & Hiasa, 2014), Schwann cells (Shin et al., 2012), epithelial cells (Sathe et al., 2011), platelets (Hiasa et al., 2014), and osteoblasts (Inoue et al., 2020). The broad range of tissues expressing VNUT underpins the diversity and complexity of its physiological roles.

Perhaps surprising is the lack of lethality of VNUT knockout in mice. With a protein that is ingrained in cellular communication, one would expect to see the damaging effects of genetic suppression. In general, $VNUT^{-/-}$ mice are healthy, showing no difference in size, consumption, locomotor activity or performance in maze tasks compared to wild-type mice (Sakamoto et al., 2014). On a

microscopic level, the effects are evident, with the disappearance of vesicular ATP storage and depolarisation-evoked ATP release in hippocampal neurons and adrenal chromaffin cells. Additionally, in the pancreas, VNUT is not present in the glucagon granules of alpha cells or insulin granules of beta cells, and glucose-responsive ATP secretion is absent (Sakamoto et al., 2014). Furthermore, VNUT$^{-/-}$ mice show a disappearance of ATP secretion from dorsal horn neurons and bladder epithelium (Masuda et al., 2016; Nakagomi et al., 2016). It is theorised that other ATP-release mechanisms are upregulated in response to VNUT knockdown and are able to compensate for its loss (Y. Moriyama et al., 2017a). Taken together, this tells us that VNUT is essential for vesicular ATP release but not essential for maintaining life.

1.3.2. The Roles of VNUT and Vesicular ATP Release

The mechanism through which vesicular ATP is released in response to stimulation has remained elusive since its discovery. VNUT knockout studies serve as a useful tool to tease apart vesicular ATP exocytosis from other release mechanisms. In the cortex, hippocampal neurons in VNUT knockout mice show a notable decrease in the release of glutamate and aspartate in response to stimulation compared to those from wild-type mice (Sakamoto et al., 2014). This effect is attributed to the disruption of positive feedback mechanisms in purinergic transmission. Vesicular ATP release is well documented in astrocytes (Coco et al., 2003; Lalo et al., 2014; Pangršič et al., 2007) and is instrumental in neuronal-glial communication. ATP released from astrocytes has been shown to work in tandem with neuronally released ATP to recruit P2XRs at excitatory synapses (Lalo et al., 2016). ATP is co-released with glutamate, which then serves to downregulate postsynaptic NMDA (N-Methyl-D-Aspartate) receptors involved in long-term potentiation and neuronal plasticity. Similarly, microglia are known to secrete ATP through exocytosis to trigger neuroprotective action (Imura et al., 2013). ATP release can serve both autocrine and paracrine roles, prompting further ATP secretion and microglia motility. This may form a positive feedback loop, driving microglia to converge on injury sites (Dou et al., 2012). In

VNUT$^{-/-}$ mice, vesicular ATP release and ATP-driven secondary responses are absent (Shinozaki et al., 2014).

Adrenal chromaffin cells in VNUT$^{-/-}$ mice show notable reductions in both the storage and release of norepinephrine and epinephrine. This happens independently of any change to VMAT1 expression levels (Sakamoto et al., 2014) and is attributed to a disruption in the vesicular-ATP-dependent synthesis and secretion and secretion of catecholamines due to a loss of a positive feedback mechanism between vesicular ATP and catecholamine release (Sakamoto et al., 2014).

Vesicular ATP and VNUT extend their influence on the islets of Langerhans within the pancreas. Islet cells release ATP upon glucose stimulation, an effect absent in VNUT knockout mice. Additionally, glucose-responsive insulin secretion and glucose tolerance are enhanced, suggesting that vesicular ATP acts as a feedback moderator in insulin secretion to manage blood glucose homeostasis (Sakamoto et al., 2014).

Vesicular ATP, and thereby VNUT, is implicated in pain perception. In response to trauma, ATP is released from epithelial cells, which act on sensory nerves to stimulate the pain centre in the CNS. ATP is also released from primary afferent sensory nerves to the spinal cord to signal pain. In VNUT$^{-/-}$ mice, extracellular ATP accumulation was diminished, demonstrating that VNUT-mediated vesicular release of ATP from spinal dorsal horn neurons is vital for pain perception (Masuda et al., 2016).

Finally, the bladder uses VNUT-mediated ATP release for storage and control of urination. VNUT$^{-/-}$ mice exhibited impaired bladder storage and frequent urination, implicating the role of VNUT in promoting the relaxation of the bladder during the filling stage.

The role of VNUT-mediated ATP secretion is diverse and highly impactful. From modulating neuronal-neuronal and neuronal-glia interactions to mediating insulin responses and pain perception, VNUT's function is critical across different systems in the body. Using knockout mice, it is possible to isolate the impact of

vesicular ATP from the abundance of intracellular ATP sources. Our understanding of the mechanisms by which VNUT-mediated vesicular ATP is secreted is still limited, which is why ongoing research on this topic is vital.

1.3.3. VNUT Subcellular Localisation

Perhaps the most important component to unearthing the release mechanisms of VNUT-mediated vesicular ATP secretion is the subcellular localisation of VNUT. This hotly debated topic is a foundational question that researchers cannot agree upon; there is likely nuance and conceivably some variation in the different cell types. The methods used to determine colocalisation of VNUT to subcellular markers are difficult due to the low specificity of organelle markers, functional inhibitors and microscopy techniques. Understanding where VNUT localises and works to load vesicles with ATP is crucial for understanding the function of vesicular purinergic signalling in each tissue type, uncovering protein interactions and regulatory mechanisms which may influence diseases, and developing therapeutic targets for novel drugs. As outlined previously, vesicular ATP release is a powerful modulator in many cell types, but its potential as a drug target is largely untapped due to our restricted understanding of VNUT-mediated vesicular ATP release. This section will explore the current literature surrounding subcellular VNUT localisation, highlighting the conflicting evidence and offering the theoretical perspective of the Poburko Lab.

ATP is known to be co-released with dopamine, norepinephrine, acetylcholine, glutamate, γ-Aminobutyric Acid (GABA) and serotonin, though what remains unclear is how cells can differentially release both neurotransmitters -- are they released from the same vesicles, vesicle pools, terminals or secretion pathways? Moriyama & Hiasa (2016) explored the expression patterns of VNUT in the mouse retina and found colocalisation between VNUT and VGLUT1 and synaptophysin in photoreceptors. In amacrine and bipolar cells, they found evidence of VNUT colocalising with VGAT, the vesicular GABA transporter. These results were drawn from

immunohistochemistry on tissue samples (shown in Figure 1.3), where colocalisation is assessed by the correlation in expression patterns rather than with subcellular resolution, meaning the images lack the specificity to draw conclusions from the subcellular localisation of VNUT.

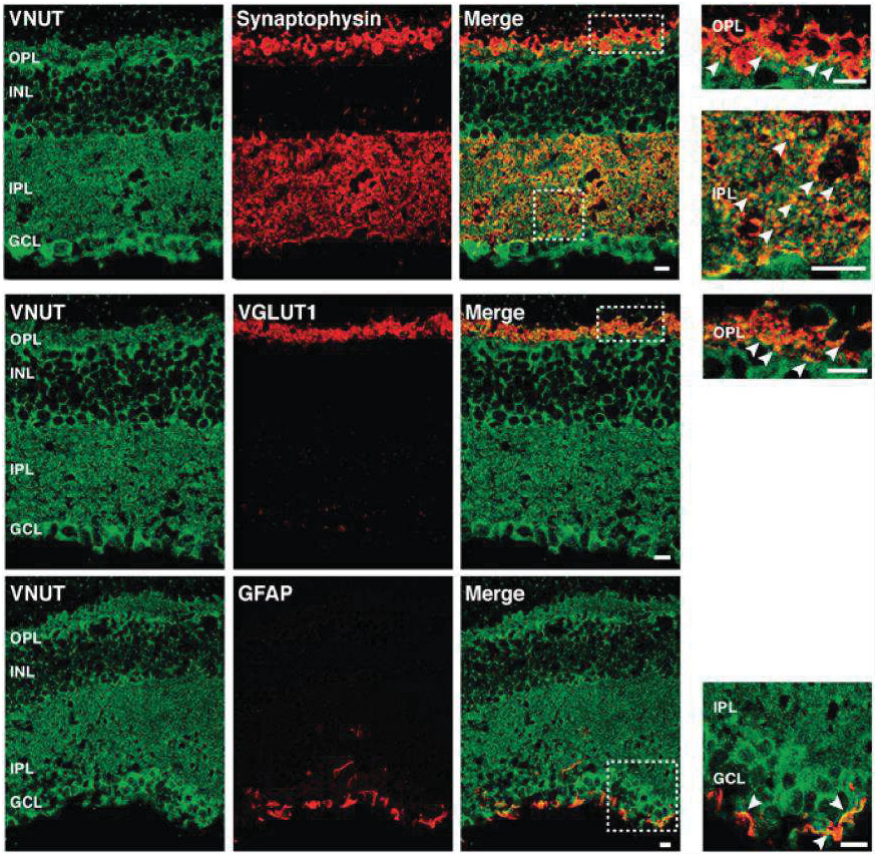

Figure 1.3: Moriyama et al 2016 VNUT co-localisation
This figure was taken from S. Moriyama & Hiasa (2016) and reproduced with permission. Sections of mouse retina immunostained against VNUT (green) and markers: synaptophysin, VGLUT1, and anti-glial fibrillary acidic protein (GFAP). Expression of VNUT overlaps that of synaptophysin, with some overlap of VGLUT1 and GFAP also present. Scale bars are 10 μm.

Several studies that conclude that VNUT is localised with lysosomes use quinacrine as a fluorescent ATP marker. For example, Zhong et al. (2016) demonstrated that lysosomes isolated from COS1 cells took up less ATP when cells were exposed to both VNUT inhibitors and VNUT shRNA. Similarly, Shin et al. (2012) drew conclusions on the lysosomal nature of ATP secretion based on a reduction in ATP-containing vesicles released following non-specific lysosomal

exocytosis inhibitors. Several high-impact papers have made similar conclusions on the lysosomal exocytosis of ATP following immunofluorescent colocalisation of ATP and lysosomal marker and reductions in fluorescent ATP-analogue release (Imura et al., 2013; Jung et al., 2013; Menéndez-Méndez et al., 2017; Nakagomi et al., 2016; Oya et al., 2013; Shin et al., 2012). However, the principal method to assess ATP transport used in these studies is quinacrine, which recently was exposed as a poor marker in a paper entitled 'Quinacrine is not a vital fluorescent probe for vesicular ATP storage' by Hasuzawa et al. (2021). Hasuzawa and colleagues criticise the use of quinacrine as a vesicular ATP marker, concluding that accumulation of quinacrine is independent of ATP and instead driven by a pH concentration gradient across any membrane. Thus, quinacrine is merely a pH probe, not a marker for ATP-containing compartments. This conclusion highlights the difficulties in surmising VNUT's subcellular localisation and highlights the need to develop more robust analysis methods.

Similar issues with specificity surround the commonly used fluorescent ATP analogue 2′/3′-O-(N′-methyl-anthraniloyl)-adenosine-5′-triphosphate (MANT-ATP). Research by Vessey & Fletcher (2012) used live imaging of ATP release kinetics to provide evidence that vesicular ATP release was calcium dependent. However, the researchers used a combination of quinacrine and MANT-ATP to label their ATP-containing vesicles. Similarly, Imura et al. (2013) use MANT-ATP and quinacrine to determine that ATP is exocytosed lysosomally in microglia. At present, the uptake mechanism for MANT-ATP into the cell has not been defined and has not been proven to be a specific marker for ATP-containing compartments. (Hasuzawa et al., 2021), in their critique of the field, emphasise that 'MANT-ATP cannot be considered a vesicular ATP probe'.

Another popular but controversial tool in assessing VNUT's subcellular localisation is 4,4′-diisothiocyanostilbene-2,2′-disulfonic acid (DIDS). Both Cao et al., (2014) and Zhong et al. (2016) used DIDS-mediated VNUT inhibition coupled with quinacrine labelling of ATP to implicate VNUT in lysosomal accumulation and exocytosis of ATP. The complexity here lies again in the specificity of the

compounds used. DIDS is a non-specific anion transporter inhibitor (Wulff, 2008), meaning inhibition is probably not limited to VNUT.

The landscape of VNUT-mediated ATP release is complex. While the field has made significant strides, it's crucial to acknowledge the nuanced perspectives and variations across cell types that add complexity to our understanding. Historical reliance on recently scrutinised methodologies reveals how the field is still evolving.

The Poburko Lab are developing novel methods to assess the subcellular localisation of VNUT. Previous research has characterised VNUT as localising to the same varicosities in rat tail arteries as norepinephrine (Mojard Kalkhoran et al., 2019). The authors used a combination of high-resolution immunocytochemistry and functional vesicle depletion experiments on a wire myograph to demonstrate that VNUT and norepinephrine inhabit separate vesicle pools and are released independently. Their research, using immunocytochemistry, provides evidence that VNUT is anti-colocalised with lysosomes and synaptic vesicle markers (Jensen, 2021). Moreover, forthcoming research using pH-dependent fluorescent probes in live-cell imaging shows that VNUT does not localise to acidic subcellular compartments, such as lysosomes or synaptic vesicles. In fact, VNUT has been found to localise to compartments with pH levels consistent with the endoplasmic reticulum (ER) and Golgi apparatus. These observations are reinforced by unpublished immunocytochemistry results (see Figure 1.4) and the discovery of an ER-retention sequence in the mammalian VNUT C-terminus (Jensen, 2021). Building upon these insights, this thesis aims to dissect VNUT's peptide sequence for molecular clues on VNUT's subcellular localisation, aiming to progress our understanding of the mechanisms governing vesicular ATP release.

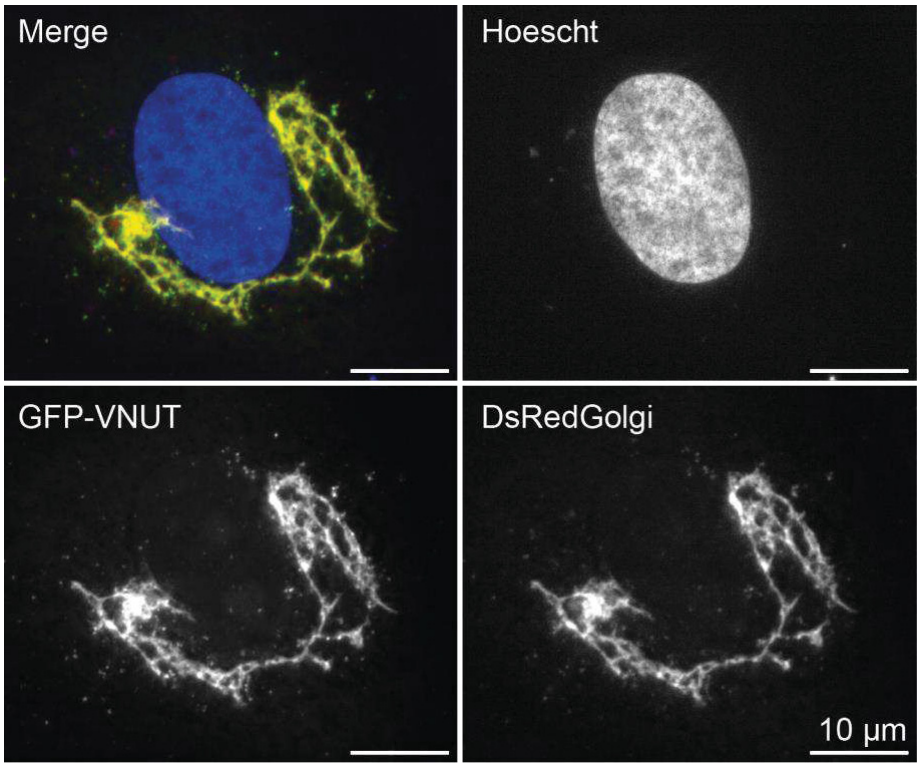

Figure 1.4: Colocalisation of VNUT and Golgi markers
This figure illustrates unpublished research from the Poburko Lab. Rat vascular smooth muscle cells (A7r5) express an EGFP-tagged VNUT, DsRed-tagged medial Golgi marker and Hoescsht33342, a nuclear stain. There is striking colocalisation between VNUT and the Golgi apparatus. Scale bars are 10 µm.

1.4. Vesicle Trafficking Dynamics

The secretory pathway transports newly synthesised proteins to their intended destination through a series of transport vesicles. An intricate network of selective adaptor proteins and vesicle coatomers ensures precise delivery of the cargo. Newly synthesised proteins are translocated into the ER, where they enter the secretory pathway. Cargo proteins converge at ER exit sites, where vesicles pinch off and migrate towards the Golgi apparatus. Anterograde transport vesicles are characterised by a coatomer protein II (COPII) vesicle coating, which can capture cargo directly or via interactions with adaptor proteins (Wilson & Hunt, 2015). Once they have departed from the ER, transport vesicles merge to form clusters, losing their COPII coating. Transport vesicle clusters

arrive at the *cis*-Golgi network, where the cargo enters the Golgi sorting system. From here, proteins may undergo post-translational modification before being directed through one of the secretory pathway avenues. Retrograde transport vesicles work in opposition to anterograde, budding from the Golgi to retrieve escaped ER-resident proteins back to the ER (Wilson & Hunt, 2015).

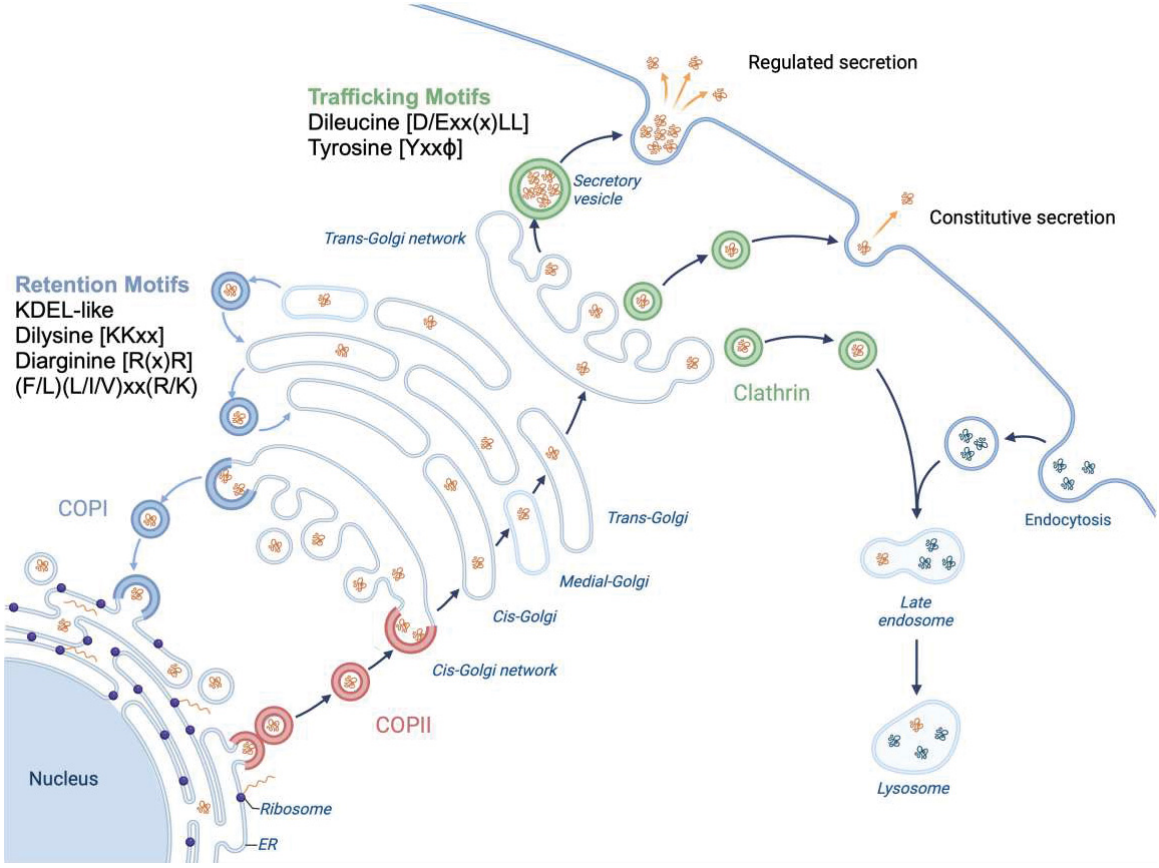

Figure 1.5: Vesicular trafficking dynamics in the secretory pathway
A cartoon illustration of the secretory pathway including transport vesicle coats and protein sorting motifs for ER-Golgi retention, endosomal and lysosomal sorting and vesicular secretion. Created with BioRender.com.

1.4.1. Retention Mechanisms

Retrograde transport is a dynamic process by which proteins are recaptured and shuttled back to the ER. Retrograde vesicles are characterised by their coatomer protein I (COPI) coating. The extent to which a protein can

escape the ER, arrive at the cis-Golgi, or be retrieved by retrograde transport vesicles is contingent upon the affinity of the cargo to bind with various chaperone and adaptor proteins, coating complexes and lipid environments of the subcellular compartments. One of the most well-characterised retrograde transport mechanisms is the KDEL receptor. Luminal chaperones and ER-resident membrane proteins possess a C-terminal K-D-E-L motif that ensures their retrieval (Munro & Pelham, 1987). The KDEL receptor is an integral membrane protein which resides in the cis-Golgi. The KDELR is thought to act in a pH-dependent manner – undergoing a conformational change in response to the differing environments of the cis-Golgi (pH 6.2) and the ER (7.2 to 7.4) to bind and deposit cargo (Bräuer et al., 2019; Wu et al., 2001). Another common ER-retention motif is the dilysine, characterised by two lysine residues (KKxx) (Teasdale & Jackson, 1996). α- and β-subunits of the COPI coating interact directly with proteins containing a dilysine motif; KKxx, KXKxx and non-canonical RKxx are all recognised retrieval motifs (W. Ma & Goldberg, 2013). A further common ER-retention motif is an arginine-based motif (RR, RxR or RxxR)(Boulaflous et al., 2009). Transmembrane proteins with dilysine motifs typically carry them in their C-terminus (Jackson et al., 2012), whereas the arginine motif location is more variable. Arginine motifs are not restricted to the C-terminus and are often N-terminally located (Abu Irqeba & Ogilvie, 2020; Sharma et al., 2010), displaying flexibility of location with the sequence while retaining its ability to bind COPI coating (Michelsen et al., 2005). While dilysine and KDEL motifs are synonymous with C-terminal localisation, the COPI-interacting arginine motif highlights the importance of the N-terminus as a crucial site for ER-retention mechanisms.

Retention of proteins in the Golgi apparatus relies on the collaboration of several dynamic processes to recapture resident proteins in the face of a constant flow. Perhaps the simplest means is transmembrane domain mediated retention; the lipid bilayer in the Golgi apparatus is thinner than that of Golgi-derived transport vesicles, meaning some Golgi resident proteins simply do not fit in secretory vesicles (Bretscher & Munro, 1993). Another proposed method of

Golgi retention relies on differing concentrations of lipids throughout the Golgi apparatus (Patterson et al., 2008). The researchers theorise that proteins have an affinity with preferred ratios of glycerophospholipids to sphingolipids, which change from cis- to trans-Golgi sections. The final mechanism to note is the interactions of amino acid motifs. The FLIXXR motif, characterised as [F/L][L/I/V]xx[R/K], is required for binding to Golgi phosphoprotein 3 (GOLPH3) (Scott et al., 2009). GOLPH3 then binds to COPI-coated vesicles for transport back to the ER. In this method, proteins which are needed in the Golgi are recycled back to the ER, where they begin the journey back to the Golgi, highlighting the dynamic nature of Golgi retention.

1.4.2. Secretory Pathways from the Golgi Apparatus

The *trans*-Golgi network (TGN) sorts all the proteins destined for post-Golgi locations. Materials are delivered from the Golgi to lysosomes through late endosomes. Most internal lysosomal enzymes are guided by mannose 6-phosphate (M6P) to endosomes and then lysosomes via clathrin-coated vesicles. Transmembrane proteins follow a different pathway. Adaptor proteins (APs) sit on the TGN membranes and recognise key sorting motifs. Five types of adaptor protein have been discovered, three of which are involved in TGN sorting, AP-1, AP-3, and AP-4. A tyrosine motif (Yxxϕ), where ϕ denotes a residue with a hydrophilic side chain, is an important sorting motif for proteins destined for lysosomes, the basolateral cell membrane of polarised epithelial cells and the somato-dendritic domain of neural cells (Farías et al., 2012; Owen et al., 2004).

The dileucine sorting motif, identified by the sequence [D/E]xx(x)L[L/I] comprises an aspartic acid (D) or glutamic acid (E) followed by two to three unspecified residues, ending in a leucine (L) and then either a leucine (L) or isoleucine (I). This motif plays a crucial role in the cytosolic domains of many transmembrane proteins associated with late endosomes and lysosomes (Bonifacino & Traub, 2003) as well as directing the VGLUT1 transporter to synaptic vesicles (Foss et al., 2013). All three of the TGN associated APs (AP-1,

AP-3 and AP-4) are able to recognise tyrosine and dileucine sorting motifs (Guo et al., 2014), though they demonstrate a varied affinity for different dileucine motif variations due to the array of unique combinations of AP subunit assemblies (Mattera et al., 2011). This specificity in AP composition and dileucine sequence interaction is thought to enhance the specificity of protein targeting, increasing the probability that proteins will be attracted towards their intended destination.

The Golgi can also direct proteins directly to the cell surface through the constitutive secretory pathway. Entry to this pathway is not contingent on any selection process. Vesicles are filled with cargo before budding from the trans-Golgi network and migrating directly to the membrane, where they fuse to deliver transmembrane proteins and secrete internal cargo. The exact mechanisms facilitating this process are poorly understood (Stalder & Gershlick, 2020).

In specialised secretory cells, including neurons, the Regulated Secretory Pathway (RSP) is used to traffic cargo destined for large dense core vesicles (LDCVs) and synaptic vesicles. This pathway is selective, using complex cargo recognition systems to ensure the accurate sorting of proteins to their appropriate locations at the nerve terminal. Transmembrane proteins are concentrated into secretory granules that mature into LDCVs or into transport vesicles that deposit the proteins at the synapse. Once there, vesicles will join reserve pools, ready for release, or fuse with the plasma membrane (Milosevic, 2018). Membrane-bound proteins can then be retrieved through endocytosis and recycled into new synaptic vesicles, filled with neurotransmitters and await a release signal (Wilson & Hunt, 2015).

1.4.3. Chimera Proteins Used for Researching Transporter Trafficking

Chimera proteins have been used to demonstrate that amino acid motifs are crucial for the accurate sorting of neurotransmitter transporters. The transporters VAChT and VMAT belong to the same transporter family, SLC18 and are responsible for the packaging of acetylcholine and monoamines into vesicles. VAChT localises to synaptic vesicles (SVs) (Weihe et al., 1996) and

VMAT2, the neurological isoform, to LDCVs (Nirenberg et al., 1995). A chimera protein was created with the body of VMAT2, the neural isoform of VMAT, and the C-terminus of VAChT (Varoqui and Erickson, (1998b, 1998a). They show that the VAChT C-terminus, which has a dileucine and tyrosine motif, was sufficient to redirect VMAT2 to SVs. In a reciprocal experiment, Yao & Hersh (2007) created a chimera between the body of VAChT and the tail of VMAT2 and found this wasn't sufficient to cause a change in VAChT sorting. They demonstrated that both the C-terminus and N-glycosylation loop between transmembrane domains one and two were necessary to redirect VAChT to LDCVs.

Similar approaches have been used to study the trafficking of VGLUTs. (Voglmaier et al., 2006a) sought to understand the differences between endocytic pathways of VGLUTs1-3. Voglmaier et al. (2006) highlighted a well-conserved dileucine motif between the isoforms in addition to two polyproline motifs in VGLUT1. They demonstrated the proline-rich region binds to endophilins to accelerate clathrin-mediated endocytosis. However, they noted the absence of proline-rich regions in the C-termini of VGLUT2-3, so examined the dileucine motif. First, using chimera proteins, they fused the C-terminus of VGLUT1 to interleukin-2 subunit Tac, a plasma membrane protein. Voglmaier et al. (2006) observed a resultant increase in reinternalisation with the VGLUT1 tail by using a pHluorin, a pH-sensitive GFP probe that is discussed further in section 1.6 Methods Featured in This Thesis. Subsequently, the authors replaced the dileucine motif with alanine residues and saw increased levels of surface VGLUT1. Together, these experiments highlight the importance of the C-terminal dileucine motif in VGLUT1-3, plus the role of the proline-rich regions of VGLUT1.

In a continuation of this research, (Foss et al., 2013) identified two more N-terminal dileucine motifs in VGLUT1 which are instrumental in its trafficking. They created several truncation variants in which they removed either the C- or N-terminus, and one with both termini removed. Truncation of either tail alone reduced but did not eliminate internalisation of VGLUT1. However, the combined truncation successfully eliminated synaptic vesicle localisation (Foss et al., 2013). In contrast, they confirmed that mutation of the C-terminal dileucine motif

in VGLUT2 was sufficient to mislocate the protein. This thesis takes inspiration from these experiments and aims to apply it to the trafficking dynamics of VNUT.

1.5. VNUT Phylogeny

Previous *in silico* research from the Poburko Lab identified a phylogenetic pattern of targeting motifs in the C-terminus of VNUT. Jensen (2021) found that most VNUT C-terminal sequences contain one or both of a dileucine and tyrosine motif -- the synaptic vesicle or lysosomal trafficking motifs. Notably, a tyrosine motif is well conserved in ray-finned fish. In amphibians, this is replaced by a dileucine motif. Tyrosine and dileucine motifs then converge in reptilian and avian sequences, where a dileucine motif directly precedes a tyrosine motif, with one residue overlapping between them. Interestingly Jensen (2021) reported that the dileucine and tyrosine motifs are absent in mammalian C-termini. The lysosomal or synaptic motifs are replaced by a KDEL-like motif, common in ER and Golgi resident proteins. The location of the KDEL-like motif is vexing, as they must typically be located on a lumen facing domain. The KDEL-like motif in VNUT is cytosolic. It is unclear whether the dileucine, tyrosine and KDEL-like motifs are sufficient to sort VNUT to lysosomes, synaptic vesicles or the ER. This thesis aims to explore the functionality of these motifs. In addition, to supplement the work from Jensen (2021) on the C-terminus of VNUT, this thesis will begin exploration of the N-terminal region of VNUT to uncover putative trafficking mechanisms.

1.6. Methods Featured in This Thesis

Neuro-2A, or N2a cells are derived from mouse neural crest neuroblastoma cells and can be differentiated into dopaminergic neurons (Tremblay et al., 2010). N2a cells have been used extensively in purinergic signalling research. N2a cells are able to release ATP through secretory vesicles and pannexin channels (Gutiérrez-Martín et al., 2011). They are also known to express $P2X_1$, $P2X_3$, $P2X_4$ and $P2X_7$ receptors (Gómez-Villafuertes et al., 2009).

N2a cells express relatively small amounts of endogenous VNUT, they are reliable models for over-expression and colocalisation experiments (Miras-Portugal et al., 2019). Retinoic acid-induced differentiation of N2a cells maintains VNUT expression in N2a cells (Menéndez-Méndez et al., 2015). Overexpression of VNUT decreases extracellular ATP, suppressing neuritogenesis in retinoic-acid differentiated N2a cells, which highlights VNUT's role in neuronal differentiation processes (Menéndez-Méndez et al., 2015). Neurite outgrowth is a defining characteristic of differentiation. Though overexpression of VNUT may frustrate efforts to differentiate cells, the N2a cell line is still a widely used and robust model for studying vesicular ATP release.

1.6.1. Image Acquisition Techniques

In this study, the image acquisition practises were designed to maximise the benefits of working with chimera proteins. The use of transfected chimeras allows the constructs to be designed with an enhanced green fluorescent protein (EGFP) or pHluorin probe, thereby ensuring that all copies are accurately fluorescently tagged. The combined use of fixed and live imaging techniques reaps the benefits of both spatial and temporal resolution. Fixed cell microscopy can be performed at higher levels of spatial resolution, allowing for the dissection of subcellular vesicle-like puncta. In addition, EGFP probes provide high signal intensity upon excitation, which reduces the risk of photobleaching (Comeau et al., 2006).

PHluorin-based live imaging probes are widely used to research the trafficking dynamics of synaptic vesicles and cargoes. A pHluorin is a pH-dependent green fluorescent protein (Kavalali & Jorgensen, 2014). PHluorins fluoresce when exposed to basic environments (see Figure 1.6) and are quenched in acidic environments (Miesenböck et al., 1998). Using the intensity of the signal, it is possible to correlate the pH value of pHluorin containing environments, which can be cross-referenced with known pH values of subcellular compartments. Live imaging using a pHluorin has the benefit of high

temporal resolution, displaying potential vesicle release kinetics. Furthermore, live imaging microscopy is undertaken in conditions closely mimicking physiological, providing a robust method to verify fixed imaging results. Previous work in the Poburko lab has created VNUT constructs with a lumen facing pHluorin probe (Kim, 2019). Given the short length of VNUT's luminal domains, the most effective construct uses the S1-2 loop of VGLUT to attach the probe. Extensive testing reveals a distribution typical of VNUT.

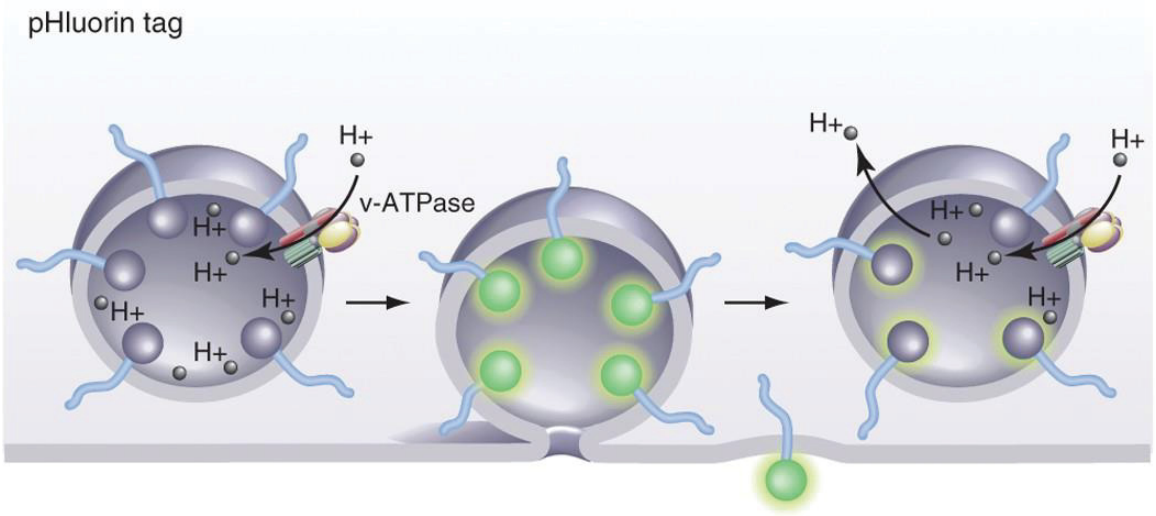

Figure 1.6: PHluorins quenching and dequenching
This figure depicts pHluorins tagged to lumenal domains of synaptic proteins. In the acidic (~ pH 5.5 environment of the vesicle, the pHluorins are quenched. Once the vesicle docks on the membrane, the probes are exposed to higher extracellular pH and dequench. Probes can remain at the membrane until recycled into new vesicles. Reprinted from Kavalali & Jorgensen (2014) with permission.

1.6.2. Image Analysis Methods

Devising methods to quantify and comparatively measure colocalisation is an intricate process that requires transforming subjective visual information into objective numerical data. Many standards have been set to ensure the validity of results. One established method is to use correlation, whereby the spread of pixel intensities in one channel is correlated against the spread in another channel of the same image. A Pearson's Correlation coefficient is generated,

with values ranging from -1 to 0 to 1, where -1 denotes perfect anti-correlation, 0 denotes no correlation, and 1 is perfect correlation. This method presents a few challenges, namely that the analysis of small points over a large area can provide very variable correlational values (Lagache et al., 2015). Our current research uses several approaches to navigate these challenges, combining correlational measures with an object-based approach to analyse fixed-cell images. Objects, puncta in this case, are defined and measured from their fitted centres of fluorescence intensity to the nearest point of the cell perimeter, therein providing a measure for their distal location. Moreover, a ratiometric approach of comparing the intensity of VNUT within the Golgi and ER subcellular compartments is also used to provide a robust and comprehensive measure of VNUT localisation.

This thesis research aims to enhance our understanding of VNUT's role in purinergic signalling. The ramifications of pathological vesicular ATP secretion are diverse and complex, ranging from neuronal communication to cardiovascular function. At the heart of this research is the subcellular localisation of VNUT. As a transporter protein which packages ATP into cells for exocytosis, it is our most promising avenue for unpacking ATP release. This research looks for molecular clues in VNUT's amino acid sequence.

1.6.3. Research Hypotheses

Colocalisation of a definitive positive marker for VNUT within varicosities and synaptic regions remains elusive. Sequestration of VNUT in the medial Golgi and in a reticular formation through the cell soma is evident. This distribution implies the existence of specific retention or retrieval mechanisms encoded within VNUT's amino acid sequence, which would facilitate its residence within the ER and/or Golgi apparatus. Such retention mechanisms often occur in the cytosolic termini of transporters (Mikros & Diallinas, 2019). Therefore, the overarching hypothesis of this research is that the mammalian VNUT contains a terminally located ER-Golgi complex retention sequence. The presence of a

genetic adaptation to retain VNUT in the ER-Golgi complex would suggest that VNUT is not merely transient in these compartments, but rather that it has a functional role in the ER and/or Golgi apparatus. Identifying this role could reveal a non-canonical mechanism of vesicle loading in the ER-Golgi complex.

Hypothesis 1 states that replacing the mammalian VNUT C-terminus with non-mammalian counterparts will reduce VNUT and ER-Golgi complex co-localisation. A three-step list of aims was devised to address Hypothesis 1. Aim 1.1: To identify non-mammalian animals with VNUT C-termini representing their phylogenetic class, containing dileucine and / or tyrosine motifs. Aim 1.2: To create chimeric proteins using a mammalian EGFP-VNUT construct combined with non-mammalian C-termini and assess VNUT localisation. Aim 1.3: To create VNUT-pHluorin chimera constructs, replacing the mammalian C-termini with representative non-mammalian counterparts and determining VNUT-containing subcellular compartments.

Hypothesis 2 states that disruption of a putative VNUT N-terminal ER-retention sequence will decrease VNUT's localisation to the ER. This will be achieved through the following aims: Aim 2.1: To use bioinformatics to ascertain likely ER-retention sequences in the mammalian VNUT N-terminus. Aim 2.2: To truncate the VNUT N-terminus on either side of the putative ER-retention sequence and measure changes to VNUT localisation.

Research methodologies to address each hypothesis are inherently similar, with a few key differences. Where the methodologies overlap, the section 'Chapter 2: General Methods' will outline the cell culture and microscopy techniques shared between the two approaches. Each hypothesis will then be addressed individually, including methods unique to each hypothesis and the associated data collected for each. Chapter 3: C-terminus describes the bioinformatics and live-imaging techniques unique to Hypothesis 1, along with all the results for this hypothesis. Bioinformatics and image analysis techniques unique to Hypothesis 2 are outlined in Chapter 4: Identification of a Putative N-terminal ER-retention Sequence in the VNUT N-terminus, alongside the data

from this hypothesis. Chapter 5: Discussion and Future Directions contains a discussion of the combined results of this research in the context of the established literature. This approach ensures a diligent exploration of the N- and. C-termini individually, and in the context of one another to provide a comprehensive analysis of the sorting motifs in the N- and C-termini of mammalian VNUT.

Chapter 2. General Methods

2.1. Molecular Biology

Molecular biology techniques differed between N- and C-terminus experiments and will be described separately. For a detailed breakdown of mammalian C-terminus substitution cloning, refer to 3.2.2 Molecular Biology. The construction of N-terminus truncations is detailed in 4.2.2 Molecular Biology.

2.2. Cell Culture

2.2.1. Maintenance and Differentiation

Mouse neuro-2A (N2a) neuroblastoma cells (American Type Culture Collection CCL-131) are widely utilised in research for exploring neuronal differentiation, axonal growth, and signalling pathways (Gutiérrez-Martín et al., 2011; Martín et al., 2022, 2024; Mathew & Keerikkattil, 2022; Menéndez-Méndez et al., 2015; Tremblay et al., 2010). They are a cancerous cell line derived from the neural crest, which can differentiate into dopaminergic-like neurons (Mathew & Keerikkattil, 2022; Tremblay et al., 2010).

N2a cells were cultured in growth medium (GM) made from Dulbecco's Modified Eagle Medium (DMEM) with 4.5 g/L D-glucose, L-glutamine and 110 mg/L sodium pyruvate (ThermoFisher Scientific, # 10569), supplemented with 10% fetal bovine serum (FBS Seradigm, LIFE SCIENCE, # 97068-085) in an incubator kept at 37 °C with 5% CO_2. To induce differentiation, growth media was substituted for differentiation media (DM), which was comprised of the same DMEM, but with 0.1% FBS and 5 µM retinoic acid (Millipore-Sigma, # R2625). Cells were incubated in DM for 3 days.

Cells were seeded in 24-well plates (Corning, # 3524) containing 12 mm coated glass coverslips. Coverslips were treated for one hour each with 1M hydrochloric acid, then with 50µg/ml poly-l-lysine hydrobromide (Sigma-Aldrich, # P2636-25MG) and stored aseptically at 4 ˚C until used for cell culture. Prior to

seeding, 10 µg/ml laminin (VWR, # CACB354232) was added to each coverslip at 20 ˚C for 20 minutes. Excess laminin was then aspirated, and a cell suspension in GM was added to each well at a density of 30,000 to 50,000 cells per ml.

2.2.2. Transfection

Following 24 hours of growth, cells were transfected with fluorescently labelled expression constructs using Lipofectamine™ 3000 Transfection Reagent (Invitrogen, # L3000008). 0.5 µg of each DNA from each plasmid was added to each well with a 1:2 DNA to transfection reagent ratio. The cells were incubated at 37 ˚C for 24 hours before the growth media, and transfection reagents were replaced with differentiation media. Cells were co-transfected with an ER marker in blue, a VNUT marker in green and a Golgi apparatus, lysosome or synaptic vesicle marker in red. mTagBFP2-ER-5 is a blue fluorescent protein conjugated to calreticulin, an ER resident protein. mDsRed-Golgi-7 is a red fluorescently labelled beta-1,4-galactosyltransferase 1 gene, a membrane-bound protein located in the medial-Golgi apparatus, LAMP1-RFP is a plasmid that encodes a red-labelled Lysosome Associated Membrane Protein 1, and VMAT-pHuji is a pH-dependent red fluorescent Vesicular Monoamine Transporter 2 plasmid, the neuronal isoform of VMAT which localises to dense core vesicles.

Table 2.1: Transfection constructs used

Construct name	Probe	Source	Catalogue #
EGFP-VNUT	EGFP (green)	Poburko Labs	N/A
VNVGS1-2pH	pHluorin (green)	Porburko Lab	N/A
mTagBFP2-ER-5	BFP (blue)	Addgene	55294

mDsRed-Golgi-7	mDsRed (red)	Addgene	55832
LAMP1-RFP	RFP (red)	Addgene	1817
VMAT-pHuji	pHuji (red)	Poburko Lab	N/A

2.3. Fixed Cell Imaging

2.3.1. Sample Preparation

All steps were carried out at 20 ˚C, incubated in the dark, and are based on Dulbecco's phosphate-buffered saline (dPBS) unless otherwise stated. The cells were fixed using 4% paraformaldehyde (Electron Microscopy Sciences, # 15710) for 15 minutes, then washed with dPBS three times for 5 minutes each before permeabilization using 0.1% Triton X-100 (Millipore-Sigma, # T8787) for 15 minutes. Another three 5-minute dPBS washes were followed by a 15-minute wash with 1 µg/ml Hoescht-33342 (Invitrogen Molecular Probes, #H3570) before a final dPBS wash. Coverslips were mounted onto glass slides using ProLong Glass Antifade Mountant (ThermoFisher Scientific, # P36984) and cured for a minimum of 48 hours before imaging.

2.3.2. Image Acquisition

Epifluorescence imaging was performed with a Nikon Ti-E inverted microscope equipped with a Zyla 5.5 CMOS camera (Andor) and CFI Plan Apo Lambda 100X 1.45 NA objective lens with an additional 1.5X magnification for C-terminal experiments. The fluorophores were excited using a Sutter Lambda XL light source. SmartShutter excitation and emission filter wheels were operated using a Sutter Lambda 10-3 controller, interfaced with Nikon NIS Elements software version 4.51.01. Blue, green and orange/red fluorophores were imaged with a Sedat filter set (i.e. single band excitation and emission filters) and a quad-

band dichroic mirror to. Minimise spectral bleed through. Images were acquired at either 200 or 300 nm z-steps.

2.4. Live Cell Imaging

Live cell imaging was performed on C-terminus variants only, and therefore, the sample preparation and microscopy methodologies are outlined in section 3.2.3: Live Imaging.

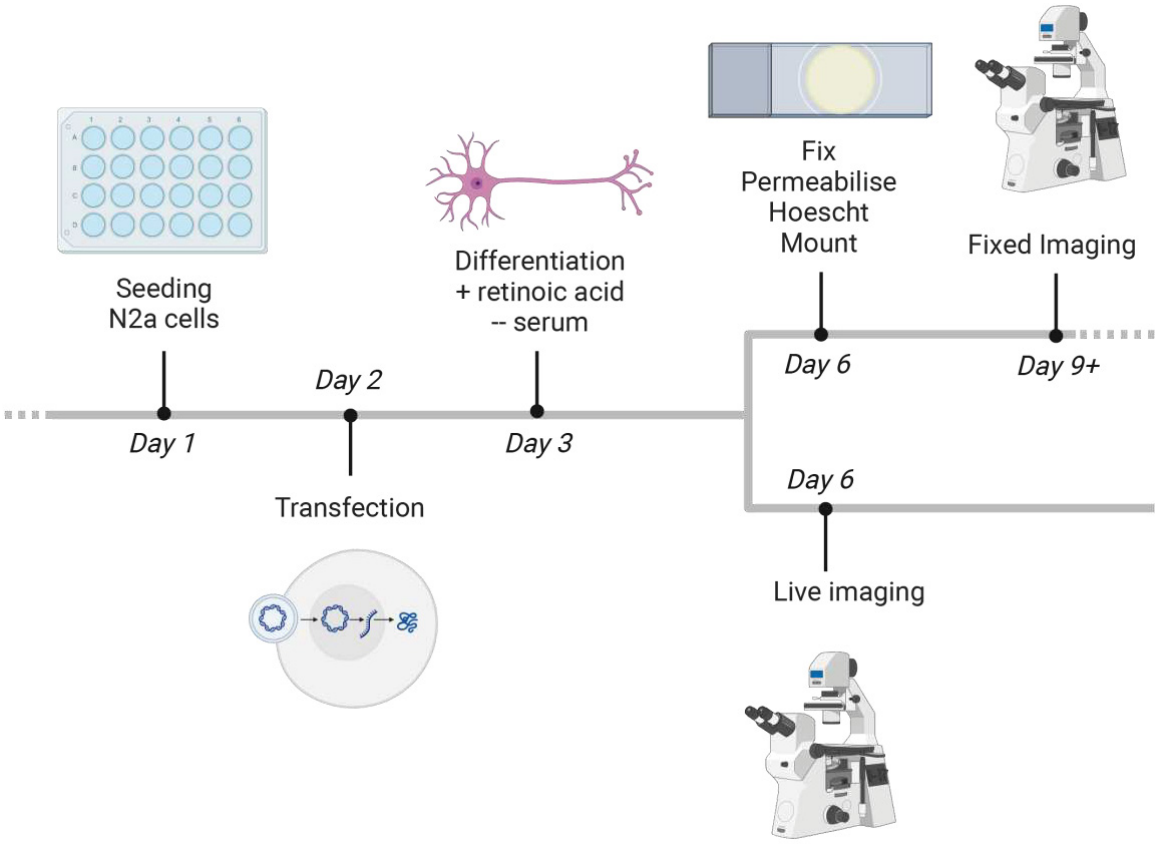

Figure 2.1: Cell seeding to microscopy workflow
Preparation of cells for imaging. Cells were seeded on poly-l-lysine and laminin treated glass coverslips in a 24 well plate with growth media. On the second day, transfection using Lipofectamine 3000 was performed. After 24 hours the media was replaced with fresh differentiation media. On the sixth day, cells were either fixed and prepared for fixed microscopy or taken directly for live imaging. Created with BioRender.com.

2.5. Image Analysis

2.5.1. ImageJ and FIJI

Fixed cell image processing was conducted using the FIJI overlay of Image J (Schindelin et al., 2012). Initially, images were cropped to isolate individual cells and their neurites, separating each cell into a distinct image whenever feasible.

2.5.2. Deconvolution

To exceed the diffraction limit, deconvolution was applied, involving points spread function (PSF) estimation for each colour channel using FIJI's PSF Generation software Field (Kirshner et al., 2013), based on the Born & Wolf model. The parameters used to create the PSF files are described in Table 2.2 and an example of the output is shown in Figure 2.2. The processing of deconvolution was automated with a custom script that processed single-cell images by separating colour channels, applying deconvolution with wavelength-specific PSFs, and reassembling the channels into multicolour image stacks.

Image deconvolution was performed using the DeconvolutionLab2 plugin in FIJI (Sage et al., 2017). This process utilised the Richardson-Lucy algorithm, which incorporates a PSF model of diffraction and employs iterative refinement to enhance image clarity. To determine the optimal number of iterations for this algorithm, a cost-benefit analysis was conducted between time, computing power and image output, leading to the selection of 50 iterations as the ideal parameter.

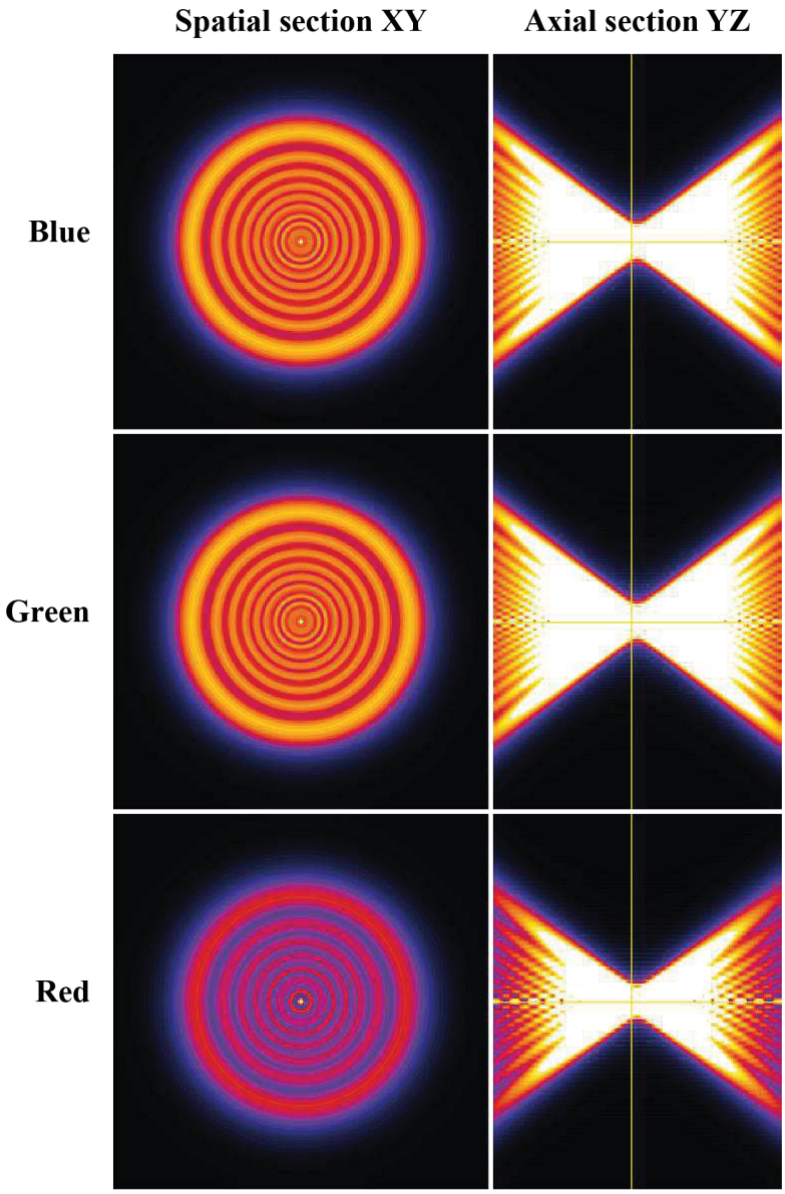

Figure 2.2: Born & Wolf PSF model of diffraction.
Point spread function (PSF) models of light diffraction were created using the PSF Generator for 456 nm (blue), 509 nm (green) and 585 nm (red) emission wavelengths. The leftmost images show the XY spatial section of the light spread, and axial YZ sections are shown on the left, with a vertical yellow line depicting the centre line from which the light spreads.

Table 2.2: Point Spread Function parameters

Setting	Value
Refractive index immersion (ni)	1.5

Accuracy computation	Better
Wavelength (nm)	456 / 509 / 585
Numerical aperture	1.45
Pixel size XY	43 / 66
Z-step (nm)	200 / 300

2.5.3. Maximal Intensity Projections

Using the deconvolved z-stacks, maximal intensity projections were generated for each cell, with slices selected from the first appearance of puncta at the cell's apical end to their last appearance at the basal end. At this stage, regions of interest (ROIs) were drawn around the cell soma by hand, as shown in panel E **of Figure** 2.3

2.5.4. RIPA

Fluorescent puncta quantification was performed using a custom-written FIJI macro, the Recursive ImageJ Particle Analyzer (RIPA) (Mojard Kalkhoran et al., 2019). After initial pre-processing with 10-pixel rolling ball background subtraction, RIPA identifies regions of interest (ROIs) around fluorescent puncta. It does so by progressively lowering intensity thresholds from the maximal pixel intensity. By incorporating parameters like size, circularity, and cell border ROIs, RIPA effectively delineates puncta ROIs within the cell soma. An example of a cell with RIPA-generated puncta is shown in panel E of **Figure** 2.3**.** The parameters fed into the plugin are listed in Table A.1 of the Appendix.

2.5.5. MINER

Hand-drawn soma ROIs and RIPA-generated puncta ROIs were then spatially analysed using a Multi-Image Neighbourhood Exploring (MINER) FIJI macro, another tool developed by the Poburko Lab (Mojard Kalkhoran et al., 2019). Centroids and perimeters are calculated for each cell soma ROI, then MINER measures the distance from the centre of puncta ROIs to the cell perimeter as seen **in Figure** 2.3 panel F. Output from this macro also includes descriptors of shape, intensity, and full width at half-maximal intensity (FWHM) to help characterise the puncta.

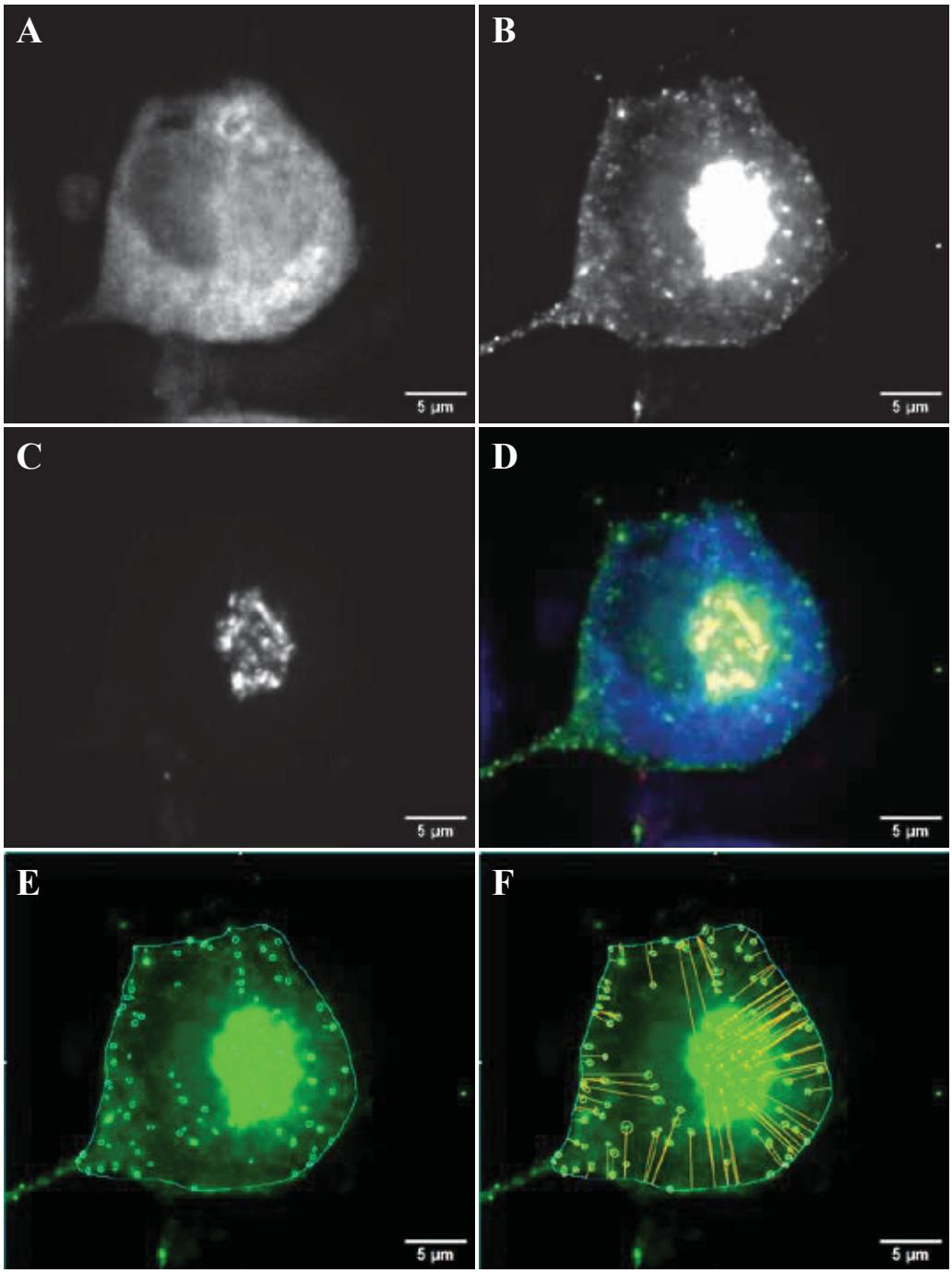

Figure 2.3: RIPA and MINER analysis Within the cell soma
An N2a cell transfected with ER-BFP-5 (A), EGFP-VNUT (B), and DsRedGolgi-7 (C) markers, with a composite overlay in panel D. Panel E displays the cell soma with a hand-drawn outline and puncta identified by RIPA in light blue. Panel F demonstrates the MINER analysis, indicating the closest distance of each punctum to the cell border.

2.5.6. JACOP

The FIJI plugin ‘Just Another Co-localisation Plugin’ (Bolte & Cordelières, 2006) enabled the quantification of pixel-wise intensity correlation between fluorescently labelled subcellular markers. This plugin takes two images and uses linear regression to describe the relationship between the patterns of fluorescent intensities. The output uses Pearson’s coefficient to measure the goodness of fit of this model, ranging from -1 to 1, where 0 equals no correlation, 1 equals perfect positive correlation, and -1 is negative correlation. I custom-built a macro to take a folder of three-channel images, match the images with hand-drawn cell-body ROIs, split the channels into three separate images and run the JaCoP plugin to analyse the correlation of intensities across each cell in all three channels and produce the results in a data table. The same cell body ROIs were used for this analysis as the puncta-based analyses.

2.6. Data Analyses

Data were collected from each cell and compiled into a table using JMP statistical software (JMP®, Version 17. SAS Institute Inc., Cary, NC, 1989–2023).

2.6.1. Correlational analyses

Pearson’s correlation coefficient values between each fluorescence wavelength were prepared in a data table for each cell as output by the JACOP FIJI plugin. Figures range from -1, indicating anti-correlation, through 0, indicating no correlation, to 1, which indicates perfect correlation. Values were compared for each experimental condition.

2.6.2. Puncta analyses

Two primary methods for data extraction were used with puncta: the ‘Onion Peel’, and the ‘Perimeter Puncta’ analyses. Both analyses use the output from the RIPA and MINER FIJI tools. The distance in pixels from the centre of

each punctum to the nearest point of the perimeter was recorded through MINER. These distances were converted into nanometers using the known resolution of the microscope objective.

For the Onion Peel analysis, puncta were then categorised by their distance from the cell perimeter in segments of 250 nm, ranging from 0-250nm to 2251-2500 nm. For each cell, the number of puncta within each segment was recorded. An example of such zones can be seen in panel A of **Figure** 2.4. The number of puncta within each zone could then be mapped onto a line graph to show the dispersion of puncta within the outer region of the cell against the VNUT variants.

The Perimeter Puncta analysis used the outermost two layers of the Onion Peel, highlighting puncta within 0-500 nm of the cell perimeter, as shown in **Figure** 2.4 panel B. This measurement was narrow enough to classify only puncta that arrive close to the cell surface but large enough to stay above the diffraction limit of light.

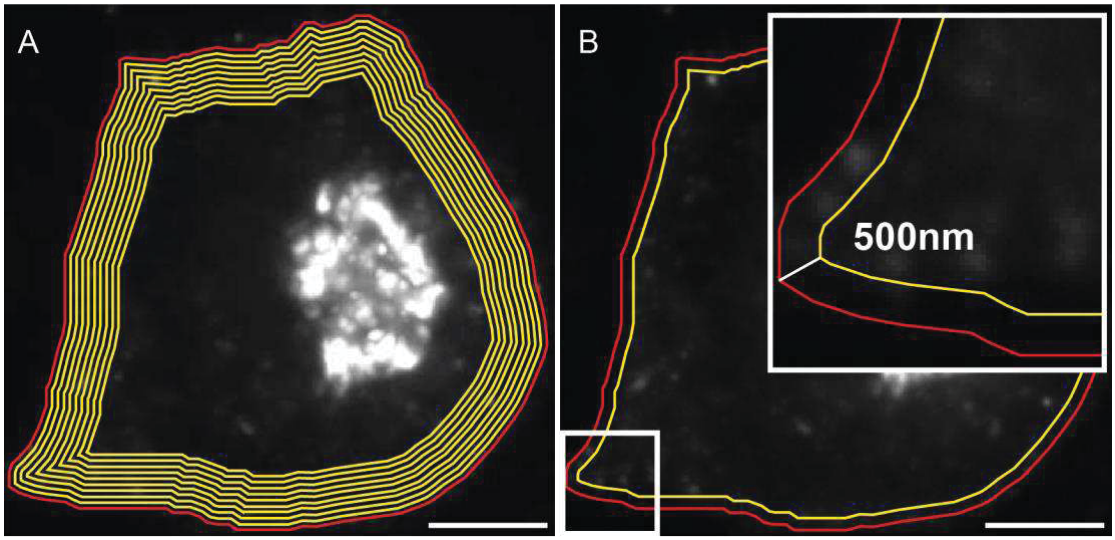

Figure 2.4: Diagrammatic representation of puncta analyses
This figure demonstrates the onion-peel and perimeter puncta analyses used on N2a cells. The red line indicates the perimeter of the cell body. Panel A shows segmented steps concentrically sectioned inwards at 250 nm steps, illustrated by yellow lines to show the zones up to 2251-2500 nm from the cell perimeter. Panel B illustrates the zone referred to as the perimeter, with the inner boundary drawn in yellow, 500 nm inwards from the red perimeter line. The scale bars are 5 μm.

2.6.3. Statistical Analyses

The data were tested with the Shapiro-Wilks goodness-of-fit test to examine whether the sample data fit a normal distribution. A non-parametric Kruskal-Wallis rank-sum test was used to test the significance between categorical data groups with a continuous outcome variable. Pairwise comparisons were made using the Wilcoxon signed-rank test. A p-value below 0.05 was accepted as statistically significant.

Chapter 3. Deciphering the C-terminal Sorting Motifs in Mammalian VNUT

3.1. Rationale

The critical role of the C-terminus in the trafficking of vesicular transporters is well-established, as evidenced by the conserved dileucine motifs in VGLUT and VMAT that are essential for vesicle targeting (Tan et al., 1998; Voglmaier et al., 2006b). Similarly, the reinternalization and localisation of VAChT to micro-vesicles is directed by a C-terminal dileucine motif (Santos et al., 2001), and a C-terminal tyrosine motif directs LAMP1 and LAP to lysosomal membranes (Obermüller et al., 2002). One or both of these motifs are present in the VNUT C-terminus sequence of most animals. Mammals, however, are conspicuous in their lack of dileucine or tyrosine clusters, where a KDEL-like sequence emerges *in situ*. Previous unpublished research from the Poburko laboratory shows strong co-localisation between VNUT and the ER and VNUT with the Golgi. Building upon this evidence, my research aims to explore the impact of the C-terminus in VNUT's subcellular localisation. Leveraging the established experimental framework of chimeric protein studies, which have previously demonstrated the influence of the C-terminus on transporter trafficking, this research will apply epifluorescence microscopy to ascertain if a non-mammalian C-terminus is sufficient to disrupt the localisation pattern of mammalian VNUT. Moreover, this study will dissect the effect of single-residue mutations within the motifs to dissect the mechanisms underlying VNUT's unique ER-Golgi complex sequestration.

3.2. Methods

3.2.1. Bioinformatics

Motif search

A dataset comprising 1,400 VNUT peptide sequences from the kingdom Animalia was obtained from the NCBI protein database (Sayers et al., 2022). For the analysis of common signalling motifs in C-terminal amino acids, a custom R script implementing a regular expression (regex) search algorithm was used. This script can be accessed on GitHub: https://github.com/dpoburko/bioInformaticsTools/blob/master/motifSearch.R. The analysis focused on three primary motifs: KDEL-like, tyrosine (including tyrosine-like), and dileucine motifs. The KDEL-like motif was defined as [(K/R/H)(D/E)(D/E)L], where each uppercase letter represents an amino acid, and alternatives within parentheses are indicated by slashes. The tyrosine motif followed the pattern [YxxΦ] and tyrosine-like as [HxxI(H/Q)I], with lowercase 'x' representing any amino acid and 'Φ' denoting a hydrophobic residue. The dileucine motif was described by [(D/E)x{2,3}ΦΦ], where 'x{2,3}' specifies two to three residues of any type."

Evolutionary Tree

VNUT peptide sequences, characterised by C-termini displaying KDEL, tyrosine, or dileucine motifs, were systematically integrated into an evolutionary framework. This integration employed taxonomic nomenclature as a foundational reference for mapping onto the phylogenetic tree TimeTree 5 (Kumar et al., 2022). Subsequently, the data was transferred to the European Molecular Biology Laboratory's (EMBL) Interactive Tree Of Life (iTOL) platform (Letunic & Bork, 2021), thereby enabling enhanced visualisation and interactive analysis.

3.2.2. Molecular Biology

Insert Design

Candidate animals were selected to make chimeric VNUT proteins based on the specific criteria. Firstly, their VNUT C-terminal sequences needed to be

representative of animals in their taxonomic class. Secondly, the animal's prominence in research was considered. For example, chicken was selected due to the common use of chick embryos as a research model. Lastly, the degree of change from one C-terminal sequence to the next was evaluated. This led to a natural stepwise change at the single residue level, as depicted in Figure 3.4. The animals selected for these experiments were Alligator, Chicken, Cod and Owl.

Next, the C-terminal domain of each sequence was determined through a transmembrane domain topology predictor, Constrained Consensus Topology prediction server (CCTOP) (Dobson et al., 2015). The C-terminus was defined as spanning from immediately after the last transmembrane domain to the end of the sequence. This region was identified for all sequences.

To make the corresponding DNA sequences suitable for HIFI Assembly (New England Biolabs), 13-20 base pairs overlaps were added to either end, so the inserts had ends which matched those of the template DNA. A further 50 base pair spacer was added after the C-terminal sequence to reduce the risk of protein misfolding, designed using NCBI Primer-Blast. Sequences were ordered from Integrated DNA Technologies (IDT).

Primer Design

Primers for the amplification of EGFP-VNUT and VNVGS1-2pH plasmids were designed using CLC Genomics Workbench software version 3. The melting temperatures (T_M) of these primers were calculated with the aid of NEB's online Tm Calculator (New England BioLabs). To amplify the entire plasmid except the C-terminus, the forward primer was placed at the end of the C-terminus and the reverse primer immediately 5' of the beginning of the C-terminus. These primers were functional on both pHluorin and EGFP-conjugated VNUT constructs.

Table 3.1: EGFP-VNUT and VNUT-pHluorin backbone amplification primers

5'-Forward-3' 5'-Reverse-3'	Amplicon length (bp)	Primer ID	T_m (˚C)

CCCAAACACCAGAAAGGTG	~7600	PR00486	64
AACGTCGCCCCCATATCT		PR00487	66

PCR Protocol

PCR backbone amplification reactions were performed using Q5 Hot Start High-Fidelity DNA Polymerase (New England BioLabs, # M0494) using 0.5 ng DNA and 0.5 µM forward and reverse primers. Samples were exposed to 2 minutes at 98˚C, followed by 35 cycles of 10 seconds of denaturation at 98˚C, 30 seconds annealing at Tm ˚C, 3 minutes 30 seconds extension at 72 ˚C and finally 2 minutes extension at 72 ˚C. Annealing temperatures were optimised using a temperature gradient based on the calculated Tm ±5 ˚C.

Gel Electrophoresis

PCR products were examined using a 0.8% agarose gel in Tris-acetate-EDTA (TAE) buffer (Sigma-Aldrich, #E4884-500G) with 0.3 µg/ml ethidium bromide (Sigma-Aldrich, # E1385-5ML). PCR product was added to TriTrack DNA Loading Dye (Thermo Scientific, # R1161) and loaded into lanes of the gel alongside GeneRuler 1 kb ready-to-use DNA Ladder (Thermo Scientific, # SM0314). Samples were run at 100 V for 30 minutes, then imaged under a UV transilluminator using GeneSnap acquisition software from SynGene.

PCR Clean-up

Following gel electrophoresis, the methylated parental DNA was digested using FastDigest DpnI (Thermo Scientific, # FD1703) at 37 ˚C for 5 minutes, then 80 ˚C for 20 minutes to inactivate the enzyme. The digested product was then purified using QIAquick PCR Purification Kit (QIAGEN # 28104), and the concentration of the DNA was measured using a NanoDrop® Spectrophotometer.

Construct Assembly

EGFP-VNUT C-terminus variant constructs were created using NEBuilder HIFI DNA Assembly Master Mix (New England BioLabs; #E5520S) to add non-mammalian inserts to the linearised EGFP-VNUT and VNVGS1-2pH template

DNA. 75ng insert DNA was used for each reaction, with a fivefold molar excess insert to vector DNA.

Transformation

Expression vectors were transformed using heat shock into NEB 5-alpha Competent E. Coli (New England BioLabs; #C2987) using the NEB transformation protocol. Samples were spread on agar plates with 100 µg/ml ampicillin and SOC media (NEB, #B9020S), and incubated at 37˚C in at shaker at 250 rpm.

Colony PCR

Individual colonies were selected were selected for screening using a sterile pipette tip. Screening was performed on the plasmid backbone and inserts using the primers described in Table 3.2: Colony PCR sequences. The product was visualised using gel electrophoresis as described above.

Colony PCR

Bacterial colonies growing independently were selected for screening.

Table 3.2: Colony PCR sequences

Target	**5'-Forward-3'** **5'-Reverse-3'**	**Amplicon length (bp)**	**Primer ID**
EGFP-VNUT backbone	GGTGGGAGGTCTATATAAGCA TAGAAGGCACAGTCGAGG	5326	492 CMV-linker 362 BGHR
VNVGS1-2pH backbone	GGTGGGAGGTCTATATAAGCA TAGAAGGCACAGTCGAGG	5200	492 CMV-linker 362 BGHR
C-terminus inserts	ACCTTTCTGGTGTTTGGGGA CTAGATATGGGGGCGACGTT	135-143	489 pVNUT-Cinsertf01 491 pVNUT-Cinsertr01

Plasmid Creation

Bacterial colonies were inoculated into LB broth (Fisher Scientific, #BP1427-500) with 100 µg/ml ampicillin and shaken at 250 rpm and 37˚C for 8 hours before being expanded and incubated for 15 hours. Subsequently,

plasmids were isolated using the PureYield Plasmid Midiprep System (Promega; #A2492) and then stored at -20°C until transfection.

3.2.3. Live Imaging

Sample Preparation

N2a cells were cultured and differentiated using the methods described in section 2.2.1: Maintenance and Differentiation. The transfection procedures followed those outlined in section 2.2.2 Transfection. Following the initial seeding and transfection, the N2a cells were incubated with differentiation media for 72 hours. Microscopy was conducted on the sixth day post-seeding.

Imaging buffers were prepared in 1L batches in advance and stored at 5˚C for use across several weeks of imaging. Monensin and nigericin were added on the day of imaging. Recipes can be found below in Table 3.3: Live imaging buffer recipes.

For live-imaging, a HEPES-buffered saline solution (HBSS) was used as a washing solution, to replicate extracellular conditions. MES-buffered saline solution (MBSS) served as a membrane-impermeable acidic wash to quench extracellular fluorophores. Sodium butyrate (NaBut) and ammonium chloride (NH_4Cl) are a membrane-permeable acid and base which quench or de-quench fluorophores, respectively. Calibration-specific versions of HBSS, MBSS and TBSS (TRIS-buffered saline solution) were created with intracellular solute levels, and K+ and Na+ ionophores: nigericin and monensin, with pH set to incremental levels for pH calibrations, discussed in pHluorin Analysis. All solutions were warmed to 37˚C for imaging.

Table 3.3: Live imaging buffer recipes

Buffer name	Recipe
HBSS	140 mM NaCl, 5 mM KCl, 10 mM HEPES, 2 mM $CaCl_2$, 1.5 mM $MgCl_2$, 10 mM Glucose; pH 7.4

MBSS	140 mM NaCl, 5 mM KCl, 10 mM MES, 2 mM $CaCl_2$, 1.5 mM $MgCl_2$, 10 mM Glucose; pH 5.5
NaBut	20 mM in HBSS
NH_4Cl	40 mM in HBSS
HBSS (Calibrations)	20 mM NaCl, 125 mM KCl, 20 mM HEPES, 0.2 mM EGTA, 0.5 mM $MgCl_2$, 10 µM monensin, 10 µM nigericin; pH 7.0-7.5
MBSS (Calibrations)	20 mM NaCl, 125 mM KCl, 20 mM MES, 0.2 mM EGTA, 0.5 mM $MgCl_2$, 10 µM monensin, 10 µM nigericin; pH 5.5-6.5
TBSS (Calibrations)	20 mM NaCl, 125 mM KCl, 20 mM TRIS, 0.2 mM EGTA, 0.5 mM $MgCl_2$, 10 µM monensin, 10 µM nigericin; pH 8.0-8.5

Image Acquisition

Cells were incubated at 37˚C with 5% CO_2 until retrieved for imaging. Coverslips (12 mm) were carefully dipped in HBSS to wash off the differentiation media, then transferred to an imaging chamber (RC-26G, Warner Instruments, Hamden, CT) with 6.7 µg/ml Hoescht-33342. The chamber floor was a #0 40 x 22 mm cover glass (VWR, #100500-808), affixed with vacuum grease.

The live-imaging chamber was placed in a Warner PM-1 heating platform that was maintained at 37˚C using a RadTemp PID controller (Radnoti). The microscope enclosure was maintained at 30-31˚C by a 550 W heater (STEGO 02700.9-00) controlled by a Dwyer TS-13021 Temperature Switch. Fluidics management was achieved through a multichannel liquid perfusion system, delivering buffers at a rate of 2 ml/minute over the coverslips. This system was controlled by a BeanShell within the Micro-Manager 2.0 microscope control software (Edelstein et al., 2014) that interfaced with peripheral hardware via a National Instruments PCIe-6321 card and BNC-2110 breakout box. Solutions

were delivered to the imaging field through parallel MicroFils (28G, World Precision Instruments) attached to solenoid valves and a ValveLink8.2 Perfusion Controller (Automate Scientific) pressurised to 3-4 PSI. Bath perfusion was controlled by a NewEra NE-1000 syringe pump (2.0 mL/min). Both the ValveLink8.2 and N-1000 pump were controlled by Micro-Manager using 5V transistor-to-transistor logic (TTL) signals. Fluorescence imaging was illuminated by a Sutter Lambda XL xenon light source, with filter changes managed by a Lambda 10-3 controlled. Imaging was performed using a Nikon Superfluor 20X 0.75 NA objective lens, capturing fluorescence emissions at 525 nm (± 30 nm) with excitation wavelengths centred around 485 nm (±20 nm).

Images were captured in the μManager overlay for Image J (Edelstein et al., 2014) and collated into frames to create a .tif stack video file for each field of view.

pH Excursions and Calibrations

The following perfusion protocol was devised to investigate the pH level within subcellular VNUT-pHluorin-containing compartments. First, HBSS was washed onto the cells to stabilise fluorescence levels. Subsequently, MBSS was washed into the bath to create an acidic extracellular environment, quenching any externalised pHluorins. An additional HBSS wash restores extracellular conditions to physiological levels. Next followed a membrane-permeable acid, NaBut, to acidify and quench intracellular pHluorin stores. After another HBSS wash, a membrane-permeable base, NH_4Cl, is washed in to raise intracellular pH levels and de-quench internal pHluorins.

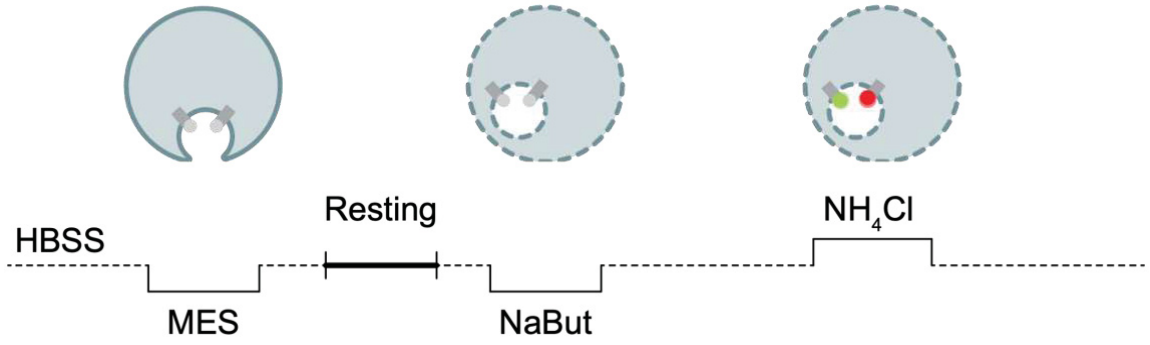

Figure 3.1: pH excursions protocol
This figure illustrates the sequence in which solutions were perfused onto the cells. First, a HEPES-buffered saline solution stabilised fluorescence levels. A MES-buffered solution quenched extracellular pHluorins, NaBut quenched intracellular stores and NH4Cl de-quenched intracellular stores.

Following the pH excursion protocol, calibration experiments were conducted to correlate pHluorin fluorescence levels with pH levels, as depicted in Figure 3.2: . These experiments involved applying a series of solutions with known pH levels in 0.5 pH steps. The solutions were designed to mimic intracellular solute concentrations, adding sodium and potassium ionophores (as outlined in Table 3.3: Live imaging buffer recipes) to equalise the pH levels across the cell membrane (Poburko et al., 2011). This technique, acting as a 'pH clamp', allows for directly comparing resting fluorescence against known pH conditions, thereby approximating the pH value for intracellular stores to measure the subcellular localisation of the VNUT-pHluorin constructs.

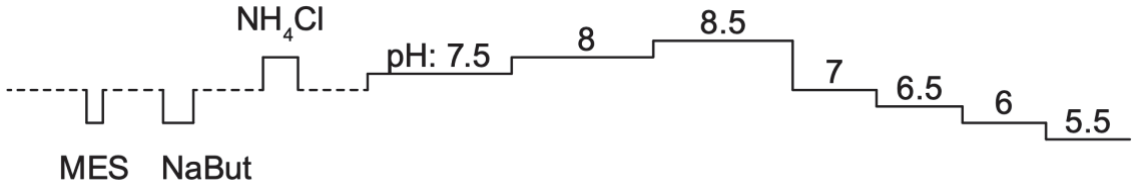

Figure 3.2: Protocol for calibrating pH values to pHluorin fluorescence
This figure provides a schematic representation of the pH calibration protocol for pHluorin experiments. The protocol is depicted through a trace indicating time from left to right. The experiment has two key phases: first, the pH excursion experiments, employing MES, NaBut and NH4Cl to manipulate intra- and extra-cellular pHluorin stores. The second phase is the calibration experiments, where solutions of a known pH are applied to cells and the resultant fluorescence intensity of pH-sensitive pHluorin is measured and used to cross-reference the resting fluorescence level and estimate the pH value of pHluorin stores.

3.2.4. Fixed Imaging

Fixed-cell microscopy followed the methodologies described in section 2.3: Fixed Cell Imaging. Images were captured at 300 nm Z-steps.

3.2.5. Image Analysis

pHluorin Analysis

Time-lapse video files were loaded into FIJI image analysis, where they were cropped to isolate individual cells, optimising computational efficiency. A custom-built macro ‘fftAlign’ was used to counteract the systematic drift of cells across the field of view, caused by fluid movement. fftAlign leverages a Fast Fourier Transformation algorithm to detect drift within user-defined parameters and apply the necessary corrections. Subsequently, the custom-built macro ‘multiMeasure current stack’ obtained the mean fluorescence intensities from hand-drawn cell perimeter ROIs across each frame, later compiled into a data table, with analysis performed in JMP.

Data normalisation for each cell involved identifying the minimum fluorescence level during the NaBut phase and the maximum during the NH4Cl phase, then applying a formula to scale all values between 0 and 1 where NaBut is 0 and NH_4Cl is 1.

Calibration traces from individual cells were modelled with a Sigmoid function in JMP’s non-linear curve-fitting platform to correlate the fluorescence and pH levels, yielding an equation to describe their relationship. The inverse of this equation was then applied to the dataset as a parameter to estimate pH values from normalised fluorescence levels.

The phase between MES and NaBut washes was designated as the resting phase due to its consistently steady fluorescence level. Fluorescence values within this phase, with a 5-10 frame buffer, were averaged to provide the resting pH value for each cell.

EGFP-Analysis

Fixed-cell microscopy with EGFP-VNUT constructs followed the image analysis pipeline of Deconvolution, Maximal Intensity Projections, RIPA puncta generation, MINER perimeter measurements, and JACOP correlational analyses as outlined in **Section 2.5: Image Analysis.**

3.2.6. Statistical Analysis

As described **in 2.6.3 Statistical Analyses**, the data were tested with the Shapiro-Wilks goodness-of-fit test to examine whether the sample data fit a normal distribution. A non-parametric Kruskal-Wallis rank-sum test was used to test the significance between categorical data groups with a continuous outcome variable. Pairwise comparisons were made using the Wilcoxon signed-rank test.

3.3. Results

This section investigates the data to determine whether the replacement of the mammalian VNUT C-terminus with non-mammalian C-termini will reduce VNUT and ER-Golgi Complex co-localisation. The target of enquiry was the unique amino acid motifs within the C-termini of mammalian VNUT and its non-mammalian orthologues. Utilising bioinformatics, we first identified non-mammalian animals from major taxonomic Classes in the kingdom *Animalia,* whose C-terminal sequences represented the broad consensus of amino acid clusters from their evolutionary kin. We then engineered chimeric proteins, substituting the mammalian C-terminus of VNUT with those from the identified non-mammals. Fluorescently tagged chimeras were expressed in mouse N2a cells, allowing precise subcellular localisation analyses using epifluorescence microscopy and pH probes. Our data then explore the distribution of VNUT at a cellular and punctate level to dissect VNUT's cellular distribution, specifically its association with the ER-Golgi apparatus.

3.3.1. Evolutionary Conservation of VNUT C-terminus Motifs Across Species

The C-terminal region of transporter proteins in the SLC superfamily are known for their regulatory functions and interactions with cellular machinery. Very little is known in this respect about VNUT’s sequence. The VNUT C-terminus exhibits a large degree of evolutionary diversity, which hints at its evolutionary

adaptation. A phylogenetic analysis was conducted to understand the evolutionary trajectory and functional implications of these motifs.

The analysis leveraged a dataset of VNUT peptide sequences acquired from the NCBI protein database. A custom-built R script scanned the sequences for common signalling motifs, specifically targeting KDEL-like, tyrosine, and dileucine motifs. These motifs were selected due to their known involvement in subcellular localisation and chaperone-protein interactions (Foss et al., 2013; Obermüller et al., 2002; Peters et al., 1990). The KDEL motif, associated with retention in the endoplasmic reticulum, and the tyrosine and dileucine motifs, associated with synaptic and lysosomal proteins, serve as key indicators of the functional roles VNUT may play in different species.

Figure 3.3 shows a phylogenetic tree which integrates motif scanning analyses within an evolutionary framework. This process uses taxonomic classification, TimeTree and the Interactive Tree of Life (iTOL) platform to review VNUT's evolutionary history and uncover the emerging patterns in these motifs.

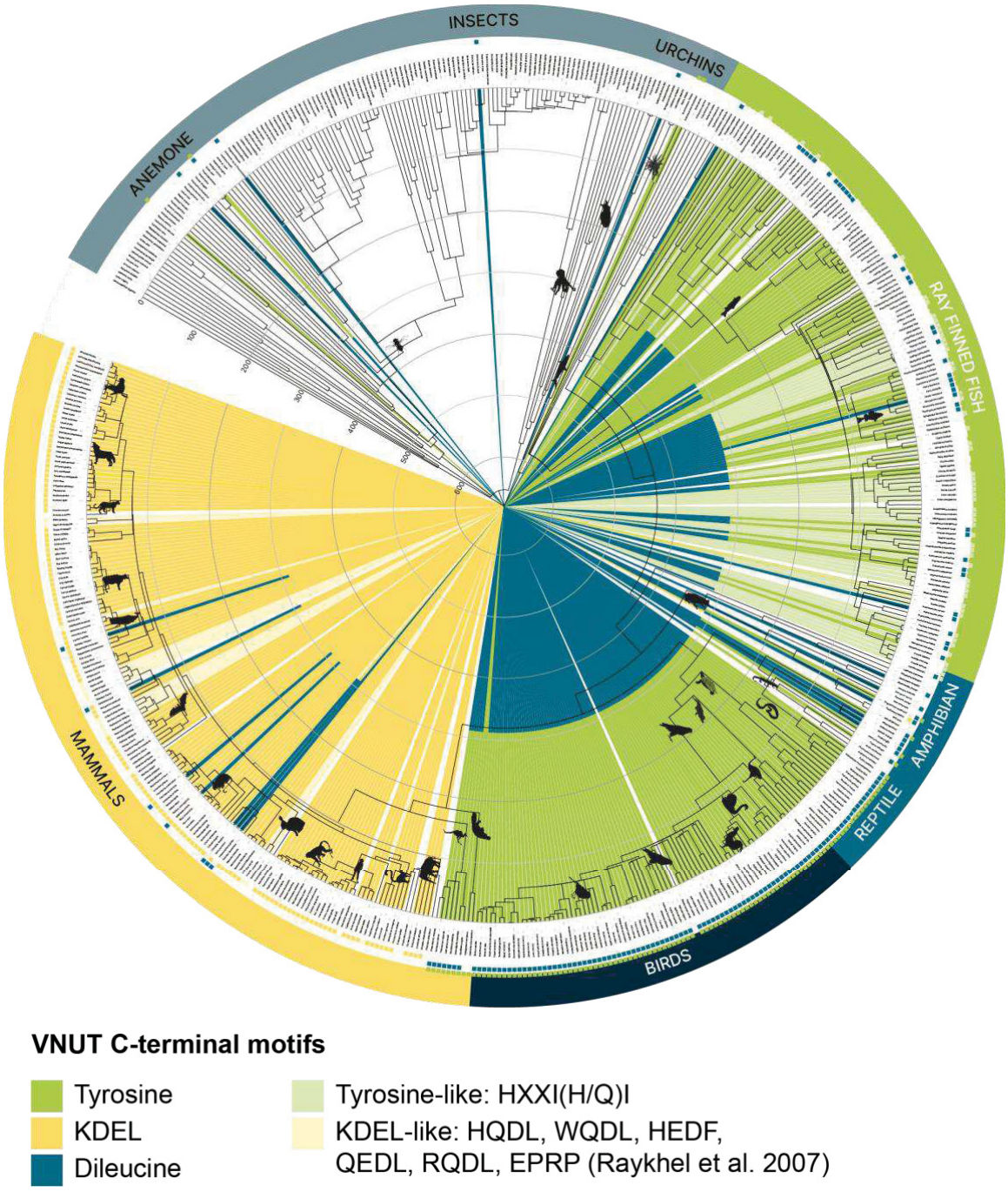

Figure 3.3: Phylogenetic tree displaying VNUT C-terminal motif change in kingdom Animalia

1400 VNUT peptide sequences were downloaded from NCBI Protein database. A custom R script using a regular expression search parameter was used to survey sequences for common C-terminal subcellular trafficking motifs: KDEL-like, Tyrosine, and Dileucine. KDEL-like was defined as ((K/R/H)(D/E)(D/E)L), Tyrosine as (Yxxϕ), and Dileucine as ((D/E)x{2,3}ϕϕ) where ϕ indicates a hydrophobic residue and x denotes any amino acid. KDEL-like and Tyrosine-like sequences outlined in the key were identified as appearing functionally similar. Each branch of the tree

represents one animal. Coloured slices denote the presence of a corresponding motif. Where there are two colours to a slice, the animal can possess both motifs in their C-terminus.

Representative animals were selected from the classes of Reptilia (reptiles), Aves (birds), and Actinopterygii (ray-finned fish) since they constituted the majority of non-mammalian VNUT sequences with C-terminal trafficking motifs. From there, the C-terminal sequences within each class were examined to identify recurring patterns. Animals were hand-picked if they met the criteria of containing amino acid sequences that were highly conserved within the class and having both the amino acid sequence and the peptide sequence available from NCBI. The Chinese alligator (*Alligator sinensis*), Atlantic cod (*Gadus morhua*), and Burrowing owl (*Athene cunicularia*) were selected at this stage to best represent their respective classes. The red junglefowl (*Gallus gallus*), better known as a chicken, was then added due to the widespread use of embryonic chicks as a research model because this could facilitate the branching of VNUT research into this model at a future date. The C-terminal sequences for each selected animal, using their colloquial name, are shown in Figure 3.4**.** The added benefit for incorporating the chicken sequence is that we now have an incremental point mutation change within the C-terminus from Alligator's "…DT**V**SAVIDL" to Chicken's "DT**D**SAYIDL", then Owl's "DTDSAY**M**DL", which allows us to assess the effect of the amino acids individually. An alignment between the human and rat C-terminus can be found in

Figure 3.4: Sequence alignment of C-terminal amino acid sequences in selected species

The C-terminal amino acid sequences of selected animals from the classes Mammalia (mammals), Reptilia (reptiles), Aves (birds), and Actinopterygii (ray-finned fish). Each letter represents an amino acid, the colour of which uses the standardised RasMol amino acid colouring system to denote similarities in structure and function. Coloured boxes behind the text

indicate amino acid motifs, where yellow denotes KDEL, teal is dileucine, and green indicates tyrosine.

As illustrated in **Figure** 3.3, the spread of motifs within and between classes is largely constant. Notably, anemones, insects, and urchins largely lack tyrosine, dileucine, and KDEL motifs in their C-termini. In contrast, ray-finned fish exhibit a small diversity of motifs: many possess a tyrosine motif, some display a tyrosine-like motif, and a few have both a tyrosine and a dileucine motif. Amphibians primarily feature dileucine motifs, whereas reptile and bird sequences consistently show a combination of tyrosine and dileucine motifs. Mammals distinguish themselves by an absence of tyrosine or dileucine motifs, coupled with the emergence of the KDEL motif. A few notable exceptions to these norms include mammals with dileucine and/or tyrosine motifs. Most striking is the presence of tyrosine and dileucine motifs in the earliest mammals -- monotremes and marsupials -- at the bottom of the circle in **Figure** 3.3 and in **Figure** 3.5**.**

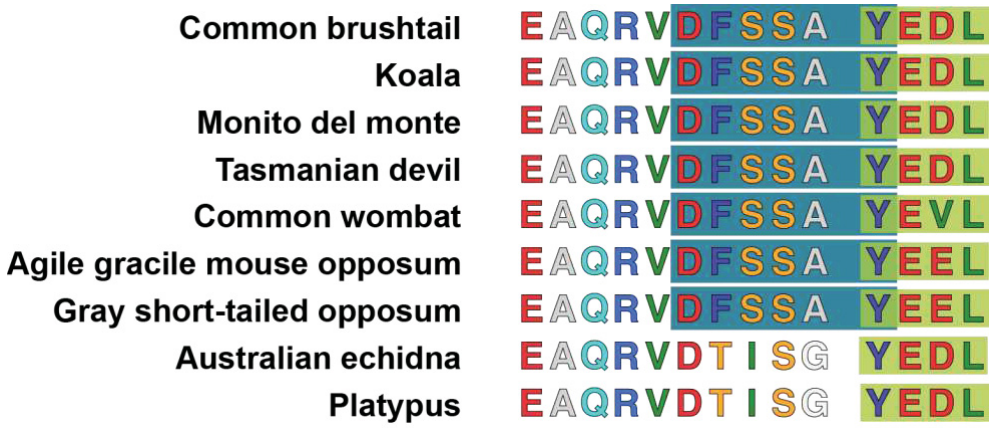

Figure 3.5: Evolutionary motif variations in monotreme and marsupial C-termini

This figure displays the C-terminal amino acid sequences of monotremes and marsupials, highlighting the presence of dileucine and tyrosine motifs using blue and green boxes, respectively. Amino acids are coloured in accordance with RasMol standardised amino acid colouring conventions.

The bioinformatics analyses have mapped motif conservation and variation across the VNUT C-termini in a diverse set of species. Through motif searches and sequence alignments, these methods identified specific regions that exhibit evolutionary conservation alongside areas of notable divergence. The comparison between mammalian and non-mammalian VNUT sequences has revealed distinct differences in their C-terminal regions, suggesting a variation in their subcellular trafficking mechanisms. This has helped us to identify candidate animal sequences to create chimeric C-terminus proteins to functionally test the trafficking properties of mammalian versus non-mammalian VNUT C-terminus motifs.

Figure 3.6: Sequence alignment of human and rat VNUT C-termini

3.3.2. Subcellular Localisation of Fixed EGFP-VNUT Chimera Constructs

Building upon the bioinformatics analyses, we compared the subcellular localisation of mammalian and non-mammalian chimeric proteins using epifluorescence microscopy. Green fluorescent protein conjugated VNUT constructs were transfected into mouse N2a neuroblastoma cells alongside fluorescently labelled organelle markers. The cells were then differentiated before fixation and microscopy.

To assess the localisation of VNUT constructs to the ER and Golgi complexes, N2a cells were co-transfected with two plasmids: mTagBFP2-ER-5, a blue fluorescent protein conjugated to calreticulin, an ER resident protein; second, mDsRed-Golgi-7, a red fluorescently labelled beta-1,4-galactosyltransferase 1 gene, a membrane-bound protein located in the medial Golgi apparatus. **Figure** 3.7 shows the subcellular localisation of the aforementioned ER, Golgi and VNUT constructs. For the purposes of these

experiments, the rat VNUT sequence is considered WT. In the first column, the ER marker is dispersed across the cell cytoplasm. In the second, the VNUT constructs follow a similar distribution pattern at the gross level, showing an expression pattern much like the Golgi marker. This is particularly evident in the final column, where the markers are all overlaid.

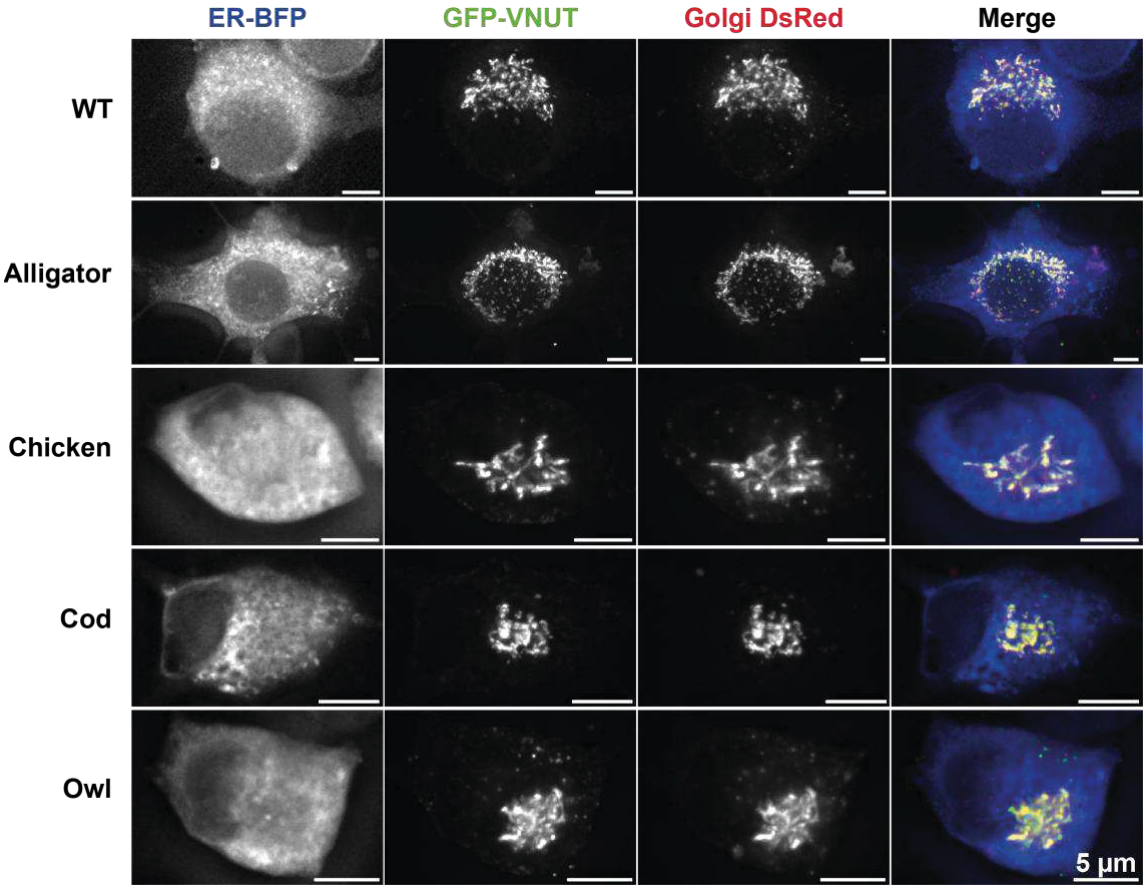

Figure 3.7: Comparative co-localisation of VNUT variants with the ER and Golgi

This figure shows representative images of the co-localisation between EGFP-tagged VNUT constructs, the endoplasmic reticulum (ER-BFP) and Golgi apparatus (Golgi DsRed) in mouse N2a cells. All scale bars are 5 µm.

Data was collected from three independent biological replicates. Quantification of co-localisation began with broad-scale correlational analyses. Using ROIs hand-drawn around the cell soma, the JACOP FIJI plugin helped analyse the correlation of pixel intensity in each of the three fluorescent colour channels. A Pearson's coefficient value was generated for each cell to measure

the correlation between each VNUT C-terminus variant compared to the ER and the Golgi. The results can be found in **Figure** 3.8 **below**.

The data do not meet the assumptions of normality, so a non-parametric test of a Kruskal-Wallis test with a Wilcoxon pairwise test was used to assess statistical significance. These tests did not identify any difference in correlation of VNUT with ER or Golgi for any of the tail variants compared to the wild type.

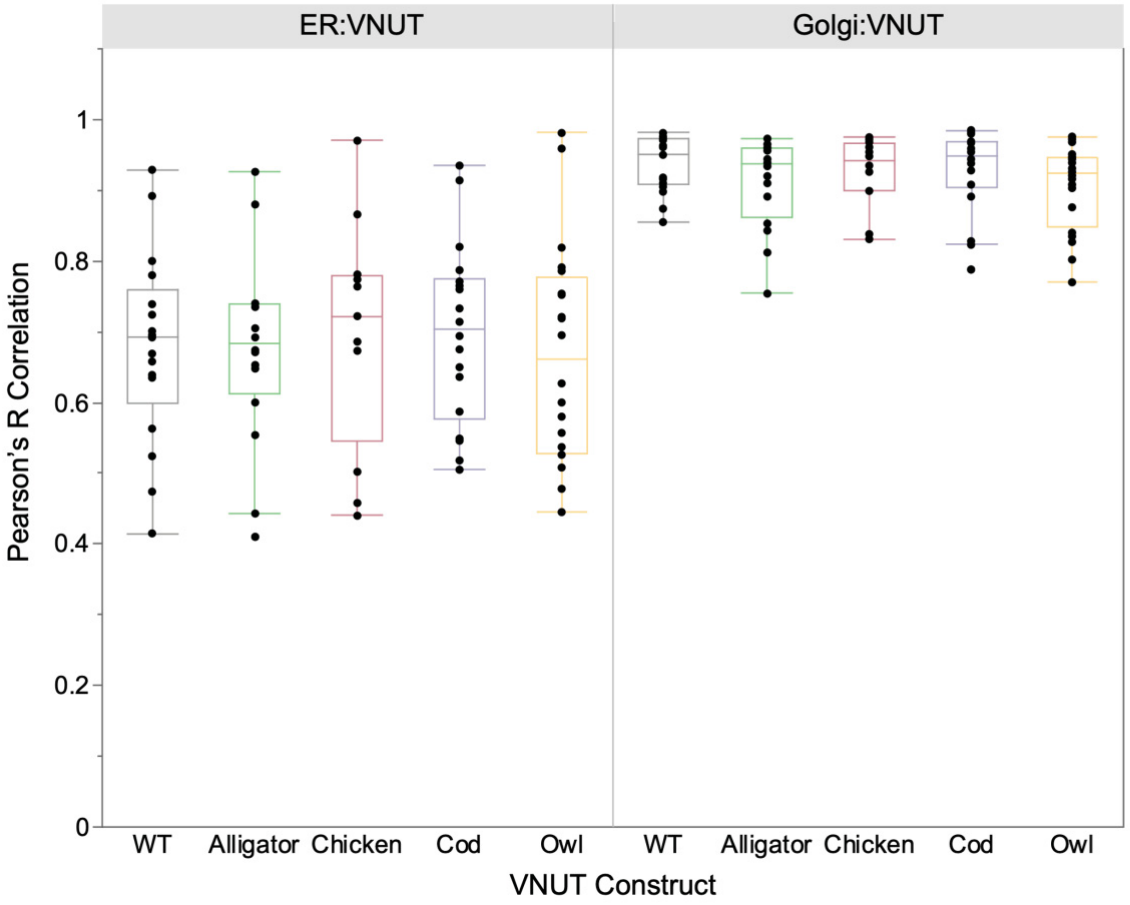

Figure 3.8: Correlation between VNUT C-terminus variants with ER and Golgi markers

This figure shows the Pearson correlation coefficients quantifying the localisation of VNUT C-terminus variants with the endoplasmic reticulum and Golgi apparatus markers in N2a cells. From left to right, the mean correlational values between ER and VNUT variants are 0.68, 0.68, 0.70, 0.70 and 0.67 for WT, Alligator, Chicken, Cod and Owl, respectively. Values for the VNUT-Golgi correlations are 0.93, 0.91, 0.93, 0.93, and 0.90 for the same variants. Each point indicates a cell, derived from three independent experiments.

Subsequently, to analyse the distribution of VNUT on a more granular level, puncta-based analyses were used to explore more subtle changes to the distribution of VNUT within the cell. Specifically, we aimed to test if there were any observable changes in the distribution of vesicle-like puncta localising to the periphery of the cells. The same cell soma ROIs were used and added to with computer-generated puncta ROIs created by the RIPA plugin for FIJI. Settings were optimised to achieve the most comprehensive puncta selection across all VNUT variants. ROIs were captured only for VNUT puncta. Next, the MINER plugin for FIJI identified the nearest point of the cell soma – using the hand-drawn ROIs – for each RIPA-created punctum. The distance from the centre of each punctum to the nearest perimeter point was recorded in a data table. Puncta close to the perimeter of each cell were then identified. A count was taken for puncta within 0 ≤ 250 nm from the perimeter of each cell, then 251 ≤ 500 nm, continuing in 250 nm increments up to 2500 nm. The number of puncta per zone was then taken for each cell, averaged for each VNUT construct and plotted to create Figure 3.9**.** We see consistently fewer puncta in the Alligator construct than in the WT. The Owl variant shows a higher dispersal toward the cell perimeter, which returns to normal levels at 1750 nm. Chicken and Cod variants show the same dispersal pattern as the wild-type rat VNUT construct. Three independent biological repetitions resulted in the following number of cells used for each condition: WT 23 (1572 puncta), Alligator 16 (739), Chicken 12 (980), Cod 20 (957), and Owl 21 (1393 puncta).

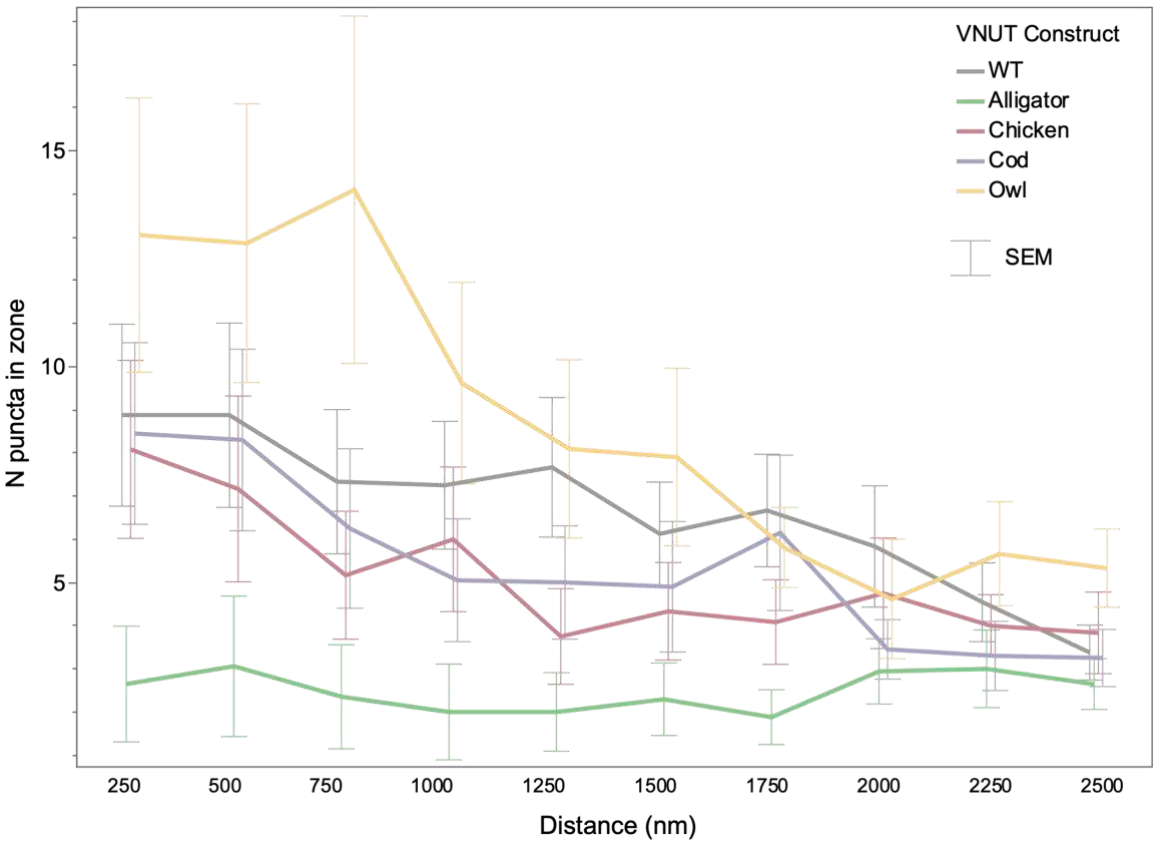

Figure 3.9: 'Onion-peel' analysis: spatial distribution of VNUT construct puncta in 250 nm slices

The distribution of VNUT puncta across 250 nm slices taken concentrically inwards from the cell perimeter. The distance inwards from the cell perimeter is plotted on the X axis, and the mean number of puncta in the slice is plotted on the Y axis, with VNUT construct marked by different colour lines The error bars show the standard error of the mean. Data from three independent experiments.

To better understand the trafficking dynamics of VNUT puncta towards the cell membrane, a 500 nm slice adjacent to the cell perimeter was designated as the perimeter zone. This selection is devised from the spatial resolution limitations of our microscopy technique and the biological expectations of vesicle aggregation near the membrane prior to exocytosis. For each cell analysed, the number of VNUT puncta within the zone was quantified, both as raw counts, and normalised against the cell's perimeter length. This normalisation is crucial as larger cells, indicated by a longer perimeter, would be inherently expected to

house more puncta. The outcomes are illustrated as raw counts in **Figure** 3.10 and the normalised data in **Figure** 3.11**.**

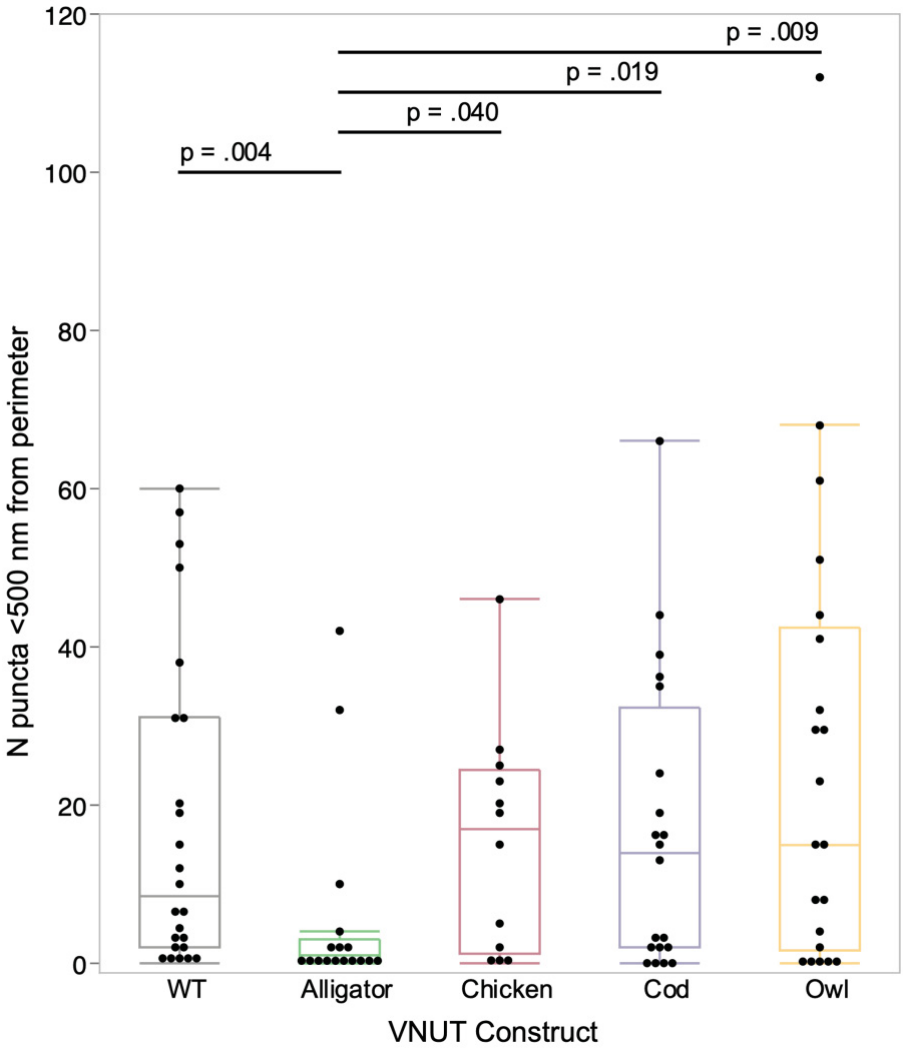

Figure 3.10: Perimeter-proximal puncta counts across VNUT C-terminus variants

The raw counts for VNUT puncta within a 500 nm slice from the cell perimeter, comparing VNUT C-terminus variants transfected into mouse N2a cells. Data were analysed with the non-parametric tests Kruskal-Wallis followed by a Wilcoxon pairwise comparison. The rat-Alligator chimera construct displayed significantly fewer puncta near the cell perimeter than all other VNUT constructs. Each data point represents one cell, derived from three independent experiments.

Figure 3.10 shows fewer puncta within 500 nm of the cell periphery in the Alligator C-terminus construct than WT, Chicken, Cod and owl. Mean values ± SD were 18 ± 20, 6 ± 12, 15 ± 14, 17 ± 19 and 26 ± 30 for WT, Alligator, Chicken,

Cod and Owl, respectively. A Shapiro-Wilks test of normal distribution showed that the data were not normally distributed. A non-parametric Kruskal-Wallis test was used to analyse the data, followed by a Wilcoxon pairwise test to examine individual differences. Pairwise analyses revealed a significant difference between the VNUT Alligator variant when compared to each of the other variants. There was no significant difference between any other variant pairs.

Figure 3.11 shows similar results when normalised against the size of the cell. The mean numbers of puncta per micron of cell perimeter ± SD are 0.4 ± 0.4, 0.1 ± 0.2, 0.3 ± 0.3, 0.4 ± 0.4, and 0.4 ± 0.4 for WT, Alligator, Cod, Chicken and Owl, respectively. Once again, the data do not meet the assumptions of normality, as determined by a Shapiro-Wilks test, so a non-parametric analysis pipeline of a Kruskal-Wallis and Wilcoxon pairwise tests were used to determine significance. Using means adjusted for cell perimeter size, we see significantly fewer puncta in the cells expressing VNUT with the Alligator C-terminus sequence than we do for rat (WT), Cod or Owl C-terminus variants. There was no significant difference between the Alligator and Chicken constructs or between any other pairs.

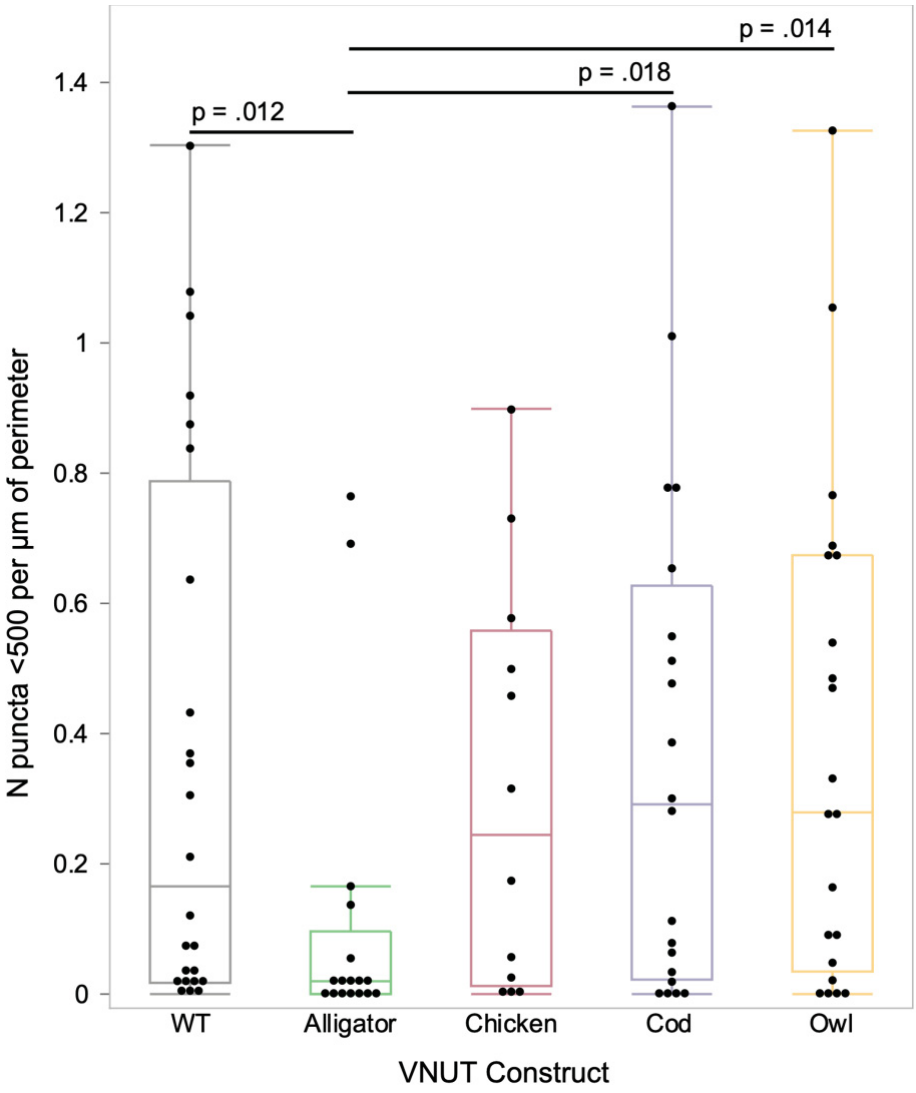

Figure 3.11: Normalised perimeter-proximal puncta distribution across VNUT C-terminus variants

This figure quantifies VNUT puncta within 500 nm of the cell perimeter, normalised by cell perimeter length. Values are displayed for WT, Alligator, Chicken, Cod and Owl chimera constructs. Statistics are generated using a Kruskal-Wallis and Wilcoxon pairwise analysis. Data show significantly fewer Alligator construct puncta in the perimeter zone than WT, Cod and Owl constructs.

A further important metric to assess how much VNUT is in the 500 nm zone is the intensity of the fluorescence values of the puncta. More VNUT molecules in one spot will fluoresce more brightly. Figure 3.12 describes this measure, where intensity is reported as the pixel values of our 16-bit images following deconvolution. Values were averaged for each cell and plotted against

the VNUT C-terminus variant. Mean values ± SD for each were 5561 ± 4752, 4512 ± 2868, 4354 ± 2368, 5413 ± 2998 and 8472 ± 5442 for WT, Alligator, Chicken, Cod and Owl, respectively. Following a Shapiro-Wilks test for normal distribution, a Kruskal-Wallis and Wilcoxon pairwise analysis framework was used to analyse puncta brightness. The VNUT puncta from the Owl variant fluoresced significantly more brightly than those from the WT, Alligator and Chicken variants. There was no significant difference between Owl and Cod puncta, or between any other data pair. This indicates each VNUT punctum with the Owl C-terminus had more molecules of VNUT associated with it.

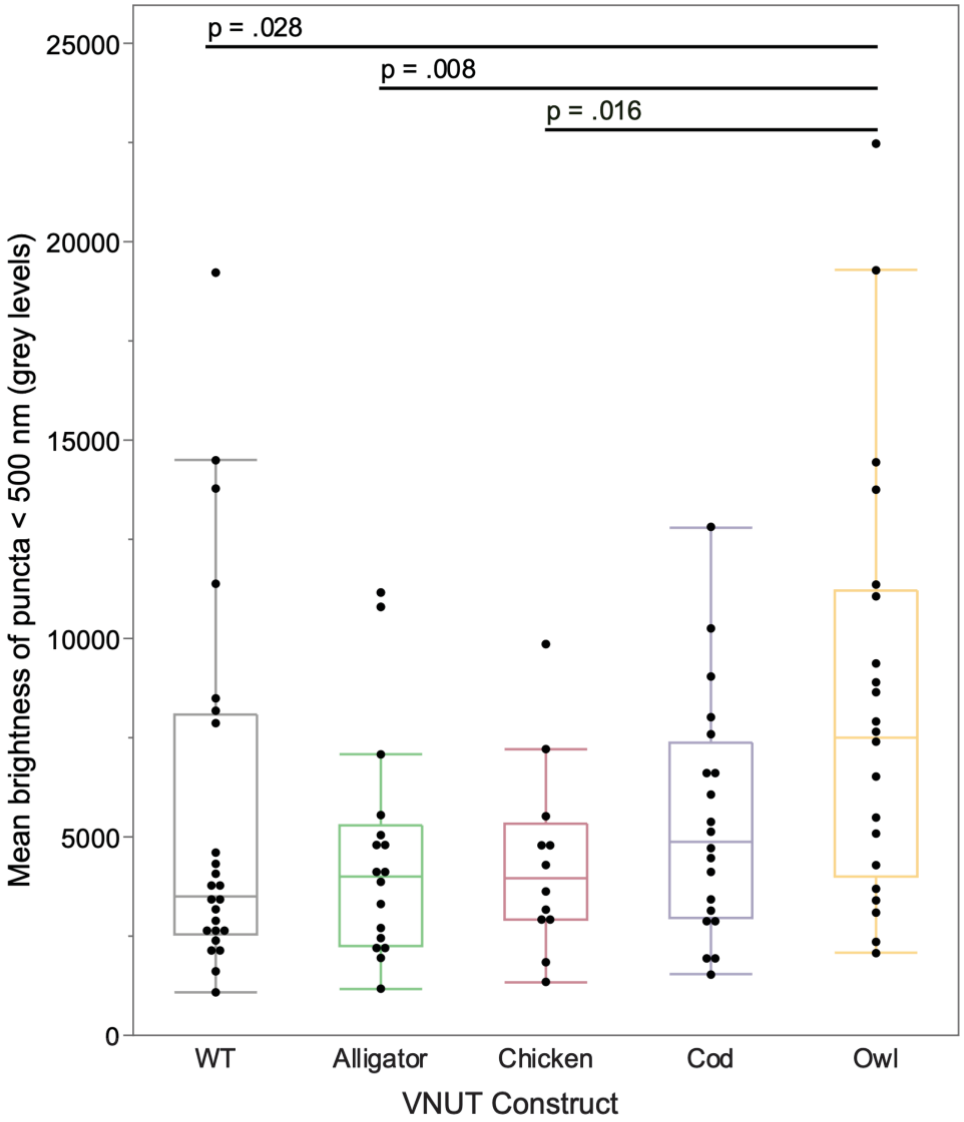

Figure 3.12: Fluorescence intensity of perimeter VNUT puncta
This figure depicts the average fluorescence intensity of VNUT puncta, measured within a 500 nm slice adjacent to the cell perimeter across the different VNUT C-terminus variants. Using a 16-bit camera, intensity values were measured on a scale from 0 – 65,535. Data were analysed using Kruskal-Wallis and Wilcoxon pairwise test to reveal a significant increase in average brightness of puncta belonging to the Owl C-terminus VNUT variant.

Using data gathered in the cell and puncta analyses, a comparison of cell and puncta areas sought to examine any relationships between VNUT variants and shape descriptors. The average area of cells in μm^2 were 220 ± 164, 294 ± 329, 199 ± 167, 136 ± 134, and 257 ± 204 for WT, Alligator, Chicken, Cod and Owl, respectively. Puncta area, measured in nm^2, were 44 ± 6, 49 ± 9, 47 ± 9, 45 ±6, 49 ± 8 in the same order. Data were analysed using Kruskal-Wallis and Wilcoxon pairwise tests and found no significant change in cell or puncta size between any variants.

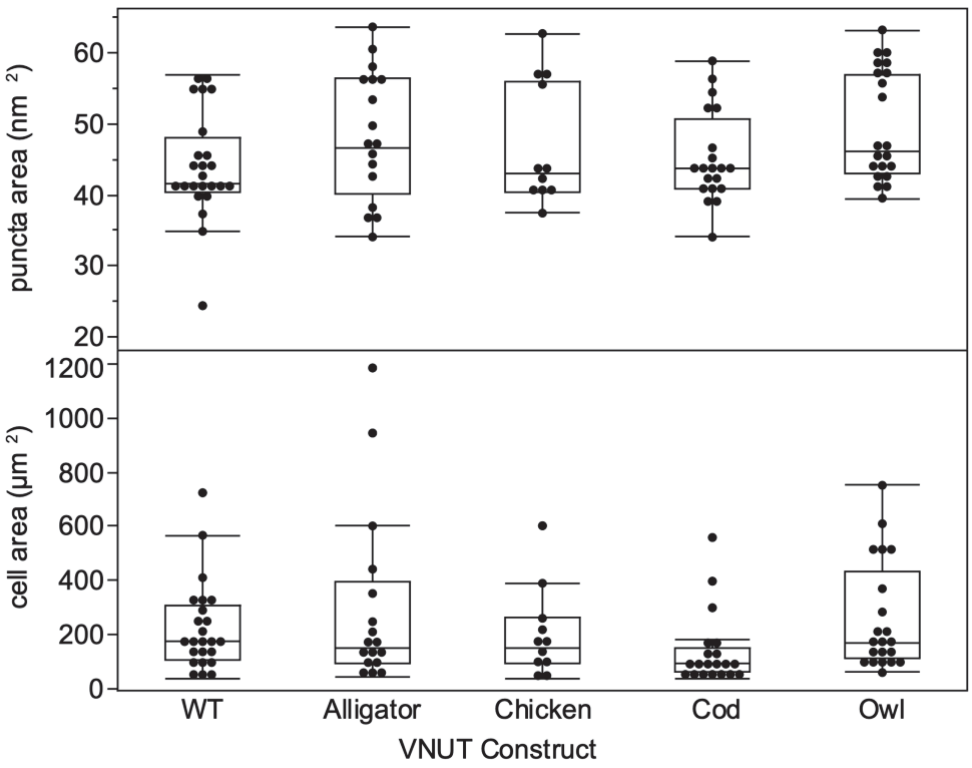

Figure 3.13: Comparison of cell and puncta area across VNU C-terminus variants.

This figure visualises the relationship between VNUT variant and both cell size and puncta size. This shows the consistency in the size of the cell and puncta for each construct.

Taken together, these results show a significant reduction in puncta localisation to the perimeter of the cell when the mammalian VNUT C-terminus is replaced with that of the Chinese alligator. When the mammalian C-terminus is replaced with that of the Burrowing owl, there is not a significant increase in the number of puncta at the cell perimeter; however, each punctum contains significantly more VNUT. Furthermore, there is no significant difference in the dispersion of VNUT puncta when the mammalian C-terminus is replaced with that of a common Chicken or Atlantic cod. These findings underscore the nuanced trafficking mechanisms of the VNUT C-terminal amino acid motifs.

3.3.3. Using pH Excursions to Determine Localisation of VNUT PHluorin Chimera Constructs

Building upon the insights gained from fixed-cell analyses, the live imaging component of this research delved into the dynamic behaviours of VNUT C-terminus variants in live cells. Using constructs tagged with a pH-dependent fluorescent probe, we aimed to provide further evidence on the subcellular trafficking behaviours of VNUT. By correlating the brightness of pHluorin fluorescence to standardised pH values, we can estimate the subcellular location based on known pH values of organelles and vesicles.

Live imaging pH excursion experiments were used to estimate the pH level of VNUT pHluorin-containing subcellular compartments. Mouse N2a cells were cultured on glass coverslips, placed into a Warner RC-26 laminar flow chamber, and mounted onto a microscope stage with a computerised perfusion system affixed. Four perfusion solutions were used in pH excursion experiments: a HEPES-buffered saline (HBSS) solution provided a stable near-physiological condition for cells at rest; a MES-buffered saline solution (MBSS) served as an extracellular acidic wash to quench external fluorophores; NaBut and NH_4Cl

served as membrane-permeable agents to quench or de-quench internal pHluorin stores respectively.

Frames were continuously acquired for the duration of pH excursion experiments, measuring the change in fluorescence levels over time in line with pH changes. PHluorins fluoresce most brightly in basic conditions, with the brightness of the signal being a direct function of the pH conditions (Mahon, 2011). Data was then normalised against NaBut and NH_4Cl conditions, where fluorescence in response to NaBut was coded as 0, and NH_4Cl as 1. Subsequently, the period of resting fluorescence was measured and the fluorescence intensity across each frame averaged to provide a relative measure of fluorescence, and pHluorin localisation estimate, for each construct. Example time traces for each construct can be found in **Figure** 3.14**.**

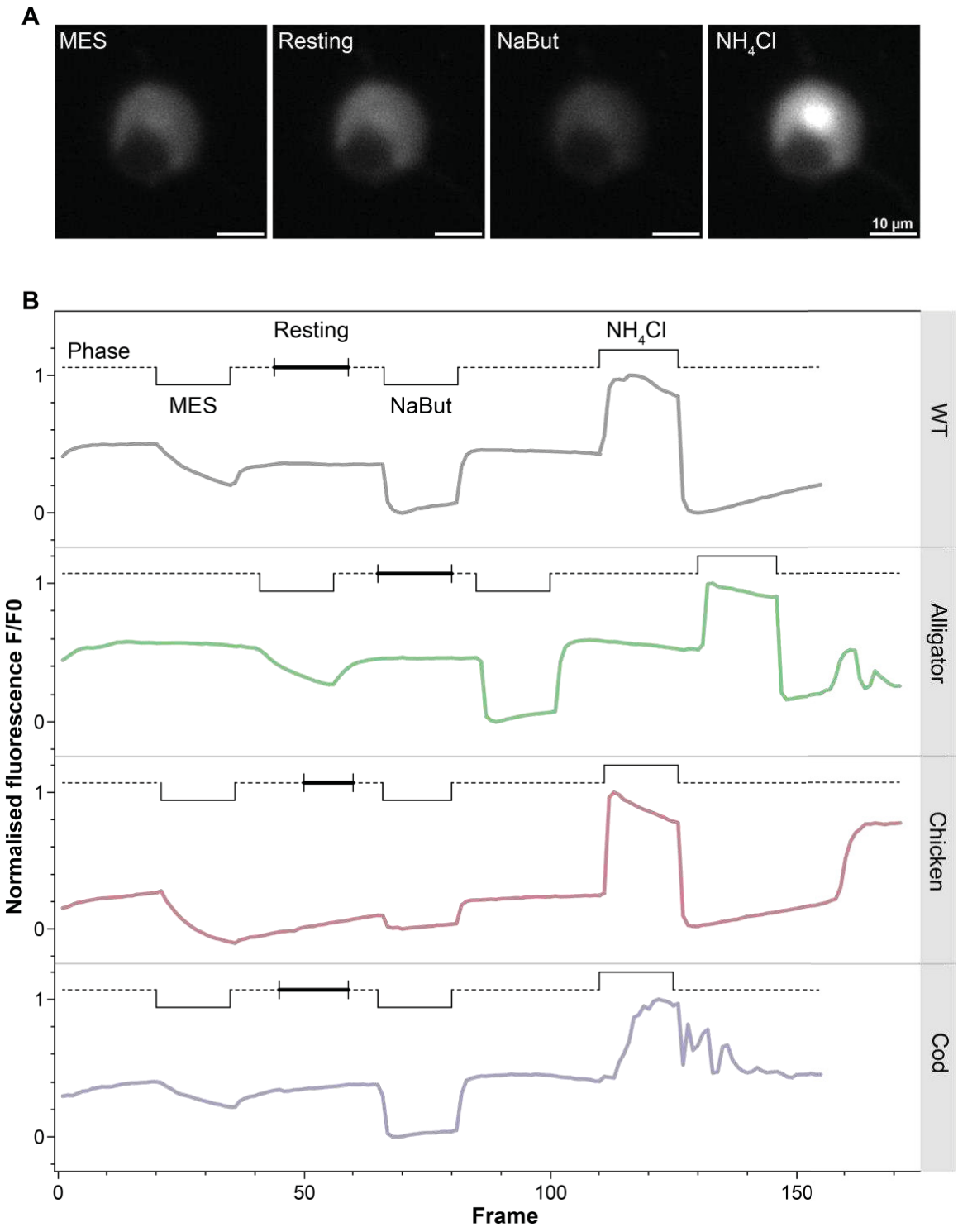

Figure 3.14: Representative normalised fluorescence trace by VNUT C-terminus variant.

This figure depicts representative time traces of fluorescence intensity measured in N2a cells transfected with VNUT-pHluorin C-terminus constructs. **A.** Images of an N2a transfected with wild-type VNUT-phluorin after perfusion of MBSS, HBSS, NaBut and then NH_4Cl. Fluorescence

intensity is depicted as white signal. Scale bars are 10 µm. **B.** Representative normalised fluorescence time traces recorded at single-cell level. Data have been normalised between 0 and 1 at the lowest NaBut and highest NH_4Cl fluorescence levels. A black line depicts the perfusion stage above each trace. A dashed line denotes a HEPES environment, solid lines deviating downwards indicate an acidic wash, solid lines deviating upwards denote a basic wash.

In Figure 3.14, a minor drop in fluorescence intensity is observed in response to the extracellular acid MES. This is likely due to a slow acidification of the cell rather than a fast-acting fluorophore quenching, as evident by the shallow gradient of the decline. Quenching of membrane-bound pHluorins would result in a sharp drop in fluorescence after perfusing MES onto the cells. An absence of this response indicates minima -- or the absence of -- VNUT on the cell surface.

Following a HEPES wash, the baseline fluorescence wash measured. Across all samples, this stage was the steadiest and the best representative resting state. Following internal acidification with NaBut, several cells showed an overcompensation in their return to baseline, which would have provided inaccurate data. A clear decrease in fluorescence can be observed in response to NaBut across all constructs, followed by a rise in intensity in response to NH_4Cl. There are some deviations in intensity outside of these points, mostly due to cells contracting or moving, which introduce noise in the data. Best efforts were made to reduce this noise by drawing a large enough ROI to encompass the movement of the cell.

pH calibration experiments facilitated the correlation between normalised fluorescence levels and pH values. After pH excursion experiments, the bath solutions were replaced with calibration solutions (recipes in **Table** 3.3). Solutions were prepared at pH 0.5 steps from pH 5.5 to 8.5, with sodium and potassium ionophores to act as a pH clamp. A calibration trace is shown in **Figure** 3.15 with pH calibration steps described in the diagram above the trace. A sigmoid curve was fit to describe the relationship between fluorescence intensity and pH, and an inverse prediction formula was then used to estimate pH values for each captured frame across live imaging experiments.

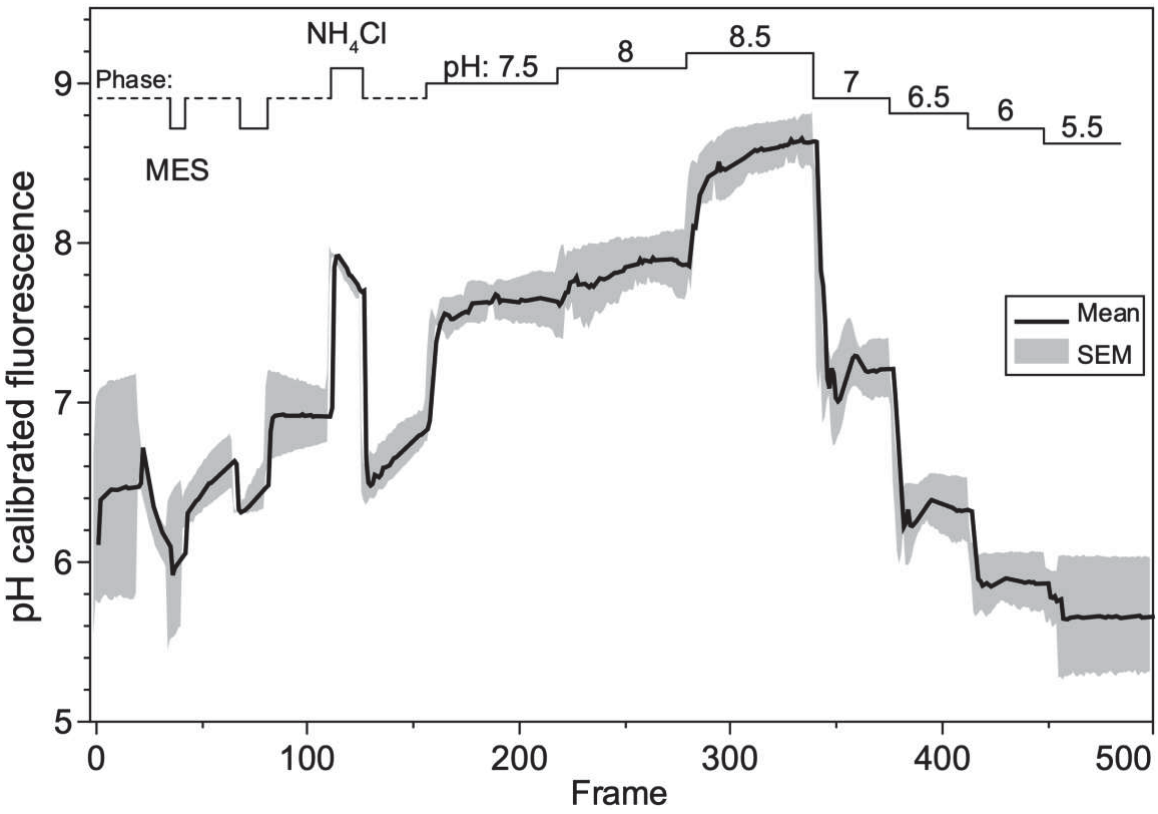

Figure 3.15: pH-calibrated fluorescence trace for VNUT pHluorin constructs
This figure shows the calibration steps for live-imaging VNUT-pHluorin constructs. Following pH excursion experiments shown in Figure 3.14, calibration steps follow, as depicted above the trace. A series of solutions of known pH levels are applied to the cells. A calibration curve was then generated to correlate fluorescence levels with pH values. The solid line indicates the mean fluorescence level, and the grey hashed area shows the SEM (n=6). Data from one independent experiment.

Once fluorescence levels were calibrated to pH values, the average pH value was taken during the resting stage for each cell. Those values were plotted by VNUT construct in **Figure** 3.16 below. Mean pH values for each construct at rest are 6.82 ± 0.1, 6.95 ± 0.2, 6.78 ± 0.3 and 6.78 ± 0.2 for WT (rat), Alligator, Chicken and Cod, respectively. Data did not meet the assumptions of normality, so they were analysed using Kruskal-Wallis ranked sum and Wilcoxon pairwise comparisons. The data showed a significant increase in environmental pH levels

in VNUT constructs possessing the Alligator C-terminus compared to WT (p = .019) and that of the Cod (p = .01). This indicates that the replacements of the mammalian C-terminus with the alligator counterpart results in an increased likelihood of VNUT sequestering in more basic environments.

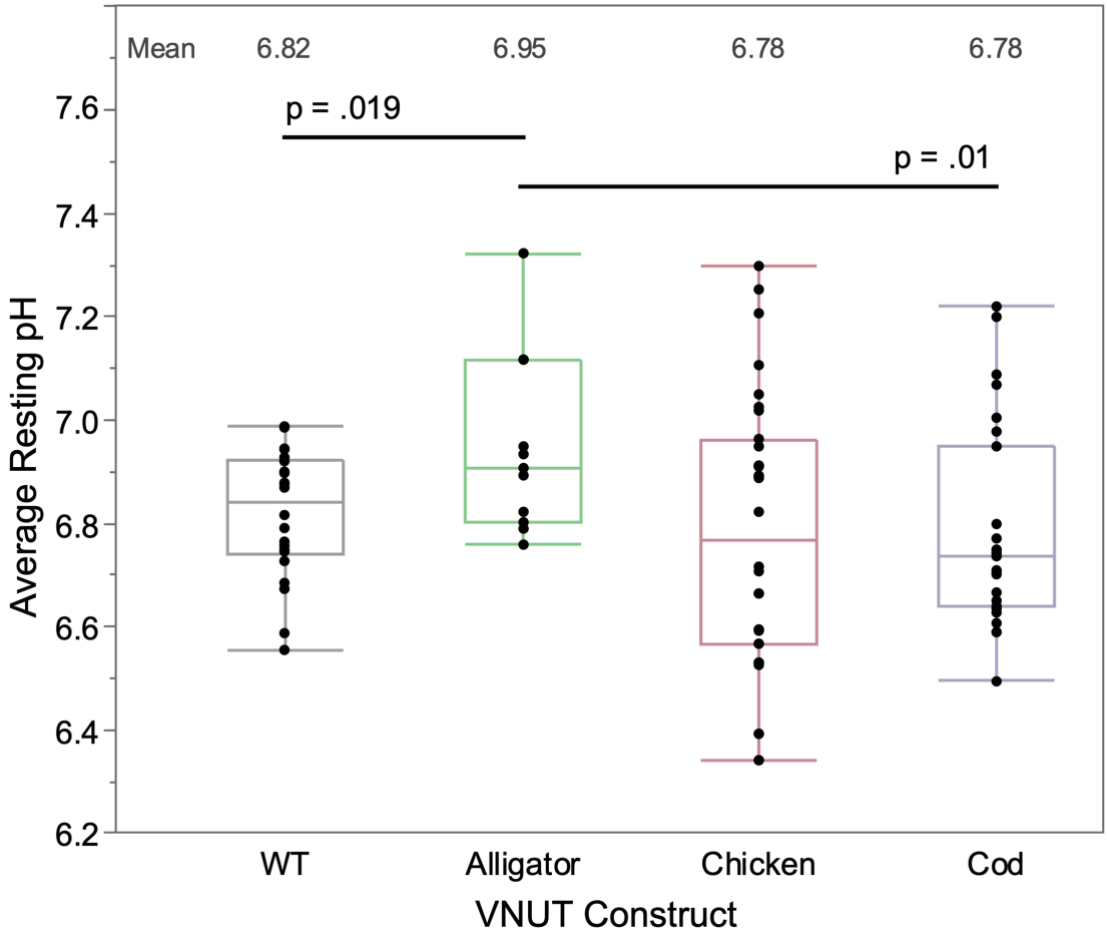

Figure 3.16: Average resting pH values for VNUT variants
This figure shows the pH levels of pHluorin-containing subcellular compartments across each VNUT C-terminus construct. Measurements were taken from N2a cells transfected with each VNUT variant in the presence of a HEPES buffered saline solution. Results show a significant change towards a more basic localisation of VNUT constructs with a reptilian C-terminus compared to that of a mammal or ray-finned fish. Each data point represents one cell, derived f rom five independent experiments.

To summarise, using pH-dependent fluorescent probes, we have measured fluorescent intensity from pHluorin-conjugated mammalian VNUT probes with either mammalian, reptilian, avian or ray-finned fish C-termini. Data

were extracted by taking the fluorescent values, normalising them against a fluorophore quenching and exciting agent, then calibrated to assign pH values to epifluorescence levels. The results indicate that a mammalian VNUT sequence with a reptilian C-terminus sequence localises to significantly more basic environments than if the C-terminal sequence matched that of a mammal or ray-finned fish. These results support the findings from fixed-imaging experiments, showing significant disruption to VNUT localisation in the presence of the Alligator C-terminus. These results have important implications for our understanding of the trafficking mechanisms of VNUT's terminal amino acids.

3.4. Summary

This chapter explored the role of VNUT's C-terminus in its subcellular localisation, with a particular focus on the evolutionary divergence in sorting motifs between mammalian and non-mammalian orthologues. Using bioinformatic analyses, we first compiled amino acid sequences of VNUT across the kingdom Animalia. Then, a motif search revealed expression patterns across species, mapped onto a phylogenetic tree to visually portray the evolutionary conservation and divergence of motifs. Bioinformatics analyses unveiled two predominant expression types within ray-finned fish: those with just tyrosine motifs, and those with both tyrosine and dileucine motifs. The conservation pattern was more consistent in reptilian and avian VNUT sequences, with strong conservation of both tyrosine and dileucine motifs. Mammalian orthologues display a conspicuous divergence from this norm, with very few sequences registering either motif. Rather, mammals may possess a KDEL-like sequence. However, the cargo-binding domain of a KDEL receptor is lumen-facing (Cabrera et al., 2003), while the mammalian KDEL sequence is cytosolic, so it is unclear whether they can interact.

This study took inspiration from previous research that utilised C-terminus chimeras between related neurotransmitter transporters to demonstrate the sorting efficacy of amino acid motifs and applied it across different species of

VNUT. The common chicken and burrowing owl were selected to represent Aves with a tyrosine and dileucine motif in their C-terminus. Trafficking of the mammalian-chicken VNUT chimera did not deviate from wild type across fixed or live microscopy analyses, whereas the mammalian-owl chimera showed elevated brightness levels in distal puncta, suggesting more copies of VNUT. Unfortunately, since the owl pHluorin construct did not generate viable bacterial colonies, the data is absent for this variant and does not allow for the corroboration of fixed-cell microscopy data for that construct at this date. The chinese alligator represented Reptilia, with a C-terminal dileucine and tyrosine motif. This chimera resulted in fewer distal VNUT puncta and a more basic localisation than wild type, suggesting the protein is not progressing through the secretory pathway at the same rate. The atlantic cod was selected to represented Actinopterygii with a C-terminal tyrosine motif and showed no significant deviation in localisation from wild type in either fixed or live cell analyses.

Live imaging analyses using pHluorins reveal the pH of VNUT-containing compartments is consistent with the ER and Golgi. These results are further corroborated by fixed-cell microscopy and correlational analyses which show a close relationship between VNUT and these organelles. In addition, the absence of signal quenching in response to MES across all variants highlights a lack of VNUT on the cell surface.

Collectively, these results indicate that the C-terminus is influential in determining the subcellular localisation of VNUT, yet it is probably not the sole mechanism driving its sorting. Indeed, it seems likely that mammalian VNUT localises to areas distinct from those of non-mammalian orthologues. However, with multiple mechanisms likely influencing their trafficking, it remains to be seen whether non-mammalian VNUT escapes the ER and Golgi to associate with synaptic vesicles or lysosomes, as is typical to proteins with their C-terminal motifs.

Discussion of these results within the context of the literature can be found in Chapter 5: Discussion and Future Directions.

Chapter 4. Identification of a Putative N-terminal ER-retention Sequence in the VNUT N-terminus

4.1. Rationale

Understanding the diverse mechanisms of protein trafficking within cells is crucial in the context of cellular processes, health, and disease. In addition to the C-terminus, the N-terminus often contains critical targeting motifs. This chapter expands the search for ER-Golgi retention motifs to the N-terminus of mammalian VNUT. The N-terminal sequence was a logical location to test for ER-Golgi retention motifs due to the known ability of N-terminal regions to direct protein trafficking, added to this was the disease-associated mutation of the ninth amino acid in humans from an arginine (R) to a cysteine (C), indicating a significant functional role at the site. Vesicles are frequently exchanged between the ER and Golgi. Retrograde transport vesicles are distinguished by a COPI coatomer complex. This complex plays a critical role in mediating the recycling of cargo back to the ER. The interaction between cargo and COPI is facilitated through binding to the alpha subunit of the coatomer, specifically at a region characterised by a beta-propeller structure. ER and Golgi resident proteins are often transported back to the ER through COPI vesicles (Cole et al., 1998), making this method a sensible route to investigate.

Previous research from the Poburko Lab (not published) shows that deletion of the entire mammalian N-terminus disrupts ER and Golgi localisation. Rather, N-terminally truncated VNUT appears to be lysosomal. This research seeks to uncover – and test the disruption of – a putative ER-retention sequence in the N-terminus of VNUT. The hypothesis is that disruption of VNUT N-terminal ER-retention sequence will decrease VNUT's localisation with the ER-Golgi complex.

To address this hypothesis, a cutting-edge AI-driven approach will be used to expedite the search for an ER-retention sequence. Scanning the residues for interactions with critical transport proteins, predicting the structure and co-folding of proteins to streamline the experimental process. Coupled with traditional molecular biology approaches, such as mutagenesis and fixed-cell microscopy, this research aims to dissect the role of a putative N-terminal ER-retention motif in VNUT's localisation.

4.2. Methods

4.2.1. Bioinformatics

Predicting Protein Interactions

Protein structures and intermolecular interactions between two target proteins were predicted using AlphaFold2 (Jumper et al., 2021; Varadi et al., 2022). Developed by DeepMind and the European Molecular Biology Laboratory (EMBL), AlphaFold uses artificial intelligence and machine learning to predict protein structures and interactions with high accuracy. The resulting predictions were visualised with the PyMOL Molecular Graphics System (Version 2.0 Schrödinger, LLC). Predicted binding energies and affinities of protein interactions were quantified using PRODIGY (PROtein binDing enerGY prediction) web service (Xue et al., 2016), which uses binding interactions identified by AlphaFold and models the resulting binding affinity.

4.2.2. Molecular Biology

Primer Design

EGFP-VNUT truncation primers were designed using NEBaseChanger v2.4.3 (New England BioLabs online tool). Primers were purchased from Integrative DNA Technologies (IDT).

Table 4.1: EGFP-VNUT N-terminus truncation primers

Construct name	5'-Forward-3' 5'-Reverse-3'	Truncation length (aa)
EGFP-VNUT ∆1-12	GAGGAGACCCGCAAGACC CATTCCGGTGCCACCGGA	12
EGFP-VNUT ∆1-17	ACCCCTTATGCGGCAGCA CATTCCGGTGCCACCGGAG	17

Site Directed Mutagenesis

All steps were followed as outlined in the NEB protocol for the Q5 Site-Directed Mutagenesis Kit (NEB, #E0554). Briefly, amplification of the pcDNA3.1-EGFP-VNUT backbone was performed using Q5 Hot Start High-Fidelity DNA Polymerase (New England BioLabs, # M0494) with 0.5 ng DNA and 0.5 µM forward and reverse primers. The PCR protocol is described in **Table** 4.2 **below**.

Table 4.2: EGFP-VNUT N-terminus truncation PCR protocol

Step	Temperature (˚C)	Time
Initial denaturation	98˚C	3 minutes
35 cycles:	98˚C	10 seconds
	69˚C (∆1-12 reaction) 72˚C (∆1-17 reaction)	30 seconds
	72˚C	5 minutes
Final extension	72˚C	2 minutes

PCR products were examined using the methodologies outlined in **3.2.2 Molecular Biology.** Kinase, Ligase & DpnI (KLD) Treatment followed the recommended protocol. DNA concentration was measured using a DeNovix DS-11 spectrophotometer.

Transformation

Expression vectors were transformed into NEB 5-alpha Competent *E. Coli* (New England BioLabs; #C2987) using NEB's heat shock transformation protocol

at shaken at 250 rpm for 60 minutes. Samples were then spread on agar plates (1% agar, Sigma Aldrich, #A1296) with 100 µg/ml ampicillin and SOC media (NEB, #B9020S), and incubated at 37˚C overnight.

Colony PCR

Colony PCR was performed using positive and negative conditions: the negative condition used a primer situated in the truncated region, which should not yield any product. The colony PCR protocol and gel electrophoresis were run according to the protocols outlined in 3.2.2: Molecular Biology, the only difference being the gel was run for 20 minutes. Clear amplicons of expected length were visible for the positive conditions, with no amplifications of the negative control, indicating all the tested colonies had the desired mutation.

Table 4.3: N-terminus truncations colony PCR primers

Condition	5'-Forward-3' 5'-Reverse-3'	Amplicon length (bp)	Primer ID
Positive	GGTGGGACGTCTATATAAGCA GAATGTCACGAAGGCCAG	477	PR00492 PR00466
Negative	CCATCCCAGCGCTCTAGC TAGAAAGACCAGTCCTTGCTGAAG	1440 - 1425	PR00424 PR00334

Plasmid Creation

Bacterial colonies were inoculated into foot cultures (3 mL) LB broth (Fisher Scientific, #BP1427-500) with 100 µg/ml ampicillin and shaken at 250 rpm and 37˚C for 8 hours before being expanded into overnight cultures (100 mL) and incubated for 15 hours. Subsequently, plasmids were isolated using the PureYield Plasmid Midiprep System (Promega; #A2492) and then stored at -20°C until transfection.

4.2.3. Cell culture

Methodologies are described in detail in section 2.2: Cell Culture.

4.2.4. Fixed Imaging

Sample Preparation

Fixed-cell sample preparation followed the methodologies described in section **2.3: Fixed Cell Imaging.** Images were captured at 200 nm Z-steps.

4.2.5. Image analysis

Correlational and puncta analyses were conducted in accordance with the methods outlined in EGFP Analyses within **Section 3.2.5: Image Analysis.** An additional measurement of the Golgi:ER signal ratio was measured in this section of the thesis.

Golgi:ER Ratio

This measurement was used to investigate whether the retrograde transport of VNUT from the Golgi apparatus to the ER had been diminished following N-terminus truncations, determining the ratio of VNUT signal held within the Golgi versus the ER. ROIs of approximately equal size were hand-drawn around subcellular regions expressing mDsRed-Golgi-7, a medial Golgi protein, and mTag-BFP-ER-5, an endoplasmic reticulum marker, as shown in **Figure** 4.1. A custom-built FIJI macro ‘measureAllChannelsWithMatchedROIs 2.4.3’ extracted fluorescence intensity levels of VNUT within the Golgi and ER ROIS for each cell, which was then compiled into a data table.

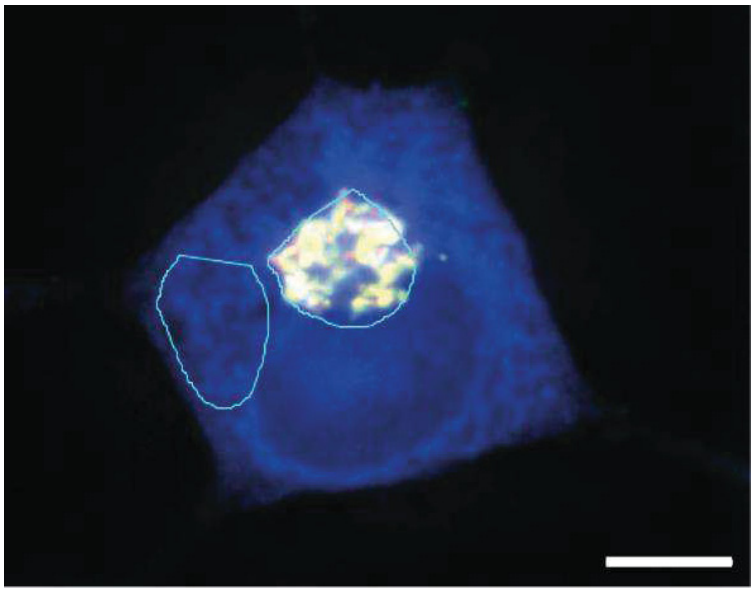

Figure 4.1: N2a ER and Golgi ROIs
An example of ROIS drawn by hand around the Golgi apparatus (white) and the ER (blue). ROIs are shown in teal.

4.2.6. Data Analyses

Data analyses for the correlational and puncta-based methods of image analysis were conducted in line with the methodologies outlined in 2.5.6: JACOP.

4.2.7. Statistical Analyses

Statistical analysis of JACOP-based correlational data, Golgi:ER ratio data and MINER-derived puncta localisation data followed the non-parametric methodologies outlined in 2.6.3 Statistical Analyses.

4.3. Results

This section describes the data surrounding the hypothesis that disruption of a putative VNUT N-terminal ER-retention sequence will decrease VNUT's localisation with the ER-Golgi complex. Our investigation sought to uncover the role of a five amino acid sequence in the mammalian N-terminus. We modelled the binding affinity of the motif with the retrograde transport vesicle coatomer,

COPI, focussing on the cargo-binding domain. We then took an EGFP—tagged mammalian VNUT sequence and created variants with truncations at key segments to isolate the effect of the motif on VNUT's retention in the ER-Golgi complex. Truncations were designed to flank the motif so that a three-way comparison could be made between WT, truncation with motif intact, and truncation with motif removed. Truncated variants were expressed in mouse N2a cells, providing a model to explore subcellular localisation precisely using epifluorescence microscopy. Our data exploration methods allowed us to achieve sub-diffraction resolution to analyse VNUT and detect changes in trafficking patterns.

4.3.1. Bioinformatics

There is well-documented evidence for the role of the N-terminus in directing protein trafficking. Cytosolic N-terminal motifs are essential for the accurate trafficking of several transporter proteins (Mikros & Diallinas, 2019). The diacidic DE motif has been linked with retention in the Golgi apparatus (Gao et al., 2014). In our search for trafficking motifs, we tested the N-terminus of VNUT for the evolutionary conservation of clusters to direct our search. Once identified, we tested the efficacy of motifs using AI-driven protein folding prediction software and quantified predicted binding affinities to direct experimental testing.

A functionally important motif would be expected to be highly conserved, so we began by analysing the N-termini of mammalian VNUT for conserved patterns. Figure 4.2 displays the N-terminal sequences of representative and common mammals. Sequences with unusually long or varied N-termini were omitted from the alignment. Mammalian VNUT orthologues show higher levels of variation between their N-terminus than the rest of the sequence (Sawada et al., 2008). However, a clear pattern emerges in Figure 4.2 of a highly conserved five amino acid DEXXR motif.

Figure 4.3 highlights the human and rat sequences individually. The human VNUT has two isoforms: Isoform 1 is 436 amino acids in length, while

isoform 2 is 430. Deviations occur only in the N-terminus, with isoform 2 exhibiting a condensed N-terminus. Most notable is the absence of the DEXXR motif and the prolines before it.

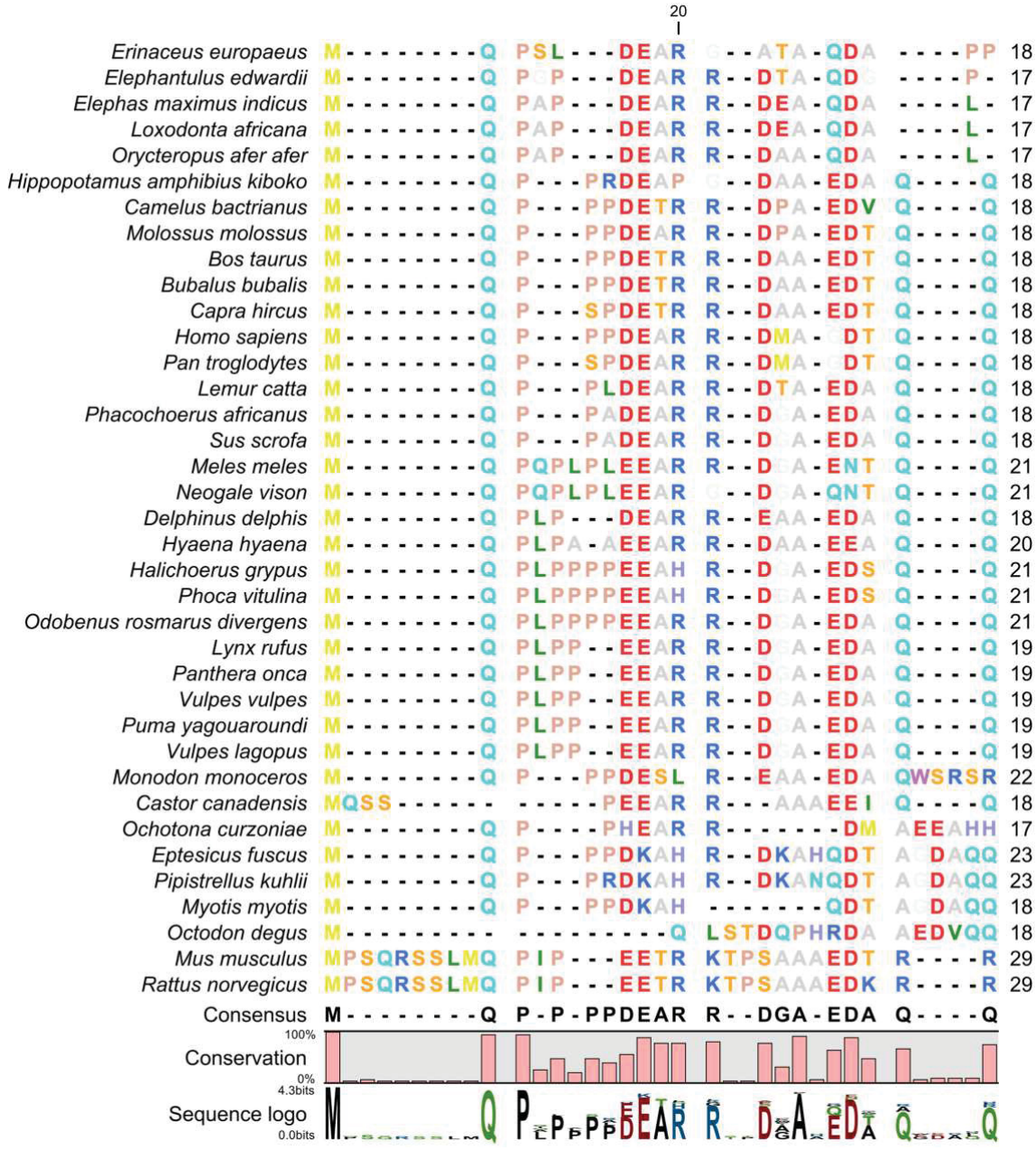

Figure 4.2: Evolutionary conservation of the Mammalian VNUT N-terminus
This figure illustrates the N-terminal amino acid sequence of the VNUT N-terminal sequence across a range of mammals. The highly conserved DEXXR motif is characterised as having two acidic residues at the start and ending in two positively charged. Residues are coloured in accordance with the RasMol standardised colour scheme. The consensus sequence is at the bottom of the figure. The conservation is mapped as a percentage and sequence logo defining the prominent amino acids.

Figure 4.3: Comparative alignment of VNUT N-Terminus between human and rat

Isolation of human and rat VNUT N-terminal sequences, showing N-terminus. Created in CLC genomics software; residues are coloured by RasMol standards.

Moreover, the region with the highest levels of conservation in the mammalian N-terminus matches an ER-Golgi recycling DE motif. We show that the key residue in R9C mutation associated with POROK8 is the second positively charged amino acid in the motif. This, coupled with its strong conservation, made the region a promising candidate to pursue. Next, I set out to test whether there could be an interaction between the N-terminus and ER-Golgi trafficking mechanisms.

We examined the predicted interactions between VNUT and αCOPI using AlphaFold. The software can predict protein-protein interactions by determining how amino acid residues interact within their spatial environment to fold into three-dimensional structures. This includes the capacity to accurately predict the interaction dynamics between two proteins.

To manage computational constraints, our modelling was limited to the interactions between VNUT and the cargo-binding β-propeller of αCOPI. The output was visualised as a 3D-rendered graphic in PyMol, as depicted in panel A of Figure 4.4. Notably, the N-terminus of VNUT is predicted to be in contact with αCOPI, suggesting this region facilitates Golgi-ER retrograde transport. Additionally, modifications to the N-terminus, within the putative motif disrupt this interaction. Panel B shows the mutation at the 9th residue associated with the disease POROK8. This change is sufficient to change the structure of the N-terminus and cause a conformational change between the two proteins. The same effect can be seen in panel C in response to the deletion of the DEXXR motif, as is characteristic of the Δ1-17 variant. From these observations, we can

infer there is likely an ER-retention sequence in the N-terminus of VNUT. Interestingly, the C-terminal KDEL-like sequence interacts with αCOPI, too, suggesting a non-KDEL receptor retrieval role of the C-terminus.

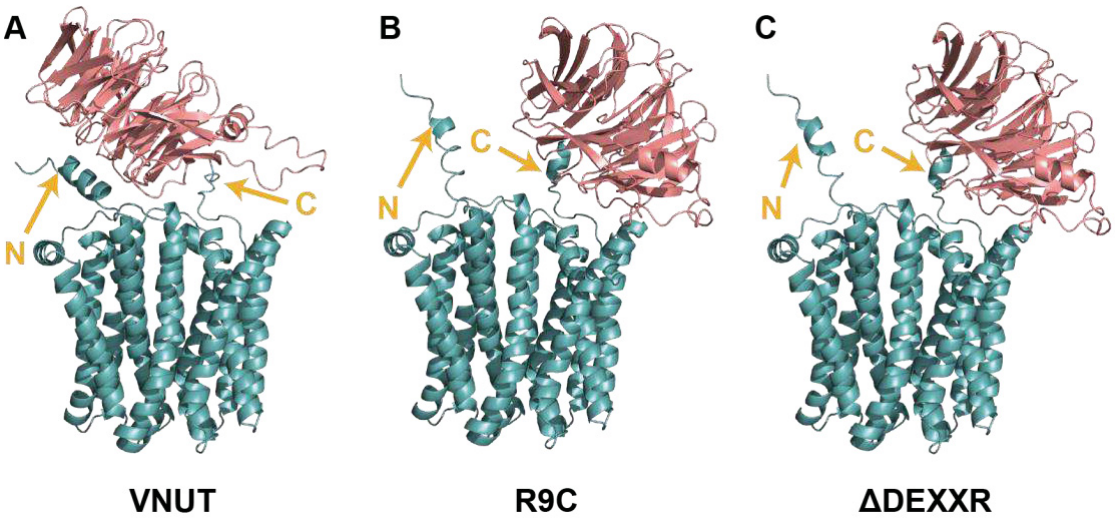

Figure 4.4: Protein folding predictions between αCOPI and human VNUT with N-terminal modifications

This figure depicts the predicted folding of αCOPI β-propeller subunit and VNUT with N-terminal modifications. αCOP is shown in pink and VNUT in teal. A. The predicted folding shape of αCOPI and intact VNUT. B. αCOPI folded with disease variant VNUT where the 9th residue is mutated. C. αCOPI folded with VNUT where the DEXXR motif is omitted. The figure was created using AlphaFold2 and PyMol.

The top five AlphaFold2-predicted interaction conformations between αCOPI and VNUT were quantified by submitting the AlphaFold2 output to PRODIGY server, where the binding affinity was calculated between the two proteins. A series of N-terminal Alanine substitutions were modelled alongside the R9C disease mutation to dissect which residues showing the greatest efficacy in binding to αCOPI. Each residue in the sequence was substituted independently with an alanine, and then clustered with neighbouring substitutions to assess whether any changed in binding affinity could be attributed to individual residues or a sum of all the changes. Figure 4.5 shows the predicted changes in binding affinity of N-terminal mutations of VNUT. The X axis is a logarithmic scale showing the change in dissociation constant (K_d) in comparison to the normal

sequence. All substitutions resulted in a lowered binding affinity, highlighting the importance of each residue in the motif.

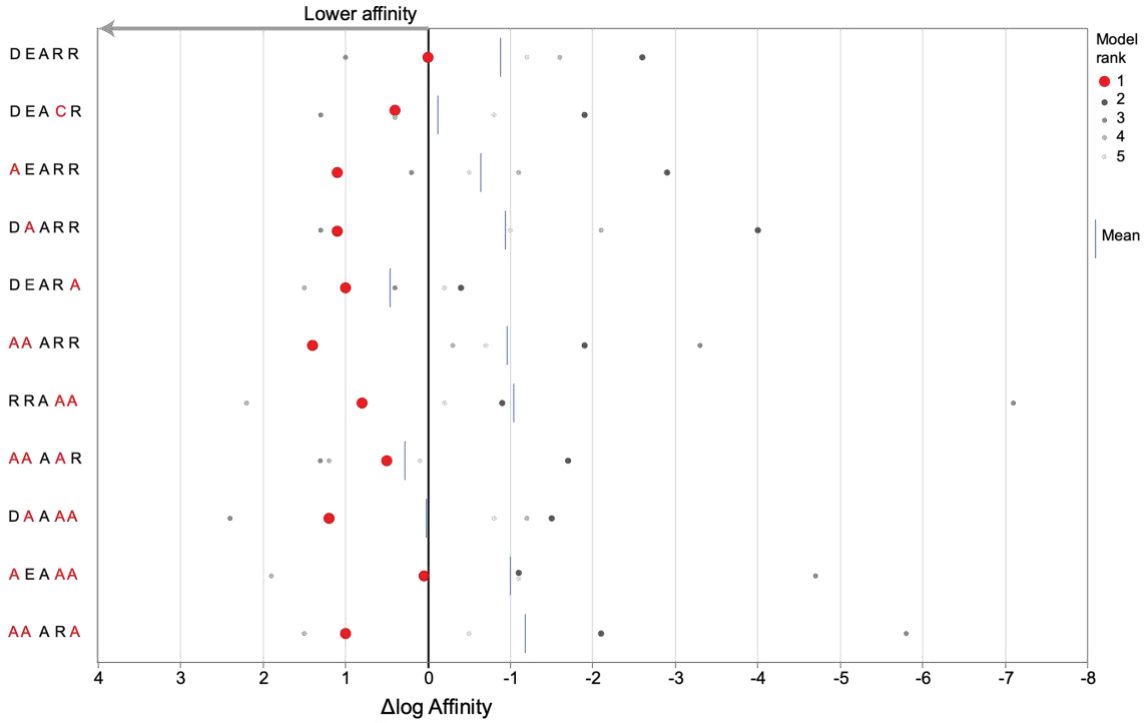

Figure 4.5: Changes in αCOPI-VNUT binding affinity due to N-Terminal alanine substitutions

This figure illustrates the effects of alanine substitutions at each position within the N-terminus of VNUT on its binding affinity to αCOPI. The y-axis represents the position of substitution, and the x-axis displays the logarithmic scale of change in binding affinity relative to the normal sequence. Positive values indicate lower binding affinity.

Since the DEXXR motif is conserved throughout mammals, we then translated these findings into the rat sequence to align with the epifluorescence tools used by the Poburko lab. There is no sequence variation between rat and human αCOPI, however rat and human VNUT N-termini show some differences as outlined in Figure 4.3

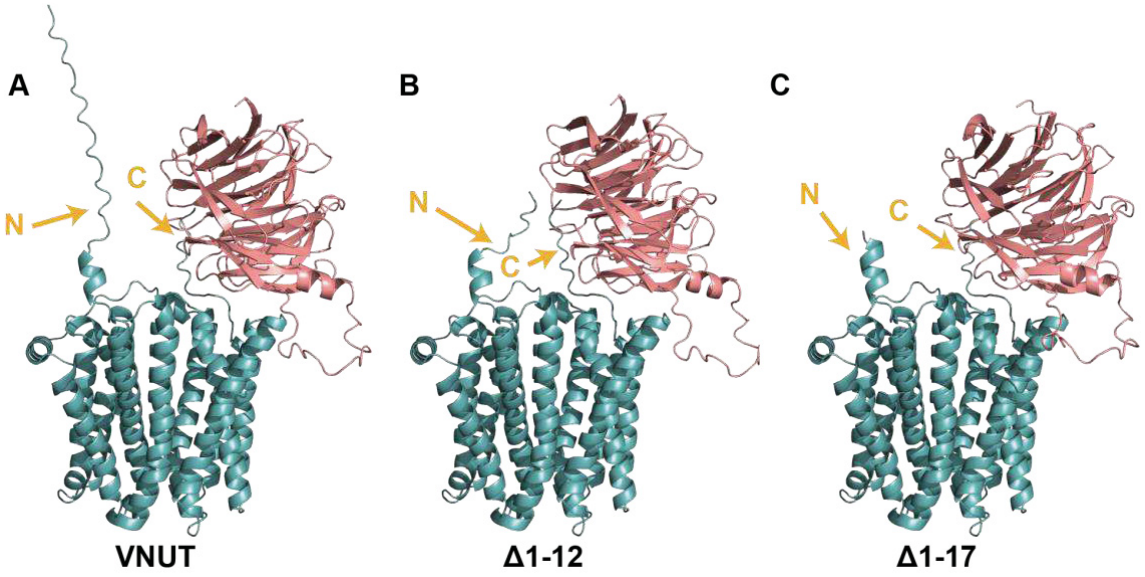

Figure 4.6: Protein folding predictions between αCOPI and rat VNUT with N-terminal truncations

AlphaFold2 and PyMol predictions of rat VNUT interactions with rat αCOPI. WT VNUT has a long N-terminus which interacts with αCOPI. When the first 12 amino acids are truncated, the N-terminus has a closer interaction with αCOPI. Deletion of 17 amino acids reduces the interaction.

Figure 4.6 illustrates the predicted folding of rat αCOP and VNUT in panel A. Panels B and C show the change in αCOPI binding in response to N-terminal truncations. The N-terminus appears to have the strongest interaction with αCOPI when the tail is truncated. Truncation of the DEXXR sequence, by removal of 17 amino acids, appears to disrupt the bond between N-terminus and αCOPI. The WT N-terminus appears rather long, which perhaps interferes with the binding ability of the motif to αCOPI.

αCOPI and VNUT binding affinities are quantified in Figure 4.7. Most striking here is the increase in interactions between VNUT-Δ1-12 and αCOPI. Deletion of the first 12 amino acids is predicted to cause a greater interaction between these two proteins. Conversely, the Δ1-17 truncation is predicted to cause a slight decrease in the interaction between VNUT and αCOPI. The large difference in binding affinity from Δ1-12 suggests a vital role in the DEXXR motif for αCOPI binding. Deletion of the first 12 amino acids appears to facilitate the action of the motif, while its deletion appreciably reduces the bond.

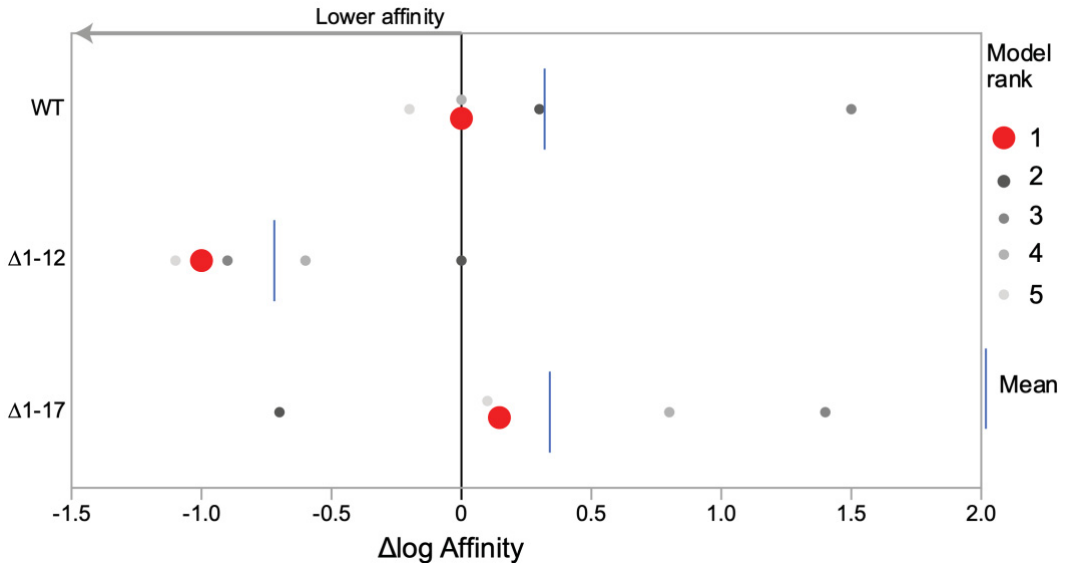

Figure 4.7: Changes in predicted αCOPI-VNUT binding affinity following N-terminal truncations

The modelled effects of N-terminal truncations of rat VNUT on its binding affinity (Kd) with αCOPI. Δlog Affinity measures the change in binding affinity on a logarithmic scale from WT as the baseline. The five best models from AlphaFold2 are plotted, with rank 1 being the conformation of highest confidence. Negative values indicate an increase in binding affinity.

To summarise, by modelling the protein dynamics between VNUT and αCOPI, we can surmise there is compelling evidence for the role the N-terminus plays in VNUTs subcellular localisation, specifically within the ER-Golgi transport pathway. The discovery of a highly conserved DEXXR motif, characterised by its acidic and positively charged residues, emphasises the importance of this region. Our AI-driven methods to predict the co-structure and interactions between VNUT and αCOPI reveal how modifications to this region may disrupt retrograde transport. These models were useful in streamlining our focus during *in vitro* experiments using rat VNUT with Δ1-12 and Δ1-17 truncations.

4.3.2. Fixed Cell Microscopy

Building upon the computational modelling, this section explores the subcellular localisation of VNUT with N-terminal truncations. EGFP-conjugated VNUT was truncated before and after the putative ER-retention sequence. These truncations are displayed diagrammatically in Figure 4.8. The constructs were transfected in mouse N2a cells before inspection against fluorescently labelled organelles.

Figure 4.8: Sequence alignment of VNUT N-terminal truncations in EGFP-VNUT

A diagram representing Rat VNUT N-terminus truncation constructs that were created for these experiments.

As in the C-terminus experiments, N2a cells were co-transfected with a red fluorescent Golgi marker and a blue ER marker. Cells were again differentiated before fixation and microscopy. Images were deconvolved to enhance the resolution of the puncta and reassign out of focus light. Representative images from each construct are shown in Figure 4.9. Images from the Δ1-12 construct are different from WT and Δ1-17; Δ1-12 expressing cells show more VNUT puncta throughout the cytosol. A few puncta can be seen towards the periphery of the cell in WT cells, as was the case for C-terminal experiments. There seems to be a general trend away from peripheral puncta in Δ1-17 expressing cells, with VNUT more localised to the Golgi.

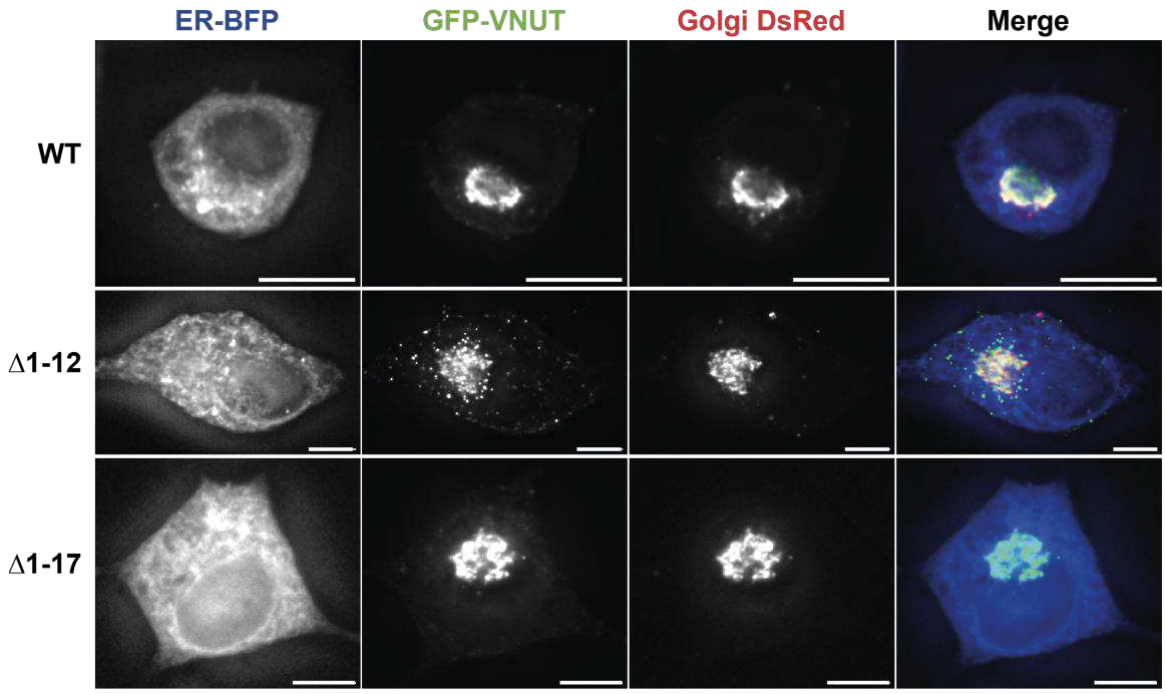

Figure 4.9: Comparative co-localisation of VNUT N-terminus variants with ER and Golgi markers

Representative microscopy images show VNUT N-terminus distribution relative to ER and Golgi markers. All scale bars are 5 μm.

Following the established image processing pipeline outlined in C-terminal experiments, co-localisation analyses began with correlational studies using the JACOP plugin in FIJI. Hand-drawn ROIs around the cell borders constrained Pearson's correlational values to assess within the cell body. Results are illustrated in Figure 4.10. Signal dispersion was measured for VNUT against four organelles: Hoescht33342, a nuclear stain, ER-BFP, DsRedGolgi and LAMP1-RFP, a lysosomal protein. In this case, Hoescht is an example of anti-colocalisation. VNUT does not localise to the nucleus, however, puncta may have been located at the apical surface. The z-slices of images were merged together as part of the image analysis process so that puncta were not spread across several slices. Any VNUT puncta located in a z-slice apical of the nucleus will have that z-position removed, and the puncta would appear within the bounds of the nucleus.

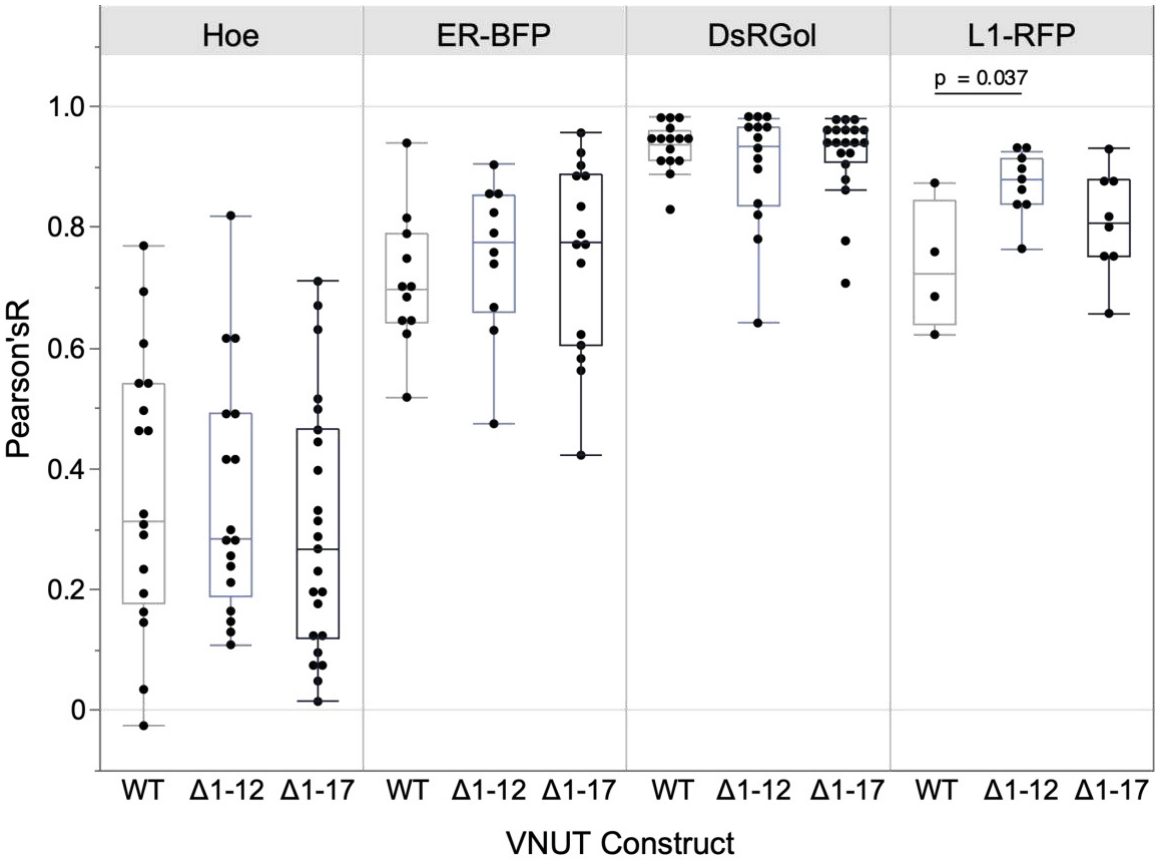

Figure 4.10: Correlational analysis of VNUT N-Terminus variants with subcellular organelle markers

The correlation between VNUT localisation and organelles is indicated by Pearson's correlation coefficients between 0 and 1. 3 independent biological replicates, each data point representing one cell.

The correlational data do not meet the assumptions of normality, so a non-parametric Kruskal-Wallis ranked rum test was used with a Wilcoxon pair-wise analysis to tease apart significant changes. According to the correlational analyses, there is no marked difference in nuclear localisation between any N-terminal variant. Again, there is no significant change in localisation against the ER and Golgi markers. A small dataset included LAMP1 co-transfection with VNUT variants. The dataset is too small to draw compelling conclusions from; however, it is worth noting that there is significantly more lysosomal localisation of VNUT with the first 12 amino acids truncated, though the dataset is small.

The purpose of the next analysis is to isolate the trafficking between the Golgi apparatus and ER. Examining the ratio of VNUT signal located with a section of Golgi versus that of the ER provided an insight into whether there was a change in accumulation in either organelle due to N-terminal truncations. A decrease in retrograde transport would likely lead to more VNUT accumulating in the Golgi compared to the ER and the normal transport routes are diminished.

Equal sized ROIs were drawn around regions of the cells clearly expressing Golgi or ER markers. Next, the mean fluorescent intensity of VNUT in those ROIs was measured in FIJI and output into a data table. The results can be found in Figure 4.11. Panel A shows the ratio of signal within the Golgi over the signal in the ER. The mean Golgi:ER VNUT signal ± 1SD is 4.5 ± 2.1, 3.7 ± 1.6, and 4.2 ± 1.3 for WT, Δ1-12 and Δ1-17 respectively. These data were assessed using Kruskal-Wallis and Wilcoxon pairwise analyses, which found a significant increase in Golgi:ER signal in Δ1-17 compared to Δ1-12. This suggests there is more VNUT in the Golgi than in the ER in the absence of residues N-terminal to the DEXXR motif. Next, I sought to uncover where the change in signal ratio originated. Panel B of Figure 4.11 deconstructs the VNUT signal location in the ER and Golgi for each variant. Absolute fluorescence intensity values using pixel intensity recorded from our 16-Bit camera. The average brightness intensities ± SD for VNUT WT are 4,487 ± 5,679 and 17,579 ± 16,115 for ER and Golgi signal; 7,814 ± 8541 and 20,239 ± 15,110 for ER and Golgi signal in Δ1-12; finally, 1,718 ± 1,296, and 7,500 ± 7,033 for the Δ1-17 ER and Golgi signal. Evidently, the VNUT signal is significantly lower in Δ1-17 than its counterparts, which may contribute to the different ratios. Both ER and Golgi signal is significantly lower for the Δ1-17 construct than Δ1-12. Moreover, The Golgi signal in Δ1-17 is significantly lower than that in WT. While there seems to be an effect of lower expression rates in the Δ1-17 variant, there is still an important reduction in ER localisation.

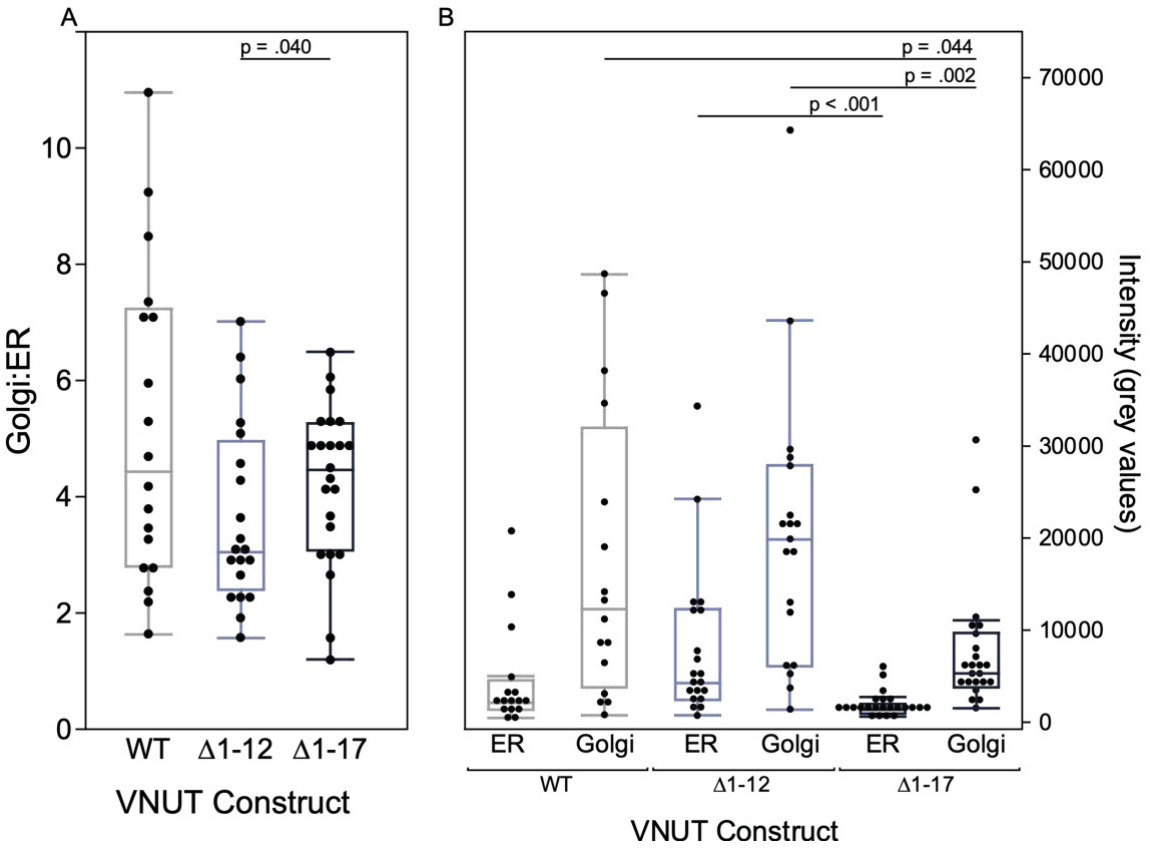

Figure 4.11: VNUT Localizationsin ER versus Golgi Across N-Terminal Variants

VNUT fluorescence intensity within the Golgi and ER compartments across different N-terminal variants. Panel A displays the ratio of Golgi to ER signal. The ratio of VNUT in the Golgi versus the ER is significantly lower in the DEXXR deletion variant (p = .040). There was no significant difference between WT and Δ1-12 (p = .0123) or Δ1-17 (p= .972). Panel B shows absolute fluorescence intensities for VNUT within the ER and Golgi. DEXXR deletion leads to a significantly less intense VNUT signal in the Golgi than in both Δ1-12 and WT and less in the ER compared to Δ1-12.

Delving into puncta-based analyses, the same cell soma ROIs were used in conjunction with RIPA and MINER FIJI plugins to analyse subtle changes to localisation. Using the RIPA plugin, puncta were systematically identified and labelled with ROIs, then fed into the MINER plugin, which measured the distance from the centre of each punctum to the nearest point on the cell border, as defined by the cell soma ROIs. Puncta close to the perimeter were once again isolated for these analyses, which used the same methodologies as C-terminal puncta analyses. First, an Onion-peel analysis revealed the distributions of VNUT

puncta within 2.5 µm of the cell perimeter. Slices of 250 nm were augmented, and punctuation within each slice was calculated. The average number of puncta within each slice is mapped against each construct in Figure 4.12. The trend shows a decrease in perimeter puncta in cells expressing Δ1-17 compared to WT, but an increase in peripheral puncta in those expressing Δ1-12. The dispersal of puncta convergences to similar levels at 2.5 µm from the perimeter.

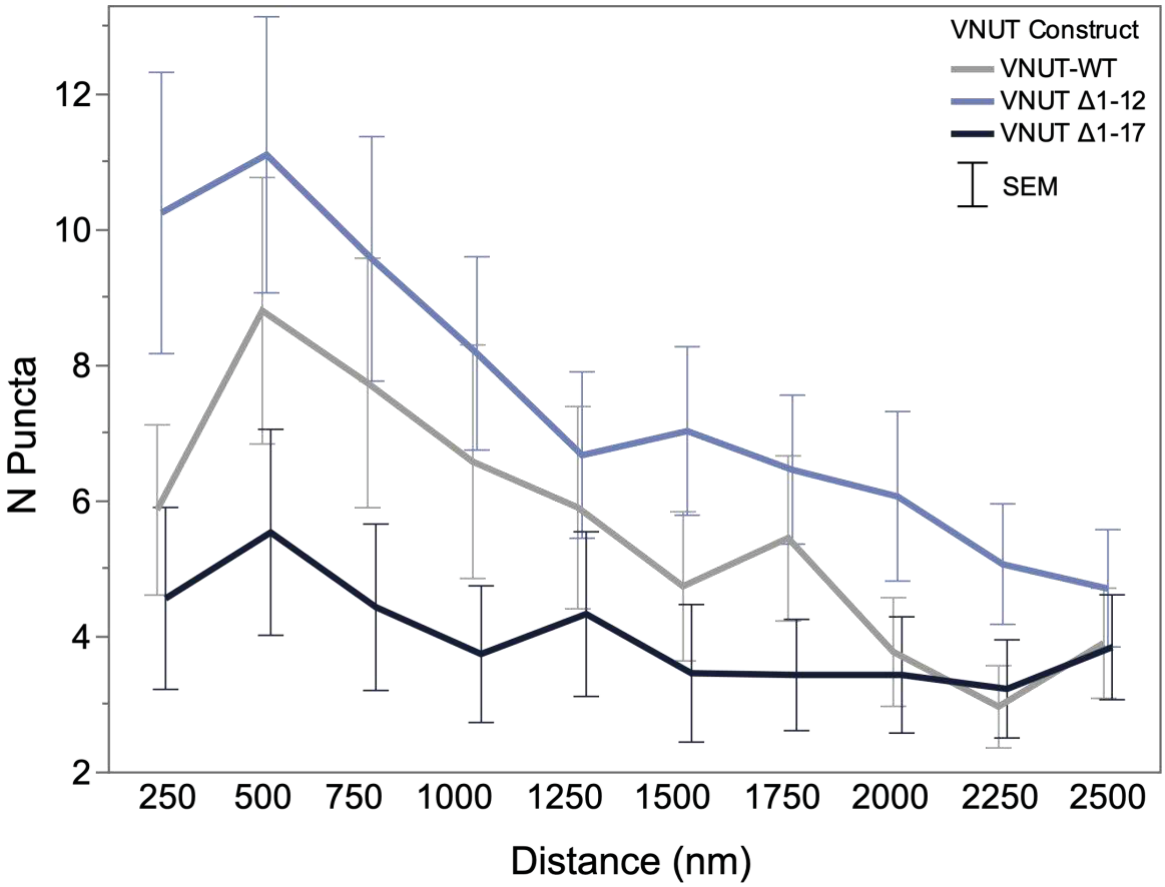

Figure 4.12: 'Onion-peel' Analysis: Distribution of VNUT N-Terminus Variants Near Cell Perimeter

The distribution of VNUT-containing puncta proximal to the cell membrane is analysed in concentric 250nm slices, revealing alterations in peripheral localisation associated with different N-terminal truncations. The analysis included three biological repeats (WT n = 31, Δ1-12 n = 28, Δ1-17 n= 39 cells).

Designation of a 500 nm perimeter zone enabled us to analyse puncta that are more likely to be closely associated with the plasma membrane at the periphery of the cell soma. The number of puncta within 500 nm from the cell

perimeter was calculated and graphed in Figure 4.13 as a raw number. The mean peripheral puncta in WT cells were 15 ± 17, 21 ± 21 for Δ1-12 and 10 ± 17 for Δ1-17. These data were analysed with nonparametric Kruskal-Wallis and Wilcoxon pairwise analyses to reveal a significant difference ($p = .008$) between the number of Δ1-12 and Δ1-17 puncta migrating towards the cell membrane. Fewer Δ1-17 puncta were peripherally located. Again, there is an opposing effect with Δ1-12 and Δ1-17 when compared to WT VNUT, highlighting the effect of the DEXXR motif and VNUT trafficking. These data were normalised against the size of the cell to account for the higher number of puncta to be expected at the periphery of a larger cell. The results can be found in Figure 4.14.

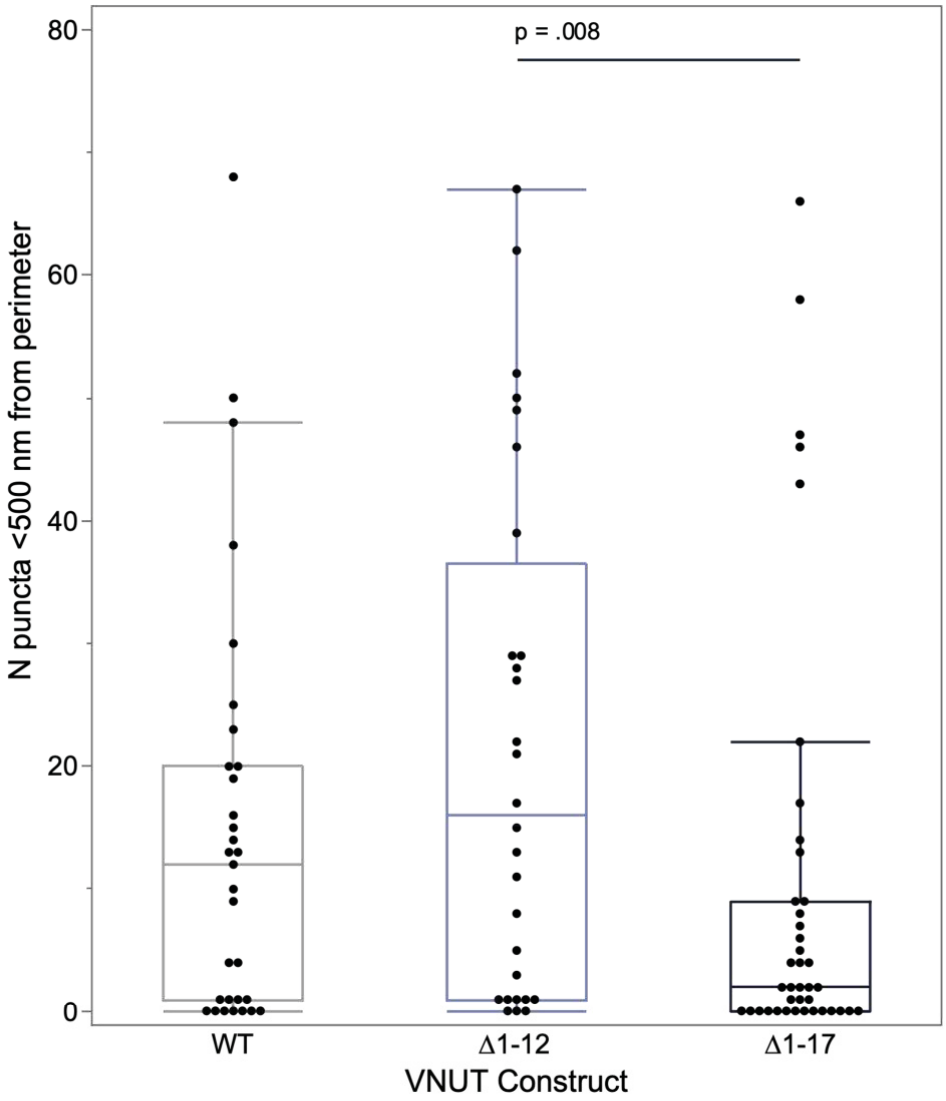

Figure 4.13: Quantifying VNUT N-Terminus Variant Localisation Near the Cell Membrane

The number of VNUT puncta located within 500nm of the cell membrane, comparing wild-type and N-terminally truncated variants. There is aa significant difference in membrane-proximal puncta between Δ1-12 and Δ1-17 variants.

Mean counts for WT, Δ1-12 and Δ1-17 were 0.27 ± 0.28, 0.40 ± 0.37, and 0.16 ± 0.25. Normalised measures for perimeter puncta show a similar trend: an opposing effect of Δ1-12 and Δ1-17 when compared to WT. There were significantly fewer puncta within 500 nm of the perimeter in cells expressing Δ1-17 than Δ1-12 ($p = .008$). There were no significant differences between WT and Δ1-12 ($p = .185$) or Δ1-17 ($p = .087$) conditions. These data were measured non-

parametrically using the same methods outlined previously.

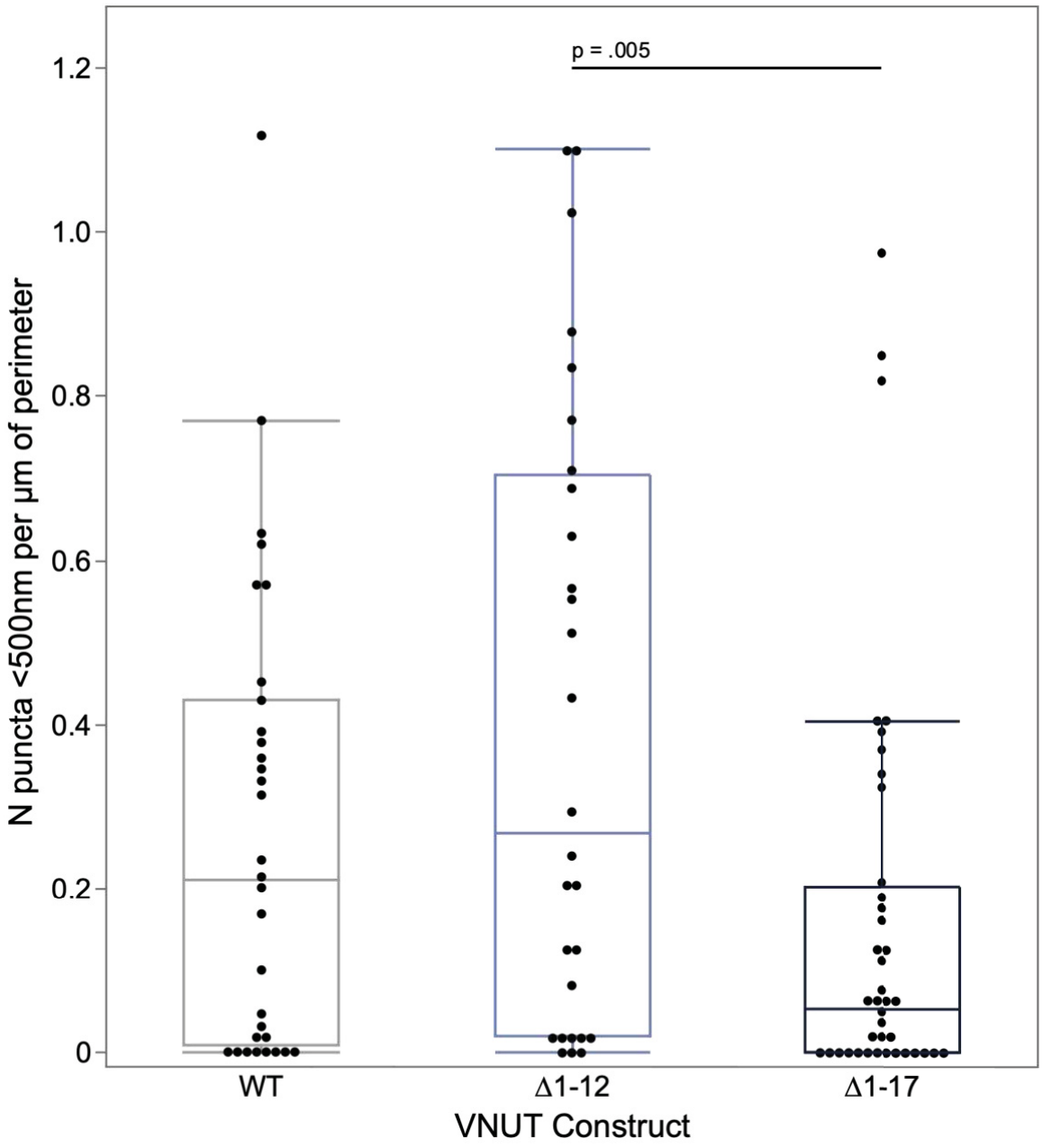

Figure 4.14: Perimeter-Localised VNUT Puncta Density by N-Terminus Variant.

Normalised data showing the frequency of VNUT puncta near the cell surface per micron of cell perimeter for each N-terminus variant.

As with C-terminal analyses, we can use puncta brightness as a further measure to discern the quantities of VNUT at the cell perimeter. Ranging from 0 to 65,535 as before, these values support the previous findings. Mean intensities

were 12,731 ± 10,714, 16,513 ± 15,661, 9,030 ± 6,655 for WT, Δ1-12, and Δ1-17 respectively. Following non-parametric assessment, the results show a significant decrease in puncta brightness at the cell perimeter for Δ1-17 variants compared to Δ1-12. There is no significant effect against WT. This suggests that the VNUT-containing compartments in Δ1-12 expressing cells have more instances of VNUT.

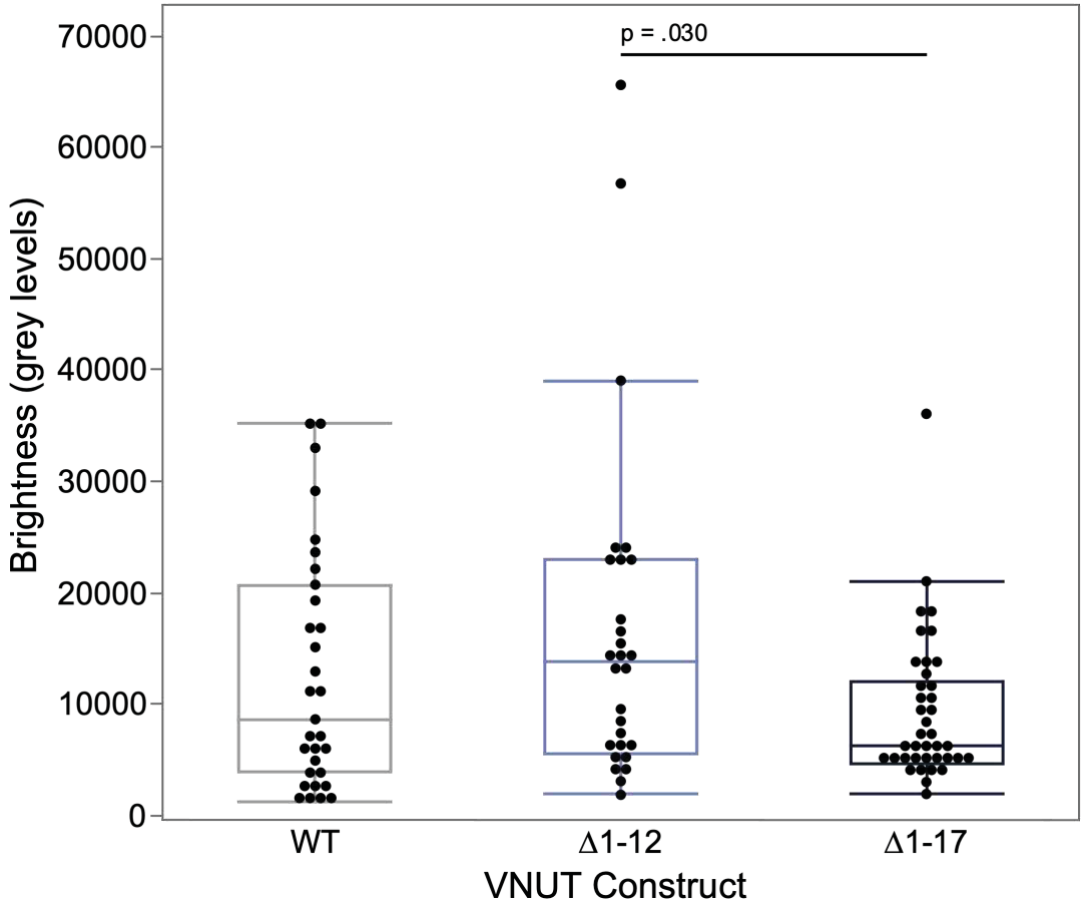

Figure 4.15: Intensity of VNUT-Containing Puncta Close to Cell Membrane Across N-Terminus Variants

This figure compares the fluorescence intensity of VNUT puncta near the cell membrane across variants using pixel values on a 16-Bit camera. There is a significant change in average puncta intensity between Δ1-12 and Δ1-17 (p = .030).

Finally, a comparative analysis measured the area of cell bodies and puncta to assess whether there were any differences in the size of the puncta or cell as a result of the cells expressing either VNUT variant. Data were analysed with Kruskal-Wallis and Wilcoxon pairwise analyses and it was concluded that

there were no significant differences to the morphology of the cells or puncta that arise from N-terminal truncations (see Figure 4.16).

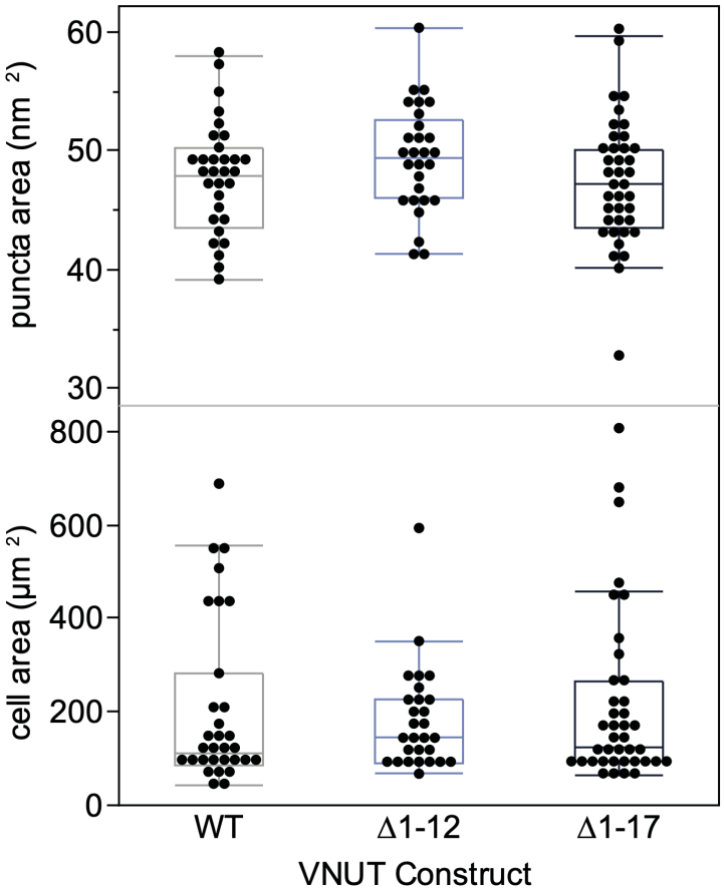

Figure 4.16: Comparative Analysis of Cell and Puncta Size Among VNUT N-Terminus Variants

The effect of N-terminal truncations on the morphology of cells and the size of VNUT-containing puncta. No significant differences.

4.4. Summary

This chapter has explored the N-terminus of mammalian VNUT for additional sorting motifs. Our approach used bioinformatic analyses to identify a highly conserved DEXXR sequence. We used AlphaFold2 to model the combined folding of VNUT with the cargo-binding domain of αCOPI and found an interaction. We then used the same model to predict how alterations to the DEXXR motif would impact VNUT's binding to αCOPI. In the human sequence, the R9C disease mutation was predicted to weaken the interaction of the two

proteins. Similarly, the substitution of any of the residues for alanine was predicted to weaken the interaction, suggesting the five residues constitute an ER-retention motif.

Testing the function of the motif began by examination of the rat sequence, predicting the interaction between VNUT and αCOPI following N-terminal truncations. Truncation of the twelve residues prior to the DEXXR sequence was predicted to increase the binding affinity between VNUT and αCOPI. In contrast, truncation of the first seventeen residues, including the DEXXR motif, was predicted to reduce αCOPI interaction. EGFP-tagged Δ1-12 and Δ1-17 constructs were created and transfected into N2a cells to assess their localisation. Both constructs colocalised strongly with the Golgi apparatus and endoplasmic reticulum. Δ1-12 showed elevated lysosomal localisation in a limited sample of cells. Additionally, the ratio of VNUT signal within the Golgi to the ER was higher in cells expressing the Δ1-17 VNUT than the Δ1-12, suggesting a disruption to retrograde transport when the DEXXR motif is removed.

Interestingly, more Δ1-12 VNUT was peripherally located than Δ1-17. Cells expressing Δ1-12 VNUT showed increased number and fluorescent intensity of distal puncta, whereas Δ1-17 VNUT resulted in fewer and less bright puncta. Neither were statistically different than wild type. However, this is surprising, given that Δ1-12 is predicted to have a stronger binding affinity to αCOPI.

The pattern of VNUT and αCOPI binding affinity between wild type, Δ1-12 and Δ1-17 reflects the change seen in distal puncta number and intensity between the three proteins. This corroborates the predicted αCOPI interaction as likely causing the change in VNUT trafficking. From this, we can surmise that the N-terminus of VNUT impacts its correct sorting through a DEXXR motif binding to αCOPI. The increase in distal Δ1-12 puncta is curious, suggesting some of these puncta could be αCOPI-associated.

Chapter 5. Discussion and Future Directions

This thesis is centred around purinergic signalling, exploring the mechanisms of VNUT-mediated vesicular ATP release in neuronal cells. Vesicular ATP is vital for a wide variety of cellular functions, including neuro- and gliotransmission, immune responses, inflammation and insulin secretion (Coco et al., 2003; Lalo et al., 2016; Linden et al., 2019; Pangršič et al., 2007; Sakamoto et al., 2014).

Little is known about the subcellular localisation of VNUT and where it loads ATP into vesicles for release as a neurotransmitter or co-transmitter. Colocalisation assays using endogenous VNUT expression and fluorescent subcellular markers have provided conflicting conclusions. This research aims to take a fresh approach, drawing upon protein engineering techniques used on related solute carriers to uncover their sorting motifs. Understanding the genetic determinants of VNUT's trafficking will provide a robust framework to draw conclusions about its subcellular localisation and pave the way to understanding the loading and release mechanisms of vesicular ATP as a neurotransmitter and co-transmitter. In the future, this knowledge can be used to facilitate the development of novel therapeutic targets for a wide range of diseases with minimal side effects.

The primary objective of the research is to determine whether the mammalian VNUT sequence contains a functional amino acid motif in either terminus that leads to its retention in the ER-Golgi complex. This research is divided into two sections. The first hypothesis focuses on the C-terminus of VNUT and states that replacing the mammalian VNUT C-terminus with non-mammalian counterparts that contain dileucine and or tyrosine motifs will reduce VNUT and ER-Golgi complex co-localisation. The second hypothesis posits that disruption of the VNUT N-terminal ER-retention sequence will decrease VNUT's localisation to the ER.

5.1. Identification of Amino Acid Motifs in VNUT's Termini

Bioinformatics analyses of the C-terminal sequences in VNUT have delineated a distinct phylogenetic pattern: non-mammalian species predominantly exhibit dileucine and/or or tyrosine motifs, whereas these motifs are conspicuously absent in mammals, which instead display KDEL-like motif. This divergence supports observations by Jensen (2021), who initially reported distinct segregation of C-terminal consensus sequences between mammalian and non-mammalian taxa. This thesis expands on these findings by incorporating a broader spectrum of animal sequences, including monotremes and marsupials.

Despite their classification as mammals, the sequences from marsupials and monotremes bear greater resemblance to avian or reptilian sequences. The similarities between early mammals and reptiles are not entirely surprising, since monotremes, such as platypuses and echidnas, lay eggs. Marsupials, despite bearing live young, employ unique reproductive strategies involving the birth of immature offspring that mature in a protective pouch. This evolutionary trajectory, particularly for species endemic to the isolated ecosystems of Australian and New Guinea, suggests ecological pressures favouring the retention of ancestral characteristics (Ferner et al., 2017).

Some placental mammals, such as minke whales, naked mole rats, and chinchillas, possess a C-terminal dileucine motif, too. These species tend to inhabit exceptional ecological niches divergent from the typical temperate, terrestrial environments of mammals near sea level. Minke whales can dive to a maximum depth of 106 metres and are known for their high frequency of diving and resurfacing (Kleivane et al., 2022). Minke whales have elevated levels of stress-resistance genes, and are particularly resilient against hypoxia (Yim et al., 2014). Similarly, naked mole rats have undergone vital adaptations to low oxygen and high carbon dioxide tolerance for their survival underground in poorly ventilated conditions (Amoroso et al., 2023), and chinchillas show similar resilience against hypoxia (Ederstrom et al., 1971). Notably, hypoxic and hypo- or hyperbaric environments are characteristic of high altitudes experienced by

birds and marine habitats experienced by ray-finned fish. These mammals may rely on signalling systems favoured by birds and fish to ensure their survival. This suggests a functional adaptation in purinergic signalling to support specialised mammalian species in harsh environments.

The C-termini of non-mammalian animals resemble those of related transporters VGLUT2 and VAChT, with their well-conserved dileucine and tyrosine motifs. VGLUT2 is characterised by a dileucine motif, which is imperative for its targeting of synaptic vesicles (Foss et al., 2013). Similarly, the tyrosine motif in VAChT is essential for its synaptic vesicle localisation (Varoqui & Erickson, 1998b). Since the incorporation of these motifs to the mammalian VNUT sequence did not abolish Golgi localisation, investigations were expanded to explore additional sorting signals beyond the C-terminus. Other neurotransmitter transporters, including VGLUT1 and VMAT2, require sorting signals at or near their N-termini for proper trafficking. VGLUT1 employs a C-terminal polyproline motif and additional N-terminal dileucine motifs for its localisation (Foss et al., 2013; Voglmaier et al., 2006a). Similarly, VMAT2 utilises a glycosylation loop proximal to its N-terminus, accompanied by a C-terminal dileucine to ensure its delivery LDCVs (Yao & Hersh, 2007). Therefore, we extended our search to the N-terminus of mammalian VNUT to elucidate mechanisms influencing its ER-Golgi localisation.

Since the release of AlphaFold2 in 2020, it has profoundly impacted the fields of structural biology, protein-protein interactions, drug discovery and more (Yang et al., 2023). Our computational analyses of mammalian VNUT revealed a highly conserved N-terminal DEXXR motif. Predictive modelling using protein folding software revealed interactions between this motif and the cargo-binding β-propeller of αCOPI. Substitution of any of the residues of the human sequence with alanine was predicted to reduce binding affinity between VNUT and αCOPI, underlining the importance of each residue within the motif.

Notably, substitution of the ninth residue from an arginine to cysteine in the human sequence is predicted to cause a conformational change in the

binding dynamics between αCOPI and VNUT, disrupting its interaction with the retrograde coatomer. The R9C mutation is characteristic of POROK8, the only known disease caused by a mutation in VNUT's sequence (Cui et al., 2014). Little is known about the cellular or molecular implications of the R9C mutation, but if typical VNUT interactions with αCOPI are disturbed, it may not reach the desired location in the quantities needed to perform its normal role. The results of this modelling are interesting in the context of this disease model and provide a foundation for more explorative studies on the trafficking of POROK8 mutated VNUT and functional analyses on the storage and release of ATP. AlphaFold2 and PRODIGY modelling of rat VNUT folding with the cargo binding domain of αCOPI predicted that a ∆1-12 amino acid truncation would increase the binding affinity of VNUT to αCOPI. ∆1-17 truncation, including removal of the DEXXR motif was predicted to reduce VNUT and αCOPI interactions below normal levels. This effect indicates that the DEXXR motif can act as a functional ER-retention sequence in the N-terminus of mammalian VNUT.

The literature lacks precedents for an established DEXXR motif in other proteins, yet analogous sequences offer insights to anticipated trafficking dynamics. The diacidic DE motifs, integral to well-characterised ER retention sequences such as KDEL and HEDL (Capitani & Sallese, 2009), and variations thereof, like DXE or DXXE, have been implicated in ER-Golgi transport through COPII-coated vesicles (Nishimura et al., 1999). Additionally, DE motifs have been implicated in the unconventional protein secretion (UPS) pathway (Padmanabhan et al., 2018), which circumvents the Golgi apparatus, directing proteins to the plasma membrane (Balmer & Faso, 2021). In mammalian cells, UPS is usually triggered by cellular stress, inflammation, ER stress, mechanical stressors or starvation (Balmer & Faso, 2021; Rabouille et al., 2012).

At the other end of the DEXXR motif are one to two arginine residues. These cytosolic N-terminal diarginine motifs are known to facilitate interactions with COPI-coated vesicles, thereby mediating the retrograde transport of transmembrane proteins from the Golgi to the ER (Boulaflous et al., 2009; Schutze et al., 1994). This suggests the arginine(s) in the DEXXR motif may be

driving the interaction between VNUT and αCOPI, though it is interesting that each residue appears to have an impact on their binding affinity.

Collectively, the positively charged arginine (R) residues have a high affinity for COPI-coated vesicles, whereas negatively charged aspartic acid (D) and Glutamic acid (E) are implicated in a variety of trafficking systems, altered by the flanking residues. While there are no other known instances of a DEXXR motif or its involvement in ER retrieval, there is some precedence for its putative action.

5.2. Correlation as a Measure of VNUT Localisation

Correlational studies into VNUT variants demonstrated that alteration to the N- or C-terminus do not result in substantial shifts in the spatial distribution of mammalian VNUT. Initial experiments examining C-terminal variants assessed their correlation with ER and Golgi markers, revealing no significant changes in their association. Notably, the correlation between VNUT and the ER exhibited considerable variability, while its association with the Golgi remained consistently strong. Similarly, truncations of the N-terminus did not significantly affect the spatial correlation of VNUT with either the nucleus, where high variability was observed, or the ER and Golgi. According to (Lagache et al., 2015), multi-channel correlational analyses can introduce high levels of variance, thereby limiting their efficacy in detecting robust changes. Nonetheless, these analyses remain useful for identifying no loss of ER and Golgi localisation following sequence alterations.

Following C-terminal substitutions and N-terminal truncations, a greater reduction in VNUT localisation to the ER-Golgi complex was expected. Several explanations may account for the observed stability in localisation patterns. One possibility is that potent retention mechanisms in VNUT remain. As previously discussed, VMAT2 and VGLUT1 localisation disruption is only achieved following alterations to both C-terminal and N-linked regions (Foss et al., 2013; Yao & Hersh, 2007). This thesis examined the termini in separation, so perhaps an

effect would be more visible following truncation or substitution of both N- and C-termini of mammalian VNUT. Furthermore, AlphaFold2 modelling revealed an interaction between COPI and cytosolic loops of VNUT, suggesting there may be further retrograde transport motifs in those areas. COPI-interacting arginine motifs are an example of a cytosolic motif which can be positioned independently of either terminus (Michelsen et al., 2005)

Another explanation to consider is the potential saturation of cellular trafficking machinery due to protein overexpression. N2a cells express relatively low quantities of endogenous VNUT (Miras-Portugal et al., 2019). The finite capacity of these cells for protein folding, post-translational modifications, and transport may become overwhelmed under conditions of high protein expression (Kintaka et al., 2016). Given that the ER and Golgi are central to these processes, oversaturation could lead to increased retention of proteins within these organelles. However, immunolabelling studies have shown that endogenous VNUT predominantly displays a perinuclear distribution (Jensen, 2021), suggesting that its accumulation in the Golgi under physiological conditions is intrinsic rather than an artefact of over-expression.

One consideration is that VNUT puncta are clearly visible within varicosities of rat tail arteries and neurites of N2a cells, demonstrating VNUT's ability to traffic to these locations outside of the Golgi (Jensen, 2021; Kim, 2019; Mojard Kalkhoran et al., 2019). Perhaps this is indicative that functional quantities of VNUT can escape the ER-Golgi complex, while most remains in the Golgi, or maybe these puncta are not vesicular. Puncta in the neurites of N2a cells do not colocalise with common synaptic vesicle markers including chromogranin A, synapsin, synaptophysin, synaptotagmins 1,2,5 and 7, synaptic vesicle glycoprotein 2A, or VMAT2 (Jensen, 2021). It is plausible that VNUT could be localised to smaller ER or Golgi structures, such as satellite ER or Golgi, at these locations. Satellite ER structures are likely to translate transmembrane proteins at the axon, such as hyperpolarization-activated cyclic nucleotide-gated channel 4 (HCN4) and calcium voltage-gated channel subunit alpha1 c (CACNA1c) (Kemal et al., 2022; Merianda et al., 2009). Similarly,

satellite Golgi, visualised using cis-, medial-, and trans-Golgi markers, are present in neuronal axons and dendrites involved in local protein synthesis and trafficking (Wang et al., 2020). There is no published research with immunolabelled endogenous VNUT and Golgi or ER markers in dendrites or varicosities, though this would be an interesting investigation.

5.3. The Effect of C-terminal Motifs in VNUT Localisation

In the analysis of C-terminus motifs through VNUT puncta, the Owl-derived C-terminus variant, containing both a dileucine (DTDSAY) and tyrosine (YMDL) motif, was distinctively effective in promoting a more peripheral localisation of VNUT within the cell. This variant exhibited an increase in both the luminosity and number of peripheral puncta. In contrast, the Alligator-derived C-terminus variant, differing by only a single amino acid in each motif (dileucine as DTVSAY and tyrosine as YIDL), showed a marked decrease in the number and brightness of distal puncta. The Chicken variant, sharing the dileucine sequence (DTDSAY) with the Owl, and the tyrosine motif (YIDL) with the alligator, did not display significant deviations from baseline localisation patterns. Similarly, the Cod variant, possessing only a tyrosine motif (YNHI), exhibited no notable differences in trafficking compared to the rat VNUT, which lacks both dileucine and tyrosine motifs.

From these observations, we can conclude that the C-terminus of VNUT is important to its subcellular localisation but is unlikely to be the sole trafficking mechanism. Interestingly, a single residue change within each motif was sufficient to account for the difference between the most and least distally localised variants. As Mattera et al. (2011) described, there are many unique combinations of subunits within each adaptor protein complex, and each one has a preferred affinity for a particular sequence of dileucine motif. Perhaps what we see in this C-terminal data is the relative increase and decrease in affinity for a particular conformation of adaptor complexes, with AP-1, AP-3 and AP-4 all recognising tyrosine and dileucine motifs. Considering the difference between

owl and chicken variants, the dileucine motif isn't sufficient to account for the difference in trafficking on its own. However, if the same can be said for tyrosine motifs and their affinity for adaptor proteins, this would explain how the owl construct is the only one to see an increase in Golgi escape. The YMDL tyrosine conformation of the owl is unique to these experiments. By some design and some fortune, these experiments allowed us to examine the effects of single residue changes on the C-terminal motifs. While the residue substitutions occur at 'wild card' locations, where the amino acid supposedly doesn't matter, it seems there is a compounding effect whereby the affinity for interactor proteins is altered.

Compounding the effects of the C-terminal tyrosine and dileucine on VNUTs, subcellular localisation could be the interaction between the mammalian C-terminus and αCOPI. AlphaFold2 predictions of both human and rat VNUT folding with αCOPI revealed interactions at both termini. Previous research has shown that removal of the final four residues from the rat sequence results in decreased colocalisation between VNUT and the ER, coupled with an increase between VNUT and the Golgi apparatus (Rayner et al., 2023). This effect was perplexing at the time since the KDEL receptor binds cargo on the luminal side of the membrane and the C-terminus of VNUT is cytosolic, meaning that the likelihood of the KDEL receptor binding this KDEL-like motif is extremely low. The αCOPI-interacting KDEL-like sequence being unique to mammals, is removed in the non-mammalian variants. An increase in distal puncta could be attributed to the loss of ER-retention, though it would be expected to see a more uniform effect across all variants.

5.4. Using pH to Locate VNUT-Containing Compartments

The secretory pathway exhibits a gradual pH gradient, with compartments becoming more acidic as they approach the cell surface. A typical gradient may range from pH 7.2 in the ER, pH 6.7 in the cis-Golgi network, pH 6.3 in the medial-Golgi and pH 6.0 in the trans-Golgi (Rivinoja et al., 2012). Secretory

vesicles are typically pH 5.5, while endosomes range from pH 5.5 to 6.5 and lysosomes are the most acidic at approximately pH 5. pH excursion experiments revealed that mammalian VNUT resides in compartments with an average pH value of 6.82, indicating that VNUT is predominantly spread between the ER, cis- and medial-Golgi. Some VNUT appears to escape this cycle and migrate towards the cell surface. However, the relatively high pH levels of VNUT indicate an overwhelming majority is retained within the ER-Golgi transport complex. The reptilian C-terminus variant localised to the most basic environment, indicating a reduced ability to migrate through the secretory pathway, sequestering in the more basic regions.

This study is the first to measure the pH levels in VNUT-containing compartments of calibrated cells, making it difficult to compare with previous research due to the lack of existing data on this topic. However, considering the typical pH value of a lysosome is very low (~ pH 5), these results do not adhere to the theory of VNUT as a lysosomal protein.

Our pHluorin analyses also contradict the concept of VNUT's localisation to synaptic vesicles. Typically, synaptic vesicle proteins are recycled between vesicles and the plasma membrane (Wilson & Hunt, 2015). They populate vesicles and the membrane in high concentrations and should be easily perceived using a pHluorin. Upon the introduction of an extracellular acidic solution, any membrane bound VNUT proteins would quench and cause an abrupt decrease in fluorescence. Membrane-bound puncta of VMAT2-pHuji, indicating a red pH-probe, shows robust quenching in N2a cells in response to extracellular acidic solutions (Jensen, 2021). Similar membrane-located puncta of pHluorin-tagged VGLUT1, VGLUT2, synaptobrevin and synaptotagmin respond to extracellular pH changes .

In the original characterisation of VNUT, Sawada et al. (2008) used immunoelectron microscopy to demonstrate the association of VNUT proteins with chromaffin granules of the adrenal medulla in mouse tissues. This remains one of the most convincing instances of VNUT localisation to vesicles. However,

our findings do not align with those of Sawada et al. (2008), which may be attributable to the differences in cell types. VNUT expression in mouse N2a cells could occur in subcellular compartments distinct from those in adrenal cells. To mitigate this issue, PC12 cells, an immortal cell line derived from the rat adrenal medulla, would enable a more direct comparison (Wiatrak et al., 2020).

An alternative hypothesis for the observed discrepancies in VNUT trafficking could be related to the specific isoform examined. The VNUT sequence provided by Sawada et al. (2008) matches that of human isoform 2. As mentioned previously, the two isoforms differ only in their N-termini. VNUT2 does not possess the DEXXR motif or preceding prolines. This poses the question of whether VNUT2 represents the vesicular isoform. The absence of an endoplasmic reticulum (ER) retention motif in VNUT2 could facilitate its escape from the Golgi apparatus and subsequent trafficking to synaptic sites. Moreover, comparative analysis suggests that the DEXXR motif in human VNUT1 interacts more robustly with α-COPI than its rat orthologue, potentially implicating a requirement for ER retention in human VNUT1 that might necessitate the existence of a synaptic isoform to compensate for enhanced retention. More research is needed to map the distribution of VNUT2 versus VNUT1 in adrenal cells to see if they are co-expressed and assess their subcellular localisation.

5.5. The Effect of N-terminal Truncations on VNUT Transport

This study quantitatively assessed the intracellular distribution of VNUT by examining the signal ratio within Golgi and ER compartments. The results indicated a disruption in Golgi to ER retrograde transport following truncation of the DEXXR motif, evidenced by accumulation of VNUT in the Golgi apparatus relative to the ER. Contrary to expectations, the loss of retrograde transport did not lead to an increase in the escape of VNUT towards the cell periphery. One might expect that with VNUT accumulating in the Golgi, unable to transport back to the ER, there would be a higher likelihood of vesicular sorting. Moreover, less

VNUT was expressed in cells expressing DEXXR-truncated VNUT, contributing to fewer puncta. Considering the lower expression levels, measuring the ratio of VNUT in the Golgi versus the ER provided a standardised measurement for where the VNUT variant was localised.

Further analysis revealed that truncation of the N-terminal DEXXR motif led to fewer puncta migrating towards the cell perimeter, evidenced by the decrease in number and intensity of distal puncta. Conversely, truncation upstream of the motif led to an increase in both these measures. It was hypothesised that truncation before the DEXXR motif would show equal or fewer distal puncta than WT due to the increased αCOPI interaction, and truncation after would show equal or more distal puncta. However, neither truncation significantly deviated from the baseline when isolated, though comparative analysis between the two demonstrated statistically significant differences. These observations may imply the association of distal puncta with the ER. Alternatively, this may suggest the involvement of the residues preceding the DEXXR motif with VNUT's localisation. Upstream of the DEXXR is a proline-rich region. Proline-rich motifs have been implicated in a wide range of subcellular trafficking mechanisms and protein-protein interactions (Ball et al., 2005; Ren & Hurley, 2011), including the trafficking of VGLUT1 to synaptic vesicles (Foss et al., 2013). Perhaps truncation of this region is changing the affinity of VNUT for other trafficking modulator proteins.

The collective observations following C-terminal substitutions and N-terminal truncations indicate a strong affinity for VNUT and the ER-Golgi complex within N2a cells. Disruption of putative ER-retention mechanisms at either terminus disrupts the subcellular localisation of VNUT, though they do not abolish ER or Golgi localisation as measured by correlation, live imaging, or signal ratio. The addition of non-mammalian trafficking motifs can disrupt the subcellular localisation of VNUT, particularly through alligator or owl sequences, however, the affinity of VNUT for the Golgi remains strong.

5.6. Caveats and Limitations

It is important to recognise the caveats and limitations that may affect the conclusions of this study. First, this research was undertaken using exogenously expressed proteins. This was a necessary step in editing VNUT's sequence; however, exogenous protein expression may cause issues with transcription and translation rates, folding kinetics, and protein interactions (Sandrock et al., 2001). It is possible that the exogenously expressed VNUT is dysfunctional in its folding or sorting mechanisms, leading us to misinterpret its subcellular localisation.

In addition, while a pH clamp was created with nigericin and monensin to allow the flow of K+, H+ and Na+ across membranes, a V-ATPase inhibitor would have improved pH stability. Across membranes, a pH gradient and electrical gradient are actively maintained by a V-ATPase pump. Bafilomycin is a potent V-ATPase inhibitor and would help stabilise pH levels by preventing V-ATPase from reacidifying any pHluorin-containing compartments (Bowman et al., 1988). Inclusion of bafilomycin would likely enhance the accuracy of pH estimations beyond the use of the ionophore pH clamp method alone. However, the relationship between the data is unlikely to change, i.e. the relative acidity of compartments containing one variant over another is likely to be reflected accurately without its inclusion. Additionally, the presence of bafilomycin is unlikely to impact the dequenching of membrane-bound pHluorins in response to ammonium chloride.

A further caveat is that the choice of fluorescently labelled organelle markers used may not fully portray the entire structures in question. The Golgi apparatus marker was a copy of the gene B4GALT1, a medial Golgi protein. As such, there may be large parts of the cis- and trans-Golgi networks which are not defined by this marker. The ER marker uses CALR, encoding calreticulin, which is abundant throughout (Dudek & Michalak, 2013).

Another issue is the variance within the data. From unpublished observations, differentiated N2a cells exhibit a few typical morphologies; some have small oval soma with few protruding neurites, whereas some are enlarged,

with many branching neurites, looking astrocytic. The quantity and dispersion of puncta tended to vary between the different morphologies, presenting an inherent complication with the cell type. Future studies may seek to mitigate this issue by categorising morphologies and exploring bimodal data analyses or using a different cell line. PC12 cells, a benchmark model for vesicular ATP release, would be a advantageous cell line to use.

Finally, truncation of the N-terminus is a blunted tool to use for researching the motif's impact as it did not isolate the effects of the motif from any other residues. This could have led to the misfolding of the N-terminus and impacted other important interactions that are yet unknown. Future experiments could isolate the removal of the DEXXR motif or replace the sequence with alanines, which have a small, chemically inert side chain that doesn't disrupt the secondary structure of surrounding residues (Weiss et al., 2000).

5.7. Implications and Future Directions

This thesis represents an advancement in our understanding on VNUT-mediated ATP secretion in neuronal cells. By revealing the role of VNUT's N- and C-terminal amino acid motifs in its subcellular localisation, we move closer to understanding the molecular mechanisms governing vesicular ATP storage and release. The findings that VNUT predominantly localises to the ER and Golgi apparatus challenge the traditional models of lysosomal or vesicular loading. We suggest that ATP may be loaded into vesicles at sites associated with the ER or Golgi, whether centrally or at satellite locations, representing a novel aspect of purinergic signalling.

The implications of a novel ATP loading system extend broadly within clinical contexts. For patients with POROK8, this opens avenues for therapeutic targets to treat the effects of their skin lesions. In addition, VNUT dysfunction is implicated in the regulation of many neuroprotective, neurodegenerative, endocrine, and cardiovascular function. With such broad interactions, VNUT is still a complex therapeutic target because of the risk of side-effects, however,

with each advancement in our understanding of its function, we move closer to a potentially life-changing treatment option.

Future research should expand upon this work by cloning the owl C-terminus on mammalian VNUT and repeating live imaging pHluorin experiments. Unfortunately, the construct that did not successfully clone with the pHluorin-containing VNUT exhibited the most interesting results for EGFP-VNUT. Additionally, I recommend replicating the C-terminus experiments with monotreme and marsupial C-termini. Moreover, I recommend expanding the chimeric protein research to VGLUTs, VMAT, and VAChT, replacing the N- and C-termini of VNUT to assess their impact on trafficking. Replacement of the C-terminus with that of VAChT should redirect VNUT to synaptic vesicles, which would act as a positive control for colocalisation assays.

Furthermore, the R9C mutation in POROK8 offers a valuable focal point. Using the human VNUT sequence, it would be interesting to know whether the R9C mutation was sufficient to redirect VNUT. In addition, exploring the DEXXR motif further with an in vitro alanine scan would ensure the protein was still able to fold correctly. Substituting each residue for an alanine in turn would enable researchers to isolate the effects of each residue and the compounded effects of all of them. Moreover, functional studies would be instrumental in determining whether the altered trafficking of VNUT impacts its ability to package ATP, particularly in relation to the R9C mutation. Paired with ATP release assays, such studies could substantially deepen our understanding of VNUT's operational dynamics.

The key to VNUT's trafficking appears to be a complex interplay of several factors. For the future of this field, I recommend trying to characterise every component of its trafficking to build a comprehensive picture. For example, there is a FLIXXR Golgi-retention motif in a region spanning the twelfth transmembrane domain and the C-terminus in the human sequence. This would be an excellent focal point to pursue to characterise the factors which govern VNUT's ER-Golgi retention.

In exploring the mechanisms of VNUT-mediated vesicular ATP release in mouse N2a cells, this thesis presents important results on the roles of the N- and C- termini of mammalian VNUT on its subcellular sorting mechanisms. This research concludes that the mammalian VNUT localises to the endoplasmic reticulum and Golgi apparatus. Furthermore, the substitution of the mammalian C-terminus with one containing a dileucine and tyrosine motif is sufficient to redirect some VNUT puncta to peripheral locations. The sequence of the tyrosine motif is especially critical to enhance peripheral sorting. Moreover, the mammalian N-terminus is instrumental in VNUT's trafficking, with a putative ER-retention DEXXR sequence that is well conserved among mammals. The localisation of VNUT at the Golgi and ER suggests a non-canonical neurotransmitter loading mechanism, unique to purinergic signalling. This thesis research advances our comprehension of the cellular and molecular mechanisms governing vesicular ATP release and highlights the potential for translating these insights into tangible clinical interventions.

References

Abu Irqeba, A., & Ogilvie, J. M. (2020). Di-arginine and FFAT-like motifs retain a subpopulation of PRA1 at ER-mitochondria membrane contact sites. *PLOS ONE*, *15*(12), e0243075. https://doi.org/10.1371/journal.pone.0243075

Amoroso, V. G., Zhao, A., Vargas, I., & Park, T. J. (2023). Naked Mole-Rats Demonstrate Profound Tolerance to Low Oxygen, High Carbon Dioxide, and Chemical Pain. *Animals: An Open Access Journal from MDPI*, *13*(5), 819. https://doi.org/10.3390/ani13050819

Ball, L. J., Kühne, R., Schneider-Mergener, J., & Oschkinat, H. (2005). Recognition of Proline-Rich Motifs by Protein–Protein-Interaction Domains. *Angewandte Chemie International Edition*, *44*(19), 2852–2869. https://doi.org/10.1002/anie.200400618

Balmer, E. A., & Faso, C. (2021). The Road Less Traveled? Unconventional Protein Secretion at Parasite–Host Interfaces. *Frontiers in Cell and Developmental Biology*, *9*, 662711. https://doi.org/10.3389/fcell.2021.662711

Bao, L., Locovei, S., & Dahl, G. (2004). Pannexin membrane channels are mechanosensitive conduits for ATP. *FEBS Letters*, *572*(1–3), 65–68. https://doi.org/10.1016/j.febslet.2004.07.009

Birkenfeld, A. L., Jordan, J., Dworak, M., Merkel, T., & Burnstock, G. (2019). Myocardial metabolism in heart failure: Purinergic signalling and other

metabolic concepts. *Pharmacology & Therapeutics*, *194*, 132–144. https://doi.org/10.1016/j.pharmthera.2018.08.015

Bolte, S., & Cordelières, F. P. (2006). A guided tour into subcellular colocalization analysis in light microscopy. *Journal of Microscopy*, *224*(3), 213–232. https://doi.org/10.1111/j.1365-2818.2006.01706.x

Bonifacino, J. S., & Traub, L. M. (2003). Signals for Sorting of Transmembrane Proteins to Endosomes and Lysosomes. *Annual Review of Biochemistry*, *72*(1), 395–447. https://doi.org/10.1146/annurev.biochem.72.121801.161800

Boulaflous, A., Saint-Jore-Dupas, C., Herranz-Gordo, M.-C., Pagny-Salehabadi, S., Plasson, C., Garidou, F., Kiefer-Meyer, M.-C., Ritzenthaler, C., Faye, L., & Gomord, V. (2009). Cytosolic N-terminal arginine-based signals together with a luminal signal target a type II membrane protein to the plant ER. *BMC Plant Biology*, *9*(1), 144. https://doi.org/10.1186/1471-2229-9-144

Bowman, E. J., Siebers, A., & Altendorf, K. (1988). Bafilomycins: A class of inhibitors of membrane ATPases from microorganisms, animal cells, and plant cells. *Proceedings of the National Academy of Sciences*, *85*(21), 7972–7976. https://doi.org/10.1073/pnas.85.21.7972

Bräuer, P., Parker, J. L., Gerondopoulos, A., Zimmermann, I., Seeger, M. A., Barr, F. A., & Newstead, S. (2019). Structural basis for pH-dependent retrieval of ER proteins from the Golgi by the KDEL receptor. *Science*, *363*(6431), 1103–1107. https://doi.org/10.1126/science.aaw2859

Bretscher, M. S., & Munro, S. (1993). Cholesterol and the Golgi Apparatus. *Science*, *261*(5126), 1280–1281. https://doi.org/10.1126/science.8362242

Brock, J. A., & Van Helden, D. F. (1995). Enhanced excitatory junction potentials in mesenteric arteries from spontaneously hypertensive rats. *Pflügers Archiv*, *430*(6), 901–908. https://doi.org/10.1007/BF01837403

Bruzzone, R., Hormuzdi, S. G., Barbe, M. T., Herb, A., & Monyer, H. (2003). Pannexins, a family of gap junction proteins expressed in brain. *Proceedings of the National Academy of Sciences*, *100*(23), 13644–13649. https://doi.org/10.1073/pnas.2233464100

Burnstock, G. (1972). Purinergic nerves. *Pharmacological Reviews*, *24*(3), 509–581.

Burnstock, G. (1976). Purinergic receptors. *Journal of Theoretical Biology*, *62*(2), 491–503. https://doi.org/10.1016/0022-5193(76)90133-8

Burnstock, G. (1990). Noradrenaline and ATP as cotransmitters in sympathetic nerves. *Neurochemistry International*, *17*(2), 357–368. https://doi.org/10.1016/0197-0186(90)90158-P

Burnstock, G. (2007). Physiology and Pathophysiology of Purinergic Neurotransmission. *Physiological Reviews*, *87*(2), 659–797. https://doi.org/10.1152/physrev.00043.2006

Burnstock, G. (2017a). Purinergic Signaling in the Cardiovascular System. *Circulation Research*, *120*(1), 207–228. https://doi.org/10.1161/CIRCRESAHA.116.309726

Burnstock, G. (2017b). Purinergic Signalling and Neurological Diseases: An Update. *CNS & Neurological Disorders - Drug Targets*, *16*(3), 257–265. https://doi.org/10.2174/1871527315666160922104848

Burnstock, G. (2018). Purine and purinergic receptors. *Brain and Neuroscience Advances*, *2*, 239821281881749. https://doi.org/10.1177/2398212818817494

Burnstock, G., & Di Virgilio, F. (2013). Purinergic signalling and cancer. *Purinergic Signalling*, *9*(4), 491–540. https://doi.org/10.1007/s11302-013-9372-5

Burnstock, G., & Pelleg, A. (2015). Cardiac purinergic signalling in health and disease. *Purinergic Signalling*, *11*(1), 1–46. https://doi.org/10.1007/s11302-014-9436-1

Burnstock, G., & Verkhratsky, A. (2010). Long-term (trophic) purinergic signalling: Purinoceptors control cell proliferation, differentiation and death. *Cell Death & Disease*, *1*(1), e9–e9. https://doi.org/10.1038/cddis.2009.11

Cabrera, M., Muñiz, M., Hidalgo, J., Vega, L., Martín, M. E., & Velasco, A. (2003). The Retrieval Function of the KDEL Receptor Requires PKA Phosphorylation of Its C-Terminus. *Molecular Biology of the Cell*, *14*(10), 4114–4125. https://doi.org/10.1091/mbc.e03-04-0194

Cao, Q., Zhao, K., Zhong, X. Z., Zou, Y., Yu, H., Huang, P., Xu, T.-L., & Dong, X.-P. (2014). SLC17A9 Protein Functions as a Lysosomal ATP Transporter and Regulates Cell Viability. *Journal of Biological Chemistry*, *289*(33), 23189–23199. https://doi.org/10.1074/jbc.M114.567107

Capitani, M., & Sallese, M. (2009). The KDEL receptor: New functions for an old protein. *FEBS Letters*, *583*(23), 3863–3871. https://doi.org/10.1016/j.febslet.2009.10.053

Chaudhury, A., He, X.-D., & Goyal, R. K. (2012). Role of myosin Va in purinergic vesicular neurotransmission in the gut. *American Journal of Physiology-Gastrointestinal and Liver Physiology*, *302*(6), G598–G607. https://doi.org/10.1152/ajpgi.00330.2011

Cheung, K., & Burnstock, G. (2002). Localization of P2X $_3$ receptors and coexpression with P2X $_2$ receptors during rat embryonic neurogenesis. *Journal of Comparative Neurology*, *443*(4), 368–382. https://doi.org/10.1002/cne.10123

Chiu, Y.-H., Medina, C. B., Doyle, C. A., Zhou, M., Narahari, A. K., Sandilos, J. K., Gonye, E. C., Gao, H.-Y., Guo, S. Y., Parlak, M., Lorenz, U. M., Conrads, T. P., Desai, B. N., Ravichandran, K. S., & Bayliss, D. A. (2021). Deacetylation as a receptor-regulated direct activation switch for pannexin channels. *Nature Communications*, *12*(1), 4482. https://doi.org/10.1038/s41467-021-24825-y

Coco, S., Calegari, F., Pravettoni, E., Pozzi, D., Taverna, E., Rosa, P., Matteoli, M., & Verderio, C. (2003). Storage and Release of ATP from Astrocytes in Culture. *Journal of Biological Chemistry*, *278*(2), 1354–1362. https://doi.org/10.1074/jbc.M209454200

Cole, N. B., Ellenberg, J., Song, J., DiEuliis, D., & Lippincott-Schwartz, J. (1998). Retrograde Transport of Golgi-localized Proteins to the ER. *The Journal of Cell Biology*, *140*(1), 1–15. https://doi.org/10.1083/jcb.140.1.1

Comeau, J. W. D., Costantino, S., & Wiseman, P. W. (2006). A Guide to Accurate Fluorescence Microscopy Colocalization Measurements. *Biophysical Journal*, *91*(12), 4611–4622. https://doi.org/10.1529/biophysj.106.089441

Contreras, J. E., Sáez, J. C., Bukauskas, F. F., & Bennett, M. V. L. (2003). Gating and regulation of connexin 43 (Cx43) hemichannels. *Proceedings of the National Academy of Sciences*, *100*(20), 11388–11393. https://doi.org/10.1073/pnas.1434298100

Coste, B., Xiao, B., Santos, J. S., Syeda, R., Grandl, J., Spencer, K. S., Kim, S. E., Schmidt, M., Mathur, J., Dubin, A. E., Montal, M., & Patapoutian, A. (2012). Piezo proteins are pore-forming subunits of mechanically activated channels. *Nature*, *483*(7388), 176–181. https://doi.org/10.1038/nature10812

Cui, H., Li, L., Wang, W., Shen, J., Yue, Z., Zheng, X., Zuo, X., Liang, B., Gao, M., Fan, X., Yin, X., Shen, C., Yang, C., Zhang, C., Zhang, X., Sheng, Y., Gao, J., Zhu, Z., Lin, D., … Zhang, X. (2014). Exome sequencing identifies *SLC17A9* pathogenic gene in two Chinese pedigrees with disseminated superficial actinic porokeratosis. *Journal of Medical Genetics*, *51*(10), 699–704. https://doi.org/10.1136/jmedgenet-2014-102486

De Vuyst, E., Decrock, E., Cabooter, L., Dubyak, G. R., Naus, C. C., Evans, W. H., & Leybaert, L. (2006). Intracellular calcium changes trigger connexin 32 hemichannel opening. *The EMBO Journal*, *25*(1), 34–44. https://doi.org/10.1038/sj.emboj.7600908

Dobson, L., Reményi, I., & Tusnády, G. E. (2015). CCTOP: A Consensus Constrained TOPology prediction web server. *Nucleic Acids Research*, *43*(W1), W408–W412. https://doi.org/10.1093/nar/gkv451

Dou, Y., Wu, H., Li, H., Qin, S., Wang, Y., Li, J., Lou, H., Chen, Z., Li, X., Luo, Q., & Duan, S. (2012). Microglial migration mediated by ATP-induced ATP release from lysosomes. *Cell Research*, *22*(6), 1022–1033. https://doi.org/10.1038/cr.2012.10

Dubyak, G. R. (2013). P2Y Receptors. In *Encyclopedia of Biological Chemistry* (pp. 375–378). Elsevier. https://doi.org/10.1016/B978-0-12-378630-2.00350-9

Dudek, E., & Michalak, M. (2013). Calnexin and Calreticulin. In R. H. Kretsinger, V. N. Uversky, & E. A. Permyakov (Eds.), *Encyclopedia of Metalloproteins* (pp. 555–562). Springer New York. https://doi.org/10.1007/978-1-4614-1533-6_42

Edelstein, A. D., Tsuchida, M. A., Amodaj, N., Pinkard, H., Vale, R. D., & Stuurman, N. (2014). Advanced methods of microscope control using μManager software. *Journal of Biological Methods*, *1*(2), e10. https://doi.org/10.14440/jbm.2014.36

Ederstrom, H. E., Akers, T. K., Keefner, K. R., & Thompson, R. E. (1971). Comparison of tolerance to hypoxia and hyperoxia in chinchillas and guinea pigs. *Space Life Sciences*, *3*(2), 171–173. https://doi.org/10.1007/BF00927991

Erb, L., Woods, L. T., Khalafalla, M. G., & Weisman, G. A. (2019). Purinergic signaling in Alzheimer's disease. *Brain Research Bulletin*, *151*, 25–37. https://doi.org/10.1016/j.brainresbull.2018.10.014

Farías, G. G., Cuitino, L., Guo, X., Ren, X., Jarnik, M., Mattera, R., & Bonifacino, J. S. (2012). Signal-Mediated, AP-1/Clathrin-Dependent Sorting of Transmembrane Receptors to the Somatodendritic Domain of Hippocampal Neurons. *Neuron*, *75*(5), 810–823. https://doi.org/10.1016/j.neuron.2012.07.007

Ferner, K., Schultz, J. A., & Zeller, U. (2017). Comparative anatomy of neonates of the three major mammalian groups (monotremes, marsupials, placentals) and implications for the ancestral mammalian neonate morphotype. *Journal of Anatomy*, *231*(6), 798–822. https://doi.org/10.1111/joa.12689

Foss, S. M., Li, H., Santos, M. S., Edwards, R. H., & Voglmaier, S. M. (2013). Multiple Dileucine-like Motifs Direct VGLUT1 Trafficking. *Journal of Neuroscience*, *33*(26), 10647–10660. https://doi.org/10.1523/JNEUROSCI.5662-12.2013

Gaitán-Peñas, H., Gradogna, A., Laparra-Cuervo, L., Solsona, C., Fernández-Dueñas, V., Barrallo-Gimeno, A., Ciruela, F., Lakadamyali, M., Pusch, M.,

& Estévez, R. (2016). Investigation of LRRC8-Mediated Volume-Regulated Anion Currents in Xenopus Oocytes. *Biophysical Journal*, *111*(7), 1429–1443. https://doi.org/10.1016/j.bpj.2016.08.030

Gao, C., Cai, Y., Wang, Y., Kang, B.-H., Aniento, F., Robinson, D. G., & Jiang, L. (2014). Retention mechanisms for ER and Golgi membrane proteins. *Trends in Plant Science*, *19*(8), 508–515. https://doi.org/10.1016/j.tplants.2014.04.004

Geisler, J. C., Corbin, K. L., Li, Q., Feranchak, A. P., Nunemaker, C. S., & Li, C. (2013). Vesicular Nucleotide Transporter-Mediated ATP Release Regulates Insulin Secretion. *Endocrinology*, *154*(2), 675–684. https://doi.org/10.1210/en.2012-1818

Gilbert, S., Oliphant, C., Hassan, S., Peille, A., Bronsert, P., Falzoni, S., Di Virgilio, F., McNulty, S., & Lara, R. (2019). ATP in the tumour microenvironment drives expression of nfP2X7, a key mediator of cancer cell survival. *Oncogene*, *38*(2), 194–208. https://doi.org/10.1038/s41388-018-0426-6

Gómez-Villafuertes, R., Del Puerto, A., Díaz-Hernández, M., Bustillo, D., Díaz-Hernández, J. I., Huerta, P. G., Artalejo, A. R., Garrido, J. J., & Miras-Portugal, M. T. (2009). Ca $^{2+}$ /calmodulin-dependent kinase II signalling cascade mediates P2X7 receptor-dependent inhibition of neuritogenesis in neuroblastoma cells. *The FEBS Journal*, *276*(18), 5307–5325. https://doi.org/10.1111/j.1742-4658.2009.07228.x

Guo, Y., Sirkis, D. W., & Schekman, R. (2014). Protein Sorting at the trans-Golgi Network. *Annual Review of Cell and Developmental Biology*, *30*(1), 169–206. https://doi.org/10.1146/annurev-cellbio-100913-013012

Gutiérrez-Martín, Y., Bustillo, D., Gómez-Villafuertes, R., Sánchez-Nogueiro, J., Torregrosa-Hetland, C., Binz, T., Gutiérrez, L. M., Miras-Portugal, M. T., & Artalejo, A. R. (2011). P2X7 Receptors Trigger ATP Exocytosis and Modify Secretory Vesicle Dynamics in Neuroblastoma Cells. *Journal of Biological Chemistry*, *286*(13), 11370–11381. https://doi.org/10.1074/jbc.M110.139410

Hanahan, D., & Weinberg, R. A. (2011). Hallmarks of Cancer: The Next Generation. *Cell*, *144*(5), 646–674. https://doi.org/10.1016/j.cell.2011.02.013

Hao, Y., & Tatonetti, N. P. (2016). Predicting G protein-coupled receptor downstream signaling by tissue expression. *Bioinformatics*, *32*(22), 3435–3443. https://doi.org/10.1093/bioinformatics/btw510

Harada, Y., & Hiasa, M. (2014). Immunological Identification of Vesicular Nucleotide Transporter in Intestinal L Cells. *Biological and Pharmaceutical Bulletin*, *37*(7), 1090–1095. https://doi.org/10.1248/bpb.b14-00275

Hasuzawa, N., Moriyama, S., Wang, L., Nagayama, A., Ashida, K., Moriyama, Y., & Nomura, M. (2021). Quinacrine is not a vital fluorescent probe for vesicular ATP storage. *Purinergic Signalling*, *17*(4), 725–735. https://doi.org/10.1007/s11302-021-09820-8

Haydon, P. G. (2017). Astrocytes and the modulation of sleep. *Current Opinion in Neurobiology*, *44*, 28–33. https://doi.org/10.1016/j.conb.2017.02.008

Herat, L., Schlaich, M., & Matthews, V. (2019). Sympathetic stimulation with norepinephrine may come at a cost. *Neural Regeneration Research*, *14*(6), 977. https://doi.org/10.4103/1673-5374.250576

Hiasa, M., Togawa, N., Miyaji, T., Omote, H., Yamamoto, A., & Moriyama, Y. (2014). Essential role of vesicular nucleotide transporter in vesicular storage and release of nucleotides in platelets. *Physiological Reports*, *2*(6), e12034. https://doi.org/10.14814/phy2.12034

Hines, D. J., & Haydon, P. G. (2014). Astrocytic adenosine: From synapses to psychiatric disorders. *Philosophical Transactions of the Royal Society B: Biological Sciences*, *369*(1654), 20130594. https://doi.org/10.1098/rstb.2013.0594

Ho, T., Jobling, A. I., Greferath, U., Chuang, T., Ramesh, A., Fletcher, E. L., & Vessey, K. A. (2015). Vesicular expression and release of ATP from dopaminergic neurons of the mouse retina and midbrain. *Frontiers in Cellular Neuroscience*, *9*. https://doi.org/10.3389/fncel.2015.00389

Huang, Z., Xie, N., Illes, P., Di Virgilio, F., Ulrich, H., Semyanov, A., Verkhratsky, A., Sperlagh, B., Yu, S.-G., Huang, C., & Tang, Y. (2021). From purines to purinergic signalling: Molecular functions and human diseases. *Signal Transduction and Targeted Therapy*, *6*(1), 162. https://doi.org/10.1038/s41392-021-00553-z

Huckstepp, R. T. R., Eason, R., Sachdev, A., & Dale, N. (2010). CO_2-dependent opening of connexin 26 and related β connexins: CO_2-dependent opening of connexins. *The Journal of Physiology*, *588*(20), 3921–3931. https://doi.org/10.1113/jphysiol.2010.192096

Iglesias, R., Locovei, S., Roque, A., Alberto, A. P., Dahl, G., Spray, D. C., & Scemes, E. (2008). $P2X_7$ receptor-Pannexin1 complex: Pharmacology and signaling. *American Journal of Physiology-Cell Physiology*, *295*(3), C752–C760. https://doi.org/10.1152/ajpcell.00228.2008

Imura, Y., Morizawa, Y., Komatsu, R., Shibata, K., Shinozaki, Y., Kasai, H., Moriishi, K., Moriyama, Y., & Koizumi, S. (2013). Microglia release ATP by exocytosis: Microglia Exocytose ATP. *Glia*, *61*(8), 1320–1330. https://doi.org/10.1002/glia.22517

Inoue, A., Nakao-Kuroishi, K., Kometani-Gunjigake, K., Mizuhara, M., Shirakawa, T., Ito-Sago, M., Yasuda, K., Nakatomi, M., Matsubara, T., Tada-Shigeyama, Y., Morikawa, K., Kokabu, S., & Kawamoto, T. (2020). VNUT/SLC17A9, a vesicular nucleotide transporter, regulates osteoblast differentiation. *FEBS Open Bio*, *10*(8), 1612–1623. https://doi.org/10.1002/2211-5463.12918

Iwatsuki, K., Ichikawa, R., Hiasa, M., Moriyama, Y., Torii, K., & Uneyama, H. (2009). Identification of the vesicular nucleotide transporter (VNUT) in taste cells. *Biochemical and Biophysical Research Communications*, *388*(1), 1–5. https://doi.org/10.1016/j.bbrc.2009.07.069

Jackson, L. P., Lewis, M., Kent, H. M., Edeling, M. A., Evans, P. R., Duden, R., & Owen, D. J. (2012). Molecular Basis for Recognition of Dilysine Trafficking Motifs by COPI. *Developmental Cell*, *23*(6), 1255–1262. https://doi.org/10.1016/j.devcel.2012.10.017

Jacobsson, J. A., Stephansson, O., & Fredriksson, R. (2010). C6ORF192 Forms a Unique Evolutionary Branch Among Solute Carriers (SLC16, SLC17, and SLC18) and Is Abundantly Expressed in Several Brain Regions. *Journal of Molecular Neuroscience*, *41*(2), 230–242. https://doi.org/10.1007/s12031-009-9222-7

Jensen, G. (2021). *Molecular Fingerprinting of VNUT-containing Compartments in Neuro-2a Cells*. Simon Fraser University.

Jentsch, T. J., Lutter, D., Planells-Cases, R., Ullrich, F., & Voss, F. K. (2016). VRAC: Molecular identification as LRRC8 heteromers with differential functions. *Pflügers Archiv - European Journal of Physiology*, *468*(3), 385–393. https://doi.org/10.1007/s00424-015-1766-5

Jumper, J., Evans, R., Pritzel, A., Green, T., Figurnov, M., Ronneberger, O., Tunyasuvunakool, K., Bates, R., Žídek, A., Potapenko, A., Bridgland, A., Meyer, C., Kohl, S. A. A., Ballard, A. J., Cowie, A., Romera-Paredes, B., Nikolov, S., Jain, R., Adler, J., … Hassabis, D. (2021). Highly accurate protein structure prediction with AlphaFold. *Nature*, *596*(7873), 583–589. https://doi.org/10.1038/s41586-021-03819-2

Jung, J., Shin, Y. H., Konishi, H., Lee, S. J., & Kiyama, H. (2013). Possible ATP release through lysosomal exocytosis from primary sensory neurons.

Biochemical and Biophysical Research Communications, *430*(2), 488–493. https://doi.org/10.1016/j.bbrc.2012.12.009

Kavalali, E. T., & Jorgensen, E. M. (2014). Visualizing presynaptic function. *Nature Neuroscience*, *17*(1), 10–16. https://doi.org/10.1038/nn.3578

Kemal, S., Richardson, H. S., Dyne, E. D., & Fu, M. (2022). ER and Golgi trafficking in axons, dendrites, and glial processes. *Current Opinion in Cell Biology*, *78*, 102119. https://doi.org/10.1016/j.ceb.2022.102119

Kennedy, C. (2015). ATP as a cotransmitter in the autonomic nervous system. *Autonomic Neuroscience*, *191*, 2–15. https://doi.org/10.1016/j.autneu.2015.04.004

Khakh, B. S., & North, R. A. (2012). Neuromodulation by Extracellular ATP and P2X Receptors in the CNS. *Neuron*, *76*(1), 51–69. https://doi.org/10.1016/j.neuron.2012.09.024

Kim, B. R. (2019). *Design and validation of genetically encoded probes for the analysis of neuronal catecholamine and ATP co-transmission*. Simon Fraser University.

Kintaka, R., Makanae, K., & Moriya, H. (2016). Cellular growth defects triggered by an overload of protein localization processes. *Scientific Reports*, *6*(1), 31774. https://doi.org/10.1038/srep31774

Kleivane, L., Kvadsheim, P. H., Bocconcelli, A., Øien, N., & Miller, P. J. O. (2022). Equipment to tag, track and collect biopsies from whales and dolphins: The ARTS, DFHorten and LKDart systems. *Animal Biotelemetry*, *10*(1), 32. https://doi.org/10.1186/s40317-022-00303-0

Kopp, R., Krautloher, A., Ramírez-Fernández, A., & Nicke, A. (2019). P2X7 Interactions and Signaling – Making Head or Tail of It. *Frontiers in Molecular Neuroscience*, *12*, 183. https://doi.org/10.3389/fnmol.2019.00183

Kumar, S., Suleski, M., Craig, J. M., Kasprowicz, A. E., Sanderford, M., Li, M., Stecher, G., & Hedges, S. B. (2022). TimeTree 5: An Expanded Resource for Species Divergence Times. *Molecular Biology and Evolution*, *39*(8), msac174. https://doi.org/10.1093/molbev/msac174

Lagache, T., Sauvonnet, N., Danglot, L., & Olivo-Marin, J. (2015). Statistical analysis of molecule colocalization in bioimaging. *Cytometry Part A*, *87*(6), 568–579. https://doi.org/10.1002/cyto.a.22629

Lalo, U., Palygin, O., Rasooli-Nejad, S., Andrew, J., Haydon, P. G., & Pankratov, Y. (2014). Exocytosis of ATP From Astrocytes Modulates Phasic and Tonic Inhibition in the Neocortex. *PLoS Biology*, *12*(1), e1001747. https://doi.org/10.1371/journal.pbio.1001747

Lalo, U., Palygin, O., Verkhratsky, A., Grant, S. G. N., & Pankratov, Y. (2016). ATP from synaptic terminals and astrocytes regulates NMDA receptors and synaptic plasticity through PSD-95 multi-protein complex. *Scientific Reports*, *6*(1), 33609. https://doi.org/10.1038/srep33609

Larsson, M., Sawada, K., Morland, C., Hiasa, M., Ormel, L., Moriyama, Y., & Gundersen, V. (2012). Functional and Anatomical Identification of a Vesicular Transporter Mediating Neuronal ATP Release. *Cerebral Cortex*, *22*(5), 1203–1214. https://doi.org/10.1093/cercor/bhr203

Letunic, I., & Bork, P. (2021). Interactive Tree Of Life (iTOL) v5: An online tool for phylogenetic tree display and annotation. *Nucleic Acids Research*, *49*(W1), W293–W296. https://doi.org/10.1093/nar/gkab301

Linden, J., Koch-Nolte, F., & Dahl, G. (2019). Purine Release, Metabolism, and Signaling in the Inflammatory Response. *Annual Review of Immunology*, *37*(1), 325–347. https://doi.org/10.1146/annurev-immunol-051116-052406

Locovei, S., Scemes, E., Qiu, F., Spray, D. C., & Dahl, G. (2007). Pannexin1 is part of the pore forming unit of the P2X $_{7}$ receptor death complex. *FEBS Letters*, *581*(3), 483–488. https://doi.org/10.1016/j.febslet.2006.12.056

Lopez-Castejon, G., & Brough, D. (2011). Understanding the mechanism of IL-1β secretion. *Cytokine & Growth Factor Reviews*, *22*(4), 189–195. https://doi.org/10.1016/j.cytogfr.2011.10.001

Ma, W., & Goldberg, J. (2013). Rules for the recognition of dilysine retrieval motifs by coatomer. *The EMBO Journal*, *32*(7), 926–937. https://doi.org/10.1038/emboj.2013.41

Ma, Z., Siebert, A. P., Cheung, K.-H., Lee, R. J., Johnson, B., Cohen, A. S., Vingtdeux, V., Marambaud, P., & Foskett, J. K. (2012). Calcium homeostasis modulator 1 (CALHM1) is the pore-forming subunit of an ion channel that mediates extracellular Ca $^{2+}$ regulation of neuronal excitability. *Proceedings of the National Academy of Sciences*, *109*(28). https://doi.org/10.1073/pnas.1204023109

Ma, Z., Taruno, A., Ohmoto, M., Jyotaki, M., Lim, J. C., Miyazaki, H., Niisato, N., Marunaka, Y., Lee, R. J., Hoff, H., Payne, R., Demuro, A., Parker, I.,

Mitchell, C. H., Henao-Mejia, J., Tanis, J. E., Matsumoto, I., Tordoff, M. G., & Foskett, J. K. (2018). CALHM3 Is Essential for Rapid Ion Channel-Mediated Purinergic Neurotransmission of GPCR-Mediated Tastes. *Neuron*, *98*(3), 547-561.e10. https://doi.org/10.1016/j.neuron.2018.03.043

Mahmood, A., Munir, R., Zia-ur-Rehman, M., Javid, N., Shah, S. J. A., Noreen, L., Sindhu, T. A., & Iqbal, J. (2021). Synthesis of Sulfonamide Tethered (Hetero)aryl ethylidenes as Potential Inhibitors of P2X Receptors: A Promising Way for the Treatment of Pain and Inflammation. *ACS Omega*, *6*(38), 25062–25075. https://doi.org/10.1021/acsomega.1c04302

Mahon, M. J. (2011). pHluorin2: An enhanced, ratiometric, pH-sensitive green florescent protein. *Advances in Bioscience and Biotechnology*, *02*(03), 132–137. https://doi.org/10.4236/abb.2011.23021

Martín, D., Bocio-Nuñez, J., Scagliusi, S. F., Pérez, P., Huertas, G., Yúfera, A., Giner, M., & Daza, P. (2022). DC electrical stimulation enhances proliferation and differentiation on N2a and MC3T3 cell lines. *Journal of Biological Engineering*, *16*(1), 27. https://doi.org/10.1186/s13036-022-00306-8

Martín, D., Ruano, D., Yúfera, A., & Daza, P. (2024). Electrical pulse stimulation parameters modulate N2a neuronal differentiation. *Cell Death Discovery*, *10*(1), 49. https://doi.org/10.1038/s41420-024-01820-y

Martin, E. A., Lasseigne, A. M., & Miller, A. C. (2020). Understanding the Molecular and Cell Biological Mechanisms of Electrical Synapse

Formation. *Frontiers in Neuroanatomy*, *14*, 12. https://doi.org/10.3389/fnana.2020.00012

Masuda, T., Ozono, Y., Mikuriya, S., Kohro, Y., Tozaki-Saitoh, H., Iwatsuki, K., Uneyama, H., Ichikawa, R., Salter, M. W., Tsuda, M., & Inoue, K. (2016). Dorsal horn neurons release extracellular ATP in a VNUT-dependent manner that underlies neuropathic pain. *Nature Communications*, *7*(1), 12529. https://doi.org/10.1038/ncomms12529

Mathew, S., & Keerikkattil, J. P. (2022). Lineage Tracking and Differentiation of Neuro 2A cells (N2a) upon exposure to Dopamine, Monosodium Glutamate and Corticosterone. *The FASEB Journal*, *36*(S1), fasebj.2022.36.S1.R3706. https://doi.org/10.1096/fasebj.2022.36.S1.R3706

Mattera, R., Boehm, M., Chaudhuri, R., Prabhu, Y., & Bonifacino, J. S. (2011). Conservation and Diversification of Dileucine Signal Recognition by Adaptor Protein (AP) Complex Variants. *Journal of Biological Chemistry*, *286*(3), 2022–2030. https://doi.org/10.1074/jbc.M110.197178

McCorry, L. K. (2007). Physiology of the Autonomic Nervous System. *American Journal of Pharmaceutical Education*, *71*(4), 78. https://doi.org/10.5688/aj710478

Menéndez-Méndez, A., Díaz-Hernández, J. I., & Miras-Portugal, M. T. (2015). The vesicular nucleotide transporter (VNUT) is involved in the extracellular ATP effect on neuronal differentiation. *Purinergic Signalling*, *11*(2), 239–249. https://doi.org/10.1007/s11302-015-9449-4

Menéndez-Méndez, A., Díaz-Hernández, J. I., Ortega, F., Gualix, J., Gómez-Villafuertes, R., & Miras-Portugal, M. T. (2017). Specific Temporal Distribution and Subcellular Localization of a Functional Vesicular Nucleotide Transporter (VNUT) in Cerebellar Granule Neurons. *Frontiers in Pharmacology*, *8*, 951. https://doi.org/10.3389/fphar.2017.00951

Merianda, T. T., Lin, A. C., Lam, J. S. Y., Vuppalanchi, D., Willis, D. E., Karin, N., Holt, C. E., & Twiss, J. L. (2009). A functional equivalent of endoplasmic reticulum and Golgi in axons for secretion of locally synthesized proteins. *Molecular and Cellular Neuroscience*, *40*(2), 128–142. https://doi.org/10.1016/j.mcn.2008.09.008

Michelsen, K., Yuan, H., & Schwappach, B. (2005). Hide and run: Arginine-based endoplasmic-reticulum-sorting motifs in the assembly of heteromultimeric membrane proteins. *EMBO Reports*, *6*(8), 717–722. https://doi.org/10.1038/sj.embor.7400480

Miesenböck, G., De Angelis, D. A., & Rothman, J. E. (1998). Visualizing secretion and synaptic transmission with pH-sensitive green fluorescent proteins. *Nature*, *394*(6689), 192–195. https://doi.org/10.1038/28190

Mikros, E., & Diallinas, G. (2019). Tales of tails in transporters. *Open Biology*, *9*(6), 190083. https://doi.org/10.1098/rsob.190083

Milosevic, I. (2018). Revisiting the Role of Clathrin-Mediated Endoytosis in Synaptic Vesicle Recycling. *Frontiers in Cellular Neuroscience*, *12*, 27. https://doi.org/10.3389/fncel.2018.00027

Miras-Portugal, M. T., Diaz-Hernandez, J. I., Gomez-Villafuertes, R., Diaz-Hernandez, M., Artalejo, A. R., & Gualix, J. (2015). Role of P2X7 and P2Y2 receptors on α-secretase-dependent APP processing: Control of amyloid plaques formation “in vivo” by P2X7 receptor. *Computational and Structural Biotechnology Journal*, *13*, 176–181. https://doi.org/10.1016/j.csbj.2015.02.005

Miras-Portugal, M. T., Menéndez-Méndez, A., Gómez-Villafuertes, R., Ortega, F., Delicado, E. G., Pérez-Sen, R., & Gualix, J. (2019). Physiopathological Role of the Vesicular Nucleotide Transporter (VNUT) in the Central Nervous System: Relevance of the Vesicular Nucleotide Release as a Potential Therapeutic Target. *Frontiers in Cellular Neuroscience*, *13*, 224. https://doi.org/10.3389/fncel.2019.00224

Mojard Kalkhoran, S., Chow, S. H. J., Walia, J. S., Gershome, C., Saraev, N., Kim, B., & Poburko, D. (2019). VNUT and VMAT2 segregate within sympathetic varicosities and localize near preferred Cav2 isoforms in the rat tail artery. *American Journal of Physiology-Heart and Circulatory Physiology*, *316*(1), H89–H105. https://doi.org/10.1152/ajpheart.00560.2018

Moriyama, S., & Hiasa, M. (2016). Expression of Vesicular Nucleotide Transporter in the Mouse Retina. *Biological & Pharmaceutical Bulletin*, *39*(4), 564–569. https://doi.org/10.1248/bpb.b15-00872

Moriyama, Y., Hiasa, M., Sakamoto, S., Omote, H., & Nomura, M. (2017a). Vesicular nucleotide transporter (VNUT): Appearance of an actress on the

stage of purinergic signaling. *Purinergic Signalling*, *13*(3), 387–404. https://doi.org/10.1007/s11302-017-9568-1

Moriyama, Y., Hiasa, M., Sakamoto, S., Omote, H., & Nomura, M. (2017b). Vesicular nucleotide transporter (VNUT): Appearance of an actress on the stage of purinergic signaling. *Purinergic Signalling*, *13*(3), 387–404. https://doi.org/10.1007/s11302-017-9568-1

Munro, S., & Pelham, H. R. B. (1987). A C-terminal signal prevents secretion of luminal ER proteins. *Cell*, *48*(5), 899–907. https://doi.org/10.1016/0092-8674(87)90086-9

Nadjar, A., Blutstein, T., Aubert, A., Laye, S., & Haydon, P. G. (2013). Astrocyte-derived adenosine modulates increased sleep pressure during inflammatory response. *Glia*, *61*(5), 724–731. https://doi.org/10.1002/glia.22465

Nakagomi, H., Yoshiyama, M., Mochizuki, T., Miyamoto, T., Komatsu, R., Imura, Y., Morizawa, Y., Hiasa, M., Miyaji, T., Kira, S., Araki, I., Fujishita, K., Shibata, K., Shigetomi, E., Shinozaki, Y., Ichikawa, R., Uneyama, H., Iwatsuki, K., Nomura, M., … Koizumi, S. (2016). Urothelial ATP exocytosis: Regulation of bladder compliance in the urine storage phase. *Scientific Reports*, *6*(1), 29761. https://doi.org/10.1038/srep29761

Narahari, A. K., Kreutzberger, A. J., Gaete, P. S., Chiu, Y.-H., Leonhardt, S. A., Medina, C. B., Jin, X., Oleniacz, P. W., Kiessling, V., Barrett, P. Q., Ravichandran, K. S., Yeager, M., Contreras, J. E., Tamm, L. K., & Bayliss, D. A. (2021). ATP and large signaling metabolites flux through caspase-

activated Pannexin 1 channels. *eLife*, *10*, e64787. https://doi.org/10.7554/eLife.64787

Nijjar, S., Maddison, D., Meigh, L., De Wolf, E., Rodgers, T., Cann, M. J., & Dale, N. (2021). Opposing modulation of Cx26 gap junctions and hemichannels by CO_2. *The Journal of Physiology*, *599*(1), 103–118. https://doi.org/10.1113/JP280747

Nirenberg, M. J., Liu, Y., Peter, D., Edwards, R. H., & Pickel, V. M. (1995). The vesicular monoamine transporter 2 is present in small synaptic vesicles and preferentially localizes to large dense core vesicles in rat solitary tract nuclei. *Proceedings of the National Academy of Sciences*, *92*(19), 8773–8777. https://doi.org/10.1073/pnas.92.19.8773

Nishida, K., Nomura, Y., Kawamori, K., Moriyama, Y., & Nagasawa, K. (2014). Expression profile of vesicular nucleotide transporter (VNUT, SLC17A9) in subpopulations of rat dorsal root ganglion neurons. *Neuroscience Letters*, *579*, 75–79. https://doi.org/10.1016/j.neulet.2014.07.017

Nishimura, N., Bannykh, S., Slabough, S., Matteson, J., Altschuler, Y., Hahn, K., & Balch, W. E. (1999). A Di-acidic (DXE) Code Directs Concentration of Cargo during Export from the Endoplasmic Reticulum. *Journal of Biological Chemistry*, *274*(22), 15937–15946. https://doi.org/10.1074/jbc.274.22.15937

Nobili, P., Shen, W., Milicevic, K., Bogdanovic Pristov, J., Audinat, E., & Nikolic, L. (2022). Therapeutic Potential of Astrocyte Purinergic Signalling in

Epilepsy and Multiple Sclerosis. *Frontiers in Pharmacology*, *13*, 900337. https://doi.org/10.3389/fphar.2022.900337

Nualart-Marti, A., Del Molino, E. M., Grandes, X., Bahima, L., Martin-Satué, M., Puchal, R., Fasciani, I., González-Nieto, D., Ziganshin, B., Llobet, A., Barrio, L. C., & Solsona, C. (2013). Role of connexin 32 hemichannels in the release of ATP from peripheral nerves: Cx32 Permeability to ATP. *Glia*, *61*(12), 1976–1989. https://doi.org/10.1002/glia.22568

Obermüller, S., Kiecke, C., Von Figura, K., & Höning, S. (2002). The tyrosine motifs of Lamp 1 and LAP determine their direct and indirect targetting to lysosomes. *Journal of Cell Science*, *115*(1), 185–194. https://doi.org/10.1242/jcs.115.1.185

Oliveira, Á., Illes, P., & Ulrich, H. (2016). Purinergic receptors in embryonic and adult neurogenesis. *Neuropharmacology*, *104*, 272–281. https://doi.org/10.1016/j.neuropharm.2015.10.008

Owen, D. J., Collins, B. M., & Evans, P. R. (2004). ADAPTORS FOR CLATHRIN COATS: Structure and Function. *Annual Review of Cell and Developmental Biology*, *20*(1), 153–191. https://doi.org/10.1146/annurev.cellbio.20.010403.104543

Oya, M., Kitaguchi, T., Yanagihara, Y., Numano, R., Kakeyama, M., Ikematsu, K., & Tsuboi, T. (2013). Vesicular nucleotide transporter is involved in ATP storage of secretory lysosomes in astrocytes. *Biochemical and Biophysical Research Communications*, *438*(1), 145–151. https://doi.org/10.1016/j.bbrc.2013.07.043

Padmanabhan, S., Biswal, M. R., Manjithaya, R., & Prakash, M. K. (2018). Exploring the context of diacidic motif DE as a signal for unconventional protein secretion in eukaryotic proteins. *Wellcome Open Research*, *3*, 148. https://doi.org/10.12688/wellcomeopenres.14914.1

Pangršič, T., Potokar, M., Stenovec, M., Kreft, M., Fabbretti, E., Nistri, A., Pryazhnikov, E., Khiroug, L., Giniatullin, R., & Zorec, R. (2007). Exocytotic Release of ATP from Cultured Astrocytes. *Journal of Biological Chemistry*, *282*(39), 28749–28758. https://doi.org/10.1074/jbc.M700290200

Patterson, G. H., Hirschberg, K., Polishchuk, R. S., Gerlich, D., Phair, R. D., & Lippincott-Schwartz, J. (2008). Transport through the Golgi Apparatus by Rapid Partitioning within a Two-Phase Membrane System. *Cell*, *133*(6), 1055–1067. https://doi.org/10.1016/j.cell.2008.04.044

Pérez de Lara, M. J., Guzmán-Aránguez, A., de la Villa, P., Díaz-Hernández, J. I., Miras-Portugal, M. T., & Pintor, J. (2015). Increased levels of extracellular ATP in glaucomatous retinas: Possible role of the vesicular nucleotide transporter during the development of the pathology. *Molecular Vision*, *21*, 1060–1070.

Peters, C., Braun, M., Weber, B., Wendland, M., Schmidt, B., Pohlmann, R., Waheed, A., & Von Figura, K. (1990). Targeting of a lysosomal membrane protein: A tyrosine-containing endocytosis signal in the cytoplasmic tail of lysosomal acid phosphatase is necessary and sufficient for targeting to lysosomes. *The EMBO Journal*, *9*(11), 3497–3506. https://doi.org/10.1002/j.1460-2075.1990.tb07558.x

Pietkiewicz, P., Korecka, K., Salwowska, N., Kohut, I., Adhikari, A., Bowszyc-Dmochowska, M., Pogorzelska-Antkowiak, A., & Navarrete-Dechent, C. (2023). Porokeratoses—A Comprehensive Review on the Genetics and Metabolomics, Imaging Methods and Management of Common Clinical Variants. *Metabolites*, *13*(12), 1176. https://doi.org/10.3390/metabo13121176

Poburko, D., Santo-Domingo, J., & Demaurex, N. (2011). Dynamic Regulation of the Mitochondrial Proton Gradient during Cytosolic Calcium Elevations. *Journal of Biological Chemistry*, *286*(13), 11672–11684. https://doi.org/10.1074/jbc.M110.159962

Pogoda, K., Kameritsch, P., Retamal, M. A., & Vega, J. L. (2016). Regulation of gap junction channels and hemichannels by phosphorylation and redox changes: A revision. *BMC Cell Biology*, *17*(S1), 11. https://doi.org/10.1186/s12860-016-0099-3

Procopio, M. C., Lauro, R., Nasso, C., Carerj, S., Squadrito, F., Bitto, A., Di Bella, G., Micari, A., Irrera, N., & Costa, F. (2021). Role of Adenosine and Purinergic Receptors in Myocardial Infarction: Focus on Different Signal Transduction Pathways. *Biomedicines*, *9*(2), 204. https://doi.org/10.3390/biomedicines9020204

Purves, D. (Ed.). (2012). *Neuroscience* (5th ed). Sinauer Associates.

Rabouille, C., Malhotra, V., & Nickel, W. (2012). Diversity in unconventional protein secretion. *Journal of Cell Science*, *125*(22), 5251–5255. https://doi.org/10.1242/jcs.103630

Rayner, S., Jensen, G., Gastaldello, L., & Poburko, D. (2023, February). *Phylogenetic and Localisation Analyses of Mammalian VNUT Reveal a Unique ER-Retention Sequence Replaces Vesicular Targeting Motifs in the C-terminus.* [Poster]. BioPhysics Society.

Reimer, R. J. (2013). SLC17: A functionally diverse family of organic anion transporters. *Molecular Aspects of Medicine*, *34*(2–3), 350–359. https://doi.org/10.1016/j.mam.2012.05.004

Ren, X., & Hurley, J. H. (2011). Proline-Rich Regions and Motifs in Trafficking: From ESCRT Interaction to Viral Exploitation. *Traffic*, *12*(10), 1282–1290. https://doi.org/10.1111/j.1600-0854.2011.01208.x

Retamal, M. A., Cortés, C. J., Reuss, L., Bennett, M. V. L., & Sáez, J. C. (2006). S-nitrosylation and permeation through connexin 43 hemichannels in astrocytes: Induction by oxidant stress and reversal by reducing agents. *Proceedings of the National Academy of Sciences*, *103*(12), 4475–4480. https://doi.org/10.1073/pnas.0511118103

Rivinoja, A., Pujol, F. M., Hassinen, A., & Kellokumpu, S. (2012). Golgi pH, its regulation and roles in human disease. *Annals of Medicine*, *44*(6), 542–554. https://doi.org/10.3109/07853890.2011.579150

Sabirov, R. Z., Dutta, A. K., & Okada, Y. (2001). Volume-Dependent Atp-Conductive Large-Conductance Anion Channel as a Pathway for Swelling-Induced Atp Release. *The Journal of General Physiology*, *118*(3), 251–266. https://doi.org/10.1085/jgp.118.3.251

Sabirov, R. Z., Merzlyak, P. G., Okada, T., Islam, M. R., Uramoto, H., Mori, T., Makino, Y., Matsuura, H., Xie, Y., & Okada, Y. (2017). The organic anion transporter SLCO 2A1 constitutes the core component of the Maxi-Cl channel. *The EMBO Journal*, *36*(22), 3309–3324. https://doi.org/10.15252/embj.201796685

Sage, D., Donati, L., Soulez, F., Fortun, D., Schmit, G., Seitz, A., Guiet, R., Vonesch, C., & Unser, M. (2017). DeconvolutionLab2: An open-source software for deconvolution microscopy. *Methods*, *115*, 28–41. https://doi.org/10.1016/j.ymeth.2016.12.015

Sakamoto, S., Miyaji, T., Hiasa, M., Ichikawa, R., Uematsu, A., Iwatsuki, K., Shibata, A., Uneyama, H., Takayanagi, R., Yamamoto, A., Omote, H., Nomura, M., & Moriyama, Y. (2014). Impairment of vesicular ATP release affects glucose metabolism and increases insulin sensitivity. *Scientific Reports*, *4*(1), 6689. https://doi.org/10.1038/srep06689

Sandrock, T. M., Risley, B., Richards, B. T., Poritz, M. A., Austin, H. A., Yoo, S., Kim, M. K.-H., Roth, B., Repetny, K., Hsu, F., Stump, M., Teng, D. H.-F., & Kamb, A. (2001). Exogenous Peptide and Protein Expression Levels Using Retroviral Vectors in Human Cells. *Molecular Therapy*, *4*(5), 398–406. https://doi.org/10.1006/mthe.2001.0476

Santos, M. S., Barbosa, J., Veloso, G. S., Ribeiro, F., Kushmerick, C., Gomez, M. V., Ferguson, S. S. G., Prado, V. F., & Prado, M. A. M. (2001). Trafficking of green fluorescent protein tagged-vesicular acetylcholine transporter to varicosities in a cholinergic cell line. *Journal of*

Neurochemistry, *78*(5), 1104–1113. https://doi.org/10.1046/j.1471-4159.2001.00494.x

Sathe, M. N., Woo, K., Kresge, C., Bugde, A., Luby-Phelps, K., Lewis, M. A., & Feranchak, A. P. (2011). Regulation of Purinergic Signaling in Biliary Epithelial Cells by Exocytosis of SLC17A9-dependent ATP-enriched Vesicles. *Journal of Biological Chemistry*, *286*(28), 25363–25376. https://doi.org/10.1074/jbc.M111.232868

Sawada, K., Echigo, N., Juge, N., Miyaji, T., Otsuka, M., Omote, H., Yamamoto, A., & Moriyama, Y. (2008). Identification of a vesicular nucleotide transporter. *Proceedings of the National Academy of Sciences*, *105*(15), 5683–5686. https://doi.org/10.1073/pnas.0800141105

Sayers, E. W., Bolton, E. E., Brister, J. R., Canese, K., Chan, J., Comeau, D. C., Connor, R., Funk, K., Kelly, C., Kim, S., Madej, T., Marchler-Bauer, A., Lanczycki, C., Lathrop, S., Lu, Z., Thibaud-Nissen, F., Murphy, T., Phan, L., Skripchenko, Y., … Sherry, S. T. (2022). Database resources of the national center for biotechnology information. *Nucleic Acids Research*, *50*(D1), D20–D26. https://doi.org/10.1093/nar/gkab1112

Schiller, I. C., Jacobson, K. A., Wen, Z., Malisetty, A., Schmalzing, G., & Markwardt, F. (2022). Dihydropyridines Potentiate ATP-Induced Currents Mediated by the Full-Length Human P2X5 Receptor. *Molecules*, *27*(6), 1846. https://doi.org/10.3390/molecules27061846

Schindelin, J., Arganda-Carreras, I., Frise, E., Kaynig, V., Longair, M., Pietzsch, T., Preibisch, S., Rueden, C., Saalfeld, S., Schmid, B., Tinevez, J.-Y.,

White, D. J., Hartenstein, V., Eliceiri, K., Tomancak, P., & Cardona, A. (2012). Fiji: An open-source platform for biological-image analysis. *Nature Methods*, *9*(7), 676–682. https://doi.org/10.1038/nmeth.2019

Schutze, M. P., Peterson, P. A., & Jackson, M. R. (1994). An N-terminal double-arginine motif maintains type II membrane proteins in the endoplasmic reticulum. *The EMBO Journal*, *13*(7), 1696–1705. https://doi.org/10.1002/j.1460-2075.1994.tb06434.x

Scott, K. L., Kabbarah, O., Liang, M.-C., Ivanova, E., Anagnostou, V., Wu, J., Dhakal, S., Wu, M., Chen, S., Feinberg, T., Huang, J., Saci, A., Widlund, H. R., Fisher, D. E., Xiao, Y., Rimm, D. L., Protopopov, A., Wong, K.-K., & Chin, L. (2009). GOLPH3 modulates mTOR signalling and rapamycin sensitivity in cancer. *Nature*, *459*(7250), 1085–1090. https://doi.org/10.1038/nature08109

Sharma, P., Ignatchenko, V., Grace, K., Ursprung, C., Kislinger, T., & Gramolini, A. O. (2010). Endoplasmic Reticulum Protein Targeting of Phospholamban: A Common Role for an N-Terminal Di-Arginine Motif in ER Retention? *PLoS ONE*, *5*(7), e11496. https://doi.org/10.1371/journal.pone.0011496

Shin, Y. H., Lee, S. J., & Jung, J. (2012). Secretion of ATP from Schwann cells through lysosomal exocytosis during Wallerian degeneration. *Biochemical and Biophysical Research Communications*, *429*(3–4), 163–167. https://doi.org/10.1016/j.bbrc.2012.10.121

Shinozaki, Y., Nomura, M., Iwatsuki, K., Moriyama, Y., Gachet, C., & Koizumi, S. (2014). Microglia trigger astrocyte-mediated neuroprotection via purinergic gliotransmission. *Scientific Reports*, *4*(1), 4329. https://doi.org/10.1038/srep04329

Stalder, D., & Gershlick, D. C. (2020). Direct trafficking pathways from the Golgi apparatus to the plasma membrane. *Seminars in Cell & Developmental Biology*, *107*, 112–125. https://doi.org/10.1016/j.semcdb.2020.04.001

Tan, P. K., Waites, C., Liu, Y., Krantz, D. E., & Edwards, R. H. (1998). A Leucine-based Motif Mediates the Endocytosis of Vesicular Monoamine and Acetylcholine Transporters. *Journal of Biological Chemistry*, *273*(28), 17351–17360. https://doi.org/10.1074/jbc.273.28.17351

Tang, Y., & Illes, P. (2017). Regulation of adult neural progenitor cell functions by purinergic signaling: Purinergic Signaling and Neural Progenitor Cells. *Glia*, *65*(2), 213–230. https://doi.org/10.1002/glia.23056

Taruno, A., Vingtdeux, V., Ohmoto, M., Ma, Z., Dvoryanchikov, G., Li, A., Adrien, L., Zhao, H., Leung, S., Abernethy, M., Koppel, J., Davies, P., Civan, M. M., Chaudhari, N., Matsumoto, I., Hellekant, G., Tordoff, M. G., Marambaud, P., & Foskett, J. K. (2013). CALHM1 ion channel mediates purinergic neurotransmission of sweet, bitter and umami tastes. *Nature*, *495*(7440), 223–226. https://doi.org/10.1038/nature11906

Teasdale, R. D., & Jackson, M. R. (1996). SIGNAL-MEDIATED SORTING OF MEMBRANE PROTEINS BETWEEN THE ENDOPLASMIC RETICULUM AND THE GOLGI APPARATUS. *Annual Review of Cell and*

Developmental Biology, *12*(1), 27–54. https://doi.org/10.1146/annurev.cellbio.12.1.27

Tóth, A., Antal, Z., Bereczki, D., & Sperlágh, B. (2019). Purinergic Signalling in Parkinson's Disease: A Multi-target System to Combat Neurodegeneration. *Neurochemical Research*, *44*(10), 2413–2422. https://doi.org/10.1007/s11064-019-02798-1

Tremblay, R. G., Sikorska, M., Sandhu, J. K., Lanthier, P., Ribecco-Lutkiewicz, M., & Bani-Yaghoub, M. (2010). Differentiation of mouse Neuro 2A cells into dopamine neurons. *Journal of Neuroscience Methods*, *186*(1), 60–67. https://doi.org/10.1016/j.jneumeth.2009.11.004

Trudeau, L.-E., & El Mestikawy, S. (2018). Glutamate Cotransmission in Cholinergic, GABAergic and Monoamine Systems: Contrasts and Commonalities. *Frontiers in Neural Circuits*, *12*, 113. https://doi.org/10.3389/fncir.2018.00113

Turovsky, E. A., Braga, A., Yu, Y., Esteras, N., Korsak, A., Theparambil, S. M., Hadjihambi, A., Hosford, P. S., Teschemacher, A. G., Marina, N., Lythgoe, M. F., Haydon, P. G., & Gourine, A. V. (2020). Mechanosensory Signaling in Astrocytes. *The Journal of Neuroscience*, *40*(49), 9364–9371. https://doi.org/10.1523/JNEUROSCI.1249-20.2020

Van Kolen, K., & Slegers, H. (2006). Integration of P2Y receptor-activated signal transduction pathways in G protein-dependent signalling networks. *Purinergic Signalling*, *2*(3), 451. https://doi.org/10.1007/s11302-006-9008-0

Varadi, M., Anyango, S., Deshpande, M., Nair, S., Natassia, C., Yordanova, G., Yuan, D., Stroe, O., Wood, G., Laydon, A., Žídek, A., Green, T., Tunyasuvunakool, K., Petersen, S., Jumper, J., Clancy, E., Green, R., Vora, A., Lutfi, M., … Velankar, S. (2022). AlphaFold Protein Structure Database: Massively expanding the structural coverage of protein-sequence space with high-accuracy models. *Nucleic Acids Research*, *50*(D1), D439–D444. https://doi.org/10.1093/nar/gkab1061

Varoqui, H., & Erickson, J. D. (1998a). Dissociation of the vesicular acetylcholine transporter domains important for high-affinity transport recognition, binding of vesamicol and targeting to synaptic vesicles. *Journal of Physiology-Paris*, *92*(2), 141–144. https://doi.org/10.1016/S0928-4257(98)80152-6

Varoqui, H., & Erickson, J. D. (1998b). The Cytoplasmic Tail of the Vesicular Acetylcholine Transporter Contains a Synaptic Vesicle Targeting Signal. *Journal of Biological Chemistry*, *273*(15), 9094–9098. https://doi.org/10.1074/jbc.273.15.9094

Verkhratsky, A., & Burnstock, G. (2014). Biology of purinergic signalling: Its ancient evolutionary roots, its omnipresence and its multiple functional significance. *BioEssays*, *36*(7), 697–705. https://doi.org/10.1002/bies.201400024

Vessey, K. A., & Fletcher, E. L. (2012). Rod and Cone Pathway Signalling Is Altered in the P2X7 Receptor Knock Out Mouse. *PLoS ONE*, *7*(1), e29990. https://doi.org/10.1371/journal.pone.0029990

Virgilio, F. D., & Solini, A. (2002). P2 receptors: New potential players in atherosclerosis. *British Journal of Pharmacology*, *135*(4), 831–842. https://doi.org/10.1038/sj.bjp.0704524

Voglmaier, S. M., Kam, K., Yang, H., Fortin, D. L., Hua, Z., Nicoll, R. A., & Edwards, R. H. (2006a). Distinct Endocytic Pathways Control the Rate and Extent of Synaptic Vesicle Protein Recycling. *Neuron*, *51*(1), 71–84. https://doi.org/10.1016/j.neuron.2006.05.027

Voglmaier, S. M., Kam, K., Yang, H., Fortin, D. L., Hua, Z., Nicoll, R. A., & Edwards, R. H. (2006b). Distinct Endocytic Pathways Control the Rate and Extent of Synaptic Vesicle Protein Recycling. *Neuron*, *51*(1), 71–84. https://doi.org/10.1016/j.neuron.2006.05.027

Wang, J., Fourriere, L., & Gleeson, P. A. (2020). Local Secretory Trafficking Pathways in Neurons and the Role of Dendritic Golgi Outposts in Different Cell Models. *Frontiers in Molecular Neuroscience*, *13*, 597391. https://doi.org/10.3389/fnmol.2020.597391

Weiss, G. A., Watanabe, C. K., Zhong, A., Goddard, A., & Sidhu, S. S. (2000). Rapid mapping of protein functional epitopes by combinatorial alanine scanning. *Proceedings of the National Academy of Sciences*, *97*(16), 8950–8954. https://doi.org/10.1073/pnas.160252097

Wiatrak, B., Kubis-Kubiak, A., Piwowar, A., & Barg, E. (2020). PC12 Cell Line: Cell Types, Coating of Culture Vessels, Differentiation and Other Culture Conditions. *Cells*, *9*(4), 958. https://doi.org/10.3390/cells9040958

Wilson, J., & Hunt, T. (2015). *Molecular biology of the cell: The problems book* (6th ed). Garland science.

Wong, Z. W., & Engel, T. (2023). More than a drug target: Purinergic signalling as a source for diagnostic tools in epilepsy. *Neuropharmacology*, *222*, 109303. https://doi.org/10.1016/j.neuropharm.2022.109303

Woo, S.-H., & Trinh, T. N. (2020). P2 Receptors in Cardiac Myocyte Pathophysiology and Mechanotransduction. *International Journal of Molecular Sciences*, *22*(1), 251. https://doi.org/10.3390/ijms22010251

Wu, M. M., Grabe, M., Adams, S., Tsien, R. Y., Moore, H.-P. H., & Machen, T. E. (2001). Mechanisms of pH Regulation in the Regulated Secretory Pathway. *Journal of Biological Chemistry*, *276*(35), 33027–33035. https://doi.org/10.1074/jbc.M103917200

Wulff, H. (2008). New Light on the “Old” Chloride Channel Blocker DIDS. *ACS Chemical Biology*, *3*(7), 399–401. https://doi.org/10.1021/cb800140m

Xue, L. C., Rodrigues, J. P., Kastritis, P. L., Bonvin, A. M., & Vangone, A. (2016). PRODIGY: A web server for predicting the binding affinity of protein–protein complexes. *Bioinformatics*, *32*(23), 3676–3678. https://doi.org/10.1093/bioinformatics/btw514

Yang, Z., Zeng, X., Zhao, Y., & Chen, R. (2023). AlphaFold2 and its applications in the fields of biology and medicine. *Signal Transduction and Targeted Therapy*, *8*(1), 115. https://doi.org/10.1038/s41392-023-01381-z

Yao, J., & Hersh, L. B. (2007). The vesicular monoamine transporter 2 contains trafficking signals in both its N-glycosylation and C-terminal domains.

Journal of Neurochemistry, *100*(5), 1387–1396. https://doi.org/10.1111/j.1471-4159.2006.04326.x

Yim, H.-S., Cho, Y. S., Guang, X., Kang, S. G., Jeong, J.-Y., Cha, S.-S., Oh, H.-M., Lee, J.-H., Yang, E. C., Kwon, K. K., Kim, Y. J., Kim, T. W., Kim, W., Jeon, J. H., Kim, S.-J., Choi, D. H., Jho, S., Kim, H.-M., Ko, J., … Lee, J.-H. (2014). Minke whale genome and aquatic adaptation in cetaceans. *Nature Genetics*, *46*(1), 88–92. https://doi.org/10.1038/ng.2835

Zhao, Y. F., Verkhratsky, A., Tang, Y., & Illes, P. (2022). Astrocytes and major depression: The purinergic avenue. *Neuropharmacology*, *220*, 109252. https://doi.org/10.1016/j.neuropharm.2022.109252

Zhong, X. Z., Cao, Q., Sun, X., & Dong, X.-P. (2016). Activation of lysosomal P2X4 by ATP transported into lysosomes via VNUT/SLC17A9 using V-ATPase generated voltage gradient as the driving force. *The Journal of Physiology*, *594*(15), 4253–4266. https://doi.org/10.1113/JP271893

Appendix. Supplemental Table

Table A.1: FIJI Plugin RIPA Puncta Identification Parameters

	Analysis parameters	C-terminus	N-terminus
Threshold settings	Step method	Step size	Step size
	Step size	50-90	300 – 1000
	First threshold	Maximum	Maximum
	Background	140-400	500-600
Puncta parameters	Minimum puncta area (px)	7-9	10-40
	Maximum puncta area (px)	30-40	40
	Minimum circularity	0.5-0.6	0.6
	Maximum circularity	1	1
	Minimum solidity	0.5-0.6	0.6
	Maximum solidity	1	1
Pre- and post-processing	Background subtraction	None	None
	Unsharp mask	None	None
	Gaussian smooth radius	1	1